COO-2234-11

MASTER

PELLETS FOR FUSION REACTOR REFUELING

Annual Progress Report
for Period January 1, 1976 - December 31, 1976

Robert J. Turnbull and Kyekyoon Kim

University of Illinois
Urbana, Illinois 61801

NOTICE

NOTICE
This report was prepared as an account of work sponsored by the United States Government. Neither the United States nor the United States Energy Research and Development Administration, nor any of their employees, nor any of their contractors, subcontractors, or their employees, makes any warranty, express or implied, or assumes any legal liability or responsibility for the accuracy, completeness or usefulness of any information, apparatus, product or process disclosed, or represents that its use would not infringe privately owned rights.

January 1977

Prepared For

THE U.S. ENERGY RESEARCH AND DEVELOPMENT ADMINISTRATION
UNDER CONTRACT NO. EY-76-S-02-2234.*000

DISCLAIMER

Abstract

The purpose of this research is to test the feasibility of refueling fusion reactors using solid pellets composed of fuel elements. A solid hydrogen pellet generator has been constructed and experiments have been done to inject the pellets into the ORMAK Tokamak. A theory has been developed to describe the pellet ablation in the plasma, and an excellent agreement has been found between the theory and the experiment. Techniques for charging the pellets have been developed in order to accelerate and control them. Other works currently under way include the development of techniques for accelerating the pellets for refueling purpose. Evaluation of electrostatic acceleration has also been performed.

I. INTRODUCTION

Conceptual designs of future fusion power reactors based on Tokamak concept will require a long sustained burn cycle time. The particle confinement time, however, is only a small fraction of the burn time. This requires that the lost fuel ions be replenished with fresh ones during the burn cycle of the reactor operation. Injection of macroscopic fuel pellets appears to be the most promising refueling scheme proposed thus far. Under this grant experiments have been performed testing the feasibility of this refueling technique. The work which has been done is as follows:

1) Spherical solid hydrogen pellet injection experiments have been performed on ORMAK,
2) Theoretical calculations have been made on the ablation of a solid hydrogen pellet in a plasma and the results compared with experiment,
3) A method of charging solid insulators has been developed,
4) A technique for producing uniform charged drops of cryogenic liquids has been developed,
5) A solid hydrogen pellet generator has been constructed and modified for more efficient generation, selection, and acceleration of large size pellets,
6) Construction of a hydrogen extruder, development of an electron beam accelerator, and development of a plasma gun accelerator are currently being investigated,
7) Evaluation on electrostatic acceleration has been made.

Each of these topics will be the subject of a section of this report.

II. SPHERICAL SOLID HYDROGEN PELLET INJECTION EXPERIMENTS ON ORMAK

See the Appendix for a paper which has been written on this subject.

III. A MODEL FOR THE ABLATION RATE OF A SOLID HYDROGEN PELLET IN A PLASMA

See the Appendix for a paper which has been written on this subject.

IV. CONTACT CHARGING OF INSULATORS

1. Introduction

The prospect of controlled thermonuclear fusion has stimulated research in a broad spectrum of areas in order to develop the technical support necessary to hasten its realization. The refueling of the fusion reactor illustrates the difficulty of the overall task just by the diversity of methods proposed to accomplish it. One such proposal calls for the injection of small frozen hydrogen (or deuterium) pellets into the reactor core, which contains a high temperature plasma. The cryogenic hydrogen pellets will evaporate very quickly in the hot plasma, and will require high velocities if they are to penetrate to the center of the plasma.

The necessary high velocities might be obtained by accelerating charged pellets in a strong electric field.[1] By equating inertial and electrostatic forces, this relation for the acceleration of a charged pellet in an electric field is obtained:

$$a = \frac{q}{m} E, \qquad (1)$$

where a is the acceleration, q is the total charge, m is the pellet's mass, and E is the applied field, all in mks units. Hence, it is obvious that the charge-to-mass ratio must be maximized for optimum performance.

The degree to which a particular material can be charged

depends on the conductivity of the material and the charging method used. Moderate and good conductors can be charged fairly easily by a variety of techniques. For example, metallic particles will become charged when placed on a metal plate which is raised to a high voltage.[2] Insulating materials require much higher electric fields to be charged. Insulating liquids such as liquid nitrogen can be charged by placing a high voltage needle within a nozzle and flowing the liquid through it.[3,4,5] The electric field strength near the tip is sufficient to charge the liquid nitrogen surrounding the needle.

Charged liquid drops are subject to a fundamental limitation, known as the Rayleigh limit. While investigating the break up of charged liquid jets, Rayleigh observed that a droplet with a given radius could contain only a certain maximum amount of charge on its surface before it broke up into smaller droplets.[6] This occured when the coulombic repulsion between charges on the surface became greater than the surface tension of the liquid. This relation can be expressed as

$$q = 4\pi\sqrt{2\varepsilon T}\, R^{3/2}, \qquad (2)$$

where q is the maximum stable charge, ε is the permittivity of the liquid, T is the surface tension of the liquid, and R is the maximum stable radius of the droplet, all in mks units.

By breaking into smaller droplets, the same amount of charge is spread over greater surface area, reducing the electrostatic stress.

This process sets an upper limit to the charge which can reside on a liquid drop of a given size. To overcome this limitation the hydrogen pellets will be frozen and then charged in a very high electric field. A solid material is not subject to the same instability as is a liquid, because the solid is bound together more tightly. If the solid droplet is placed in contact with a very sharp high voltage needle, the resulting charge will hopefully be much higher than the limit for a liquid drop of the same size. The limiting factors in contact charging of solid insulators will involve the intensity of the applied electric field and the nature of the charge transfer in the insulator.

In this sense, the intense field required for charge transfer will be produced by etching a thin metal wire to a fine point, and then raising the wire to a high potential. The type of wire used, the etching process, and the limit to sharpness will be discussed.

Since solid hydrogen drops are difficult to generate, and the environment necessary is far from ideal to investigate the performance of a charging system, it is advantageous to sub-

stitute a material which has properties similar to frozen hydrogen but which does not require cryogenic temperatures and carefully controlled pressures. The information gathered with polystyrene beads should demonstrate the utility of contact charging of insulating solid drops.

2. Objectives

The major objectives to be investigated in this experiment are threefold: (1) producing the highest possible charge-to-mass ratio, (2) determining conditions under which the usable lifetime of the charging electrode is longest, and (3) developing a reliable method to measure the charge-to-mass ratio of a solid pellet.

The mechanism of charge transfer for an insulator in a strong electric field will be investigated in order to predict and interpret the results of the experiment. The relative merits of positive and negative charging and the effects of different voltages will be discussed.

The difficulties of working with high voltages and strong electric fields will be discussed and remedies presented. These lead to restrictions on the atmosphere surrounding the charging electrode, specifically the need for a vacuum system, which complicates the charging system.

Finally, there are a number of ways to measure charge and

charge-to-mass ratios, all with varying degrees of complexity and applicability. The nature of each must be explored to find which is most suitable in the expected environment.

3. Theory of Contact Charging

In order to predict the performance and to understand the limitations of contact charging, the mechanism of charge transfer due to intense electric fields must be investigated. Essentially, four quantum mechanical phenomena can occur under this condition: field ionization, field emission, field adsorption, and field desorption.[7,8,9] The first two are useful charging methods including the tunneling of electrons between the field-producing electrode and the material to be charged. The latter two effects are unwanted limitations on the electric field which a material can withstand before positive ions are adsorbed or emitted from the surface of the material. These processes must be considered in pairs (ionization-desorption and emission-adsorption) in order to determine the best needle material, diameter, and charging potential - in view of the nature of the material to be charged.

Field emission occurs from a sharp negative high voltage electrode when the field at the surface has sufficiently reduced the barrier confining electrons and tunneling from the surface to free space becomes more probable. If some

material is placed in contact with the tip, tunneling into this material becomes even more likely because the induced image charge further decreases the barrier. Electrons would be transferred until the resulting charge of the material in contact has reduced the applied field below that which is necessary for field emission. For the case of a spherical pellet in contact with a sharp tip, the charging can occur only very near the point of contact (of the order of angstroms) since greater distances reduce the probability of tunneling tremendously. Thus, the resulting charge on the pellet will be quite localized and only a tiny fraction of that possible if the entire surface was charged.

Another limitation occurs if the field is strong enough to cause molecules to be torn from the pellet and adsorbed into the tip. In some materials this phenomenon may occur before field emission and could cause the pellet to break up. Since this occurs when the charging potential is negative, a positive potential may prove more desirable.

If the tip is positive, field ionization, a process exactly the reverse of field emission, can occur and electrons will tunnel out of the pellet and into the tip. Charging will suffer the same localization effect as before, but one important advantage can be derived. In this case, sufficiently

high fields will tear atoms from the tip and deposit them on the pellet. Metals such as tungsten have a very high resistance to this field desorption process, and therefore, make excellent needle materials. Using a tungsten tip it should be possible to produce fields high enough to give good charging, but still low enough to limit damage to the tip.

The erosion of the tip will be a serious problem during the course of the experiment. If field desorption does occur from the tip, it will leave a rough surface with localized sharp projections. These points will produce strong fields and contribute to further desorption. If the field is high enough initially, the tip will be quickly dulled, and the field thereby reduced. Also, ions in the surrounding gas would bombard and damage a negative needle, so a positive potential may lead to less damage from the residual gas in the vacuum system.

4. Charge Measurement Techniques

A number of methods exist by which the charge on a small pellet, or stream of pellets, can be measured. Three alternatives will be discussed here, in order to point out the particular restrictions imposed by the nature of the experiment.

The simplest technique requires that a stream of charged

pellets be collected in a metal cup and the resultant current be discharged through a sensitive ammeter (See Figure 1). If the number of charged pellets landing in the cup per second is known, then the average charge per pellet can be computed. It would be given by

$$q = I/N, \qquad (3)$$

where I is the current measured by the ammeter, in coulombs per second, and N is the number of pellets per second.

However, this technique will be quite inadequate if the flow rate is not well known or not constant. When a stream of pellets is charged by contact it may be possible that the amount of charge on a particular pellet will vary significantly from one pellet to another. This is especially so if the stream does not strike the needle in the same place every time. Also, once the pellets are charged they will be scattered in many directions. It seems unlikely that a uniform current will be produced or that an accurate value of average charge-per-drop can be obtained.

A technique more suited to determining the charge-to-mass ratio of a single drop requires the measurement of the deflection of a charged pellet in a known electric field. A constant electric field will exist between two flat, parallel

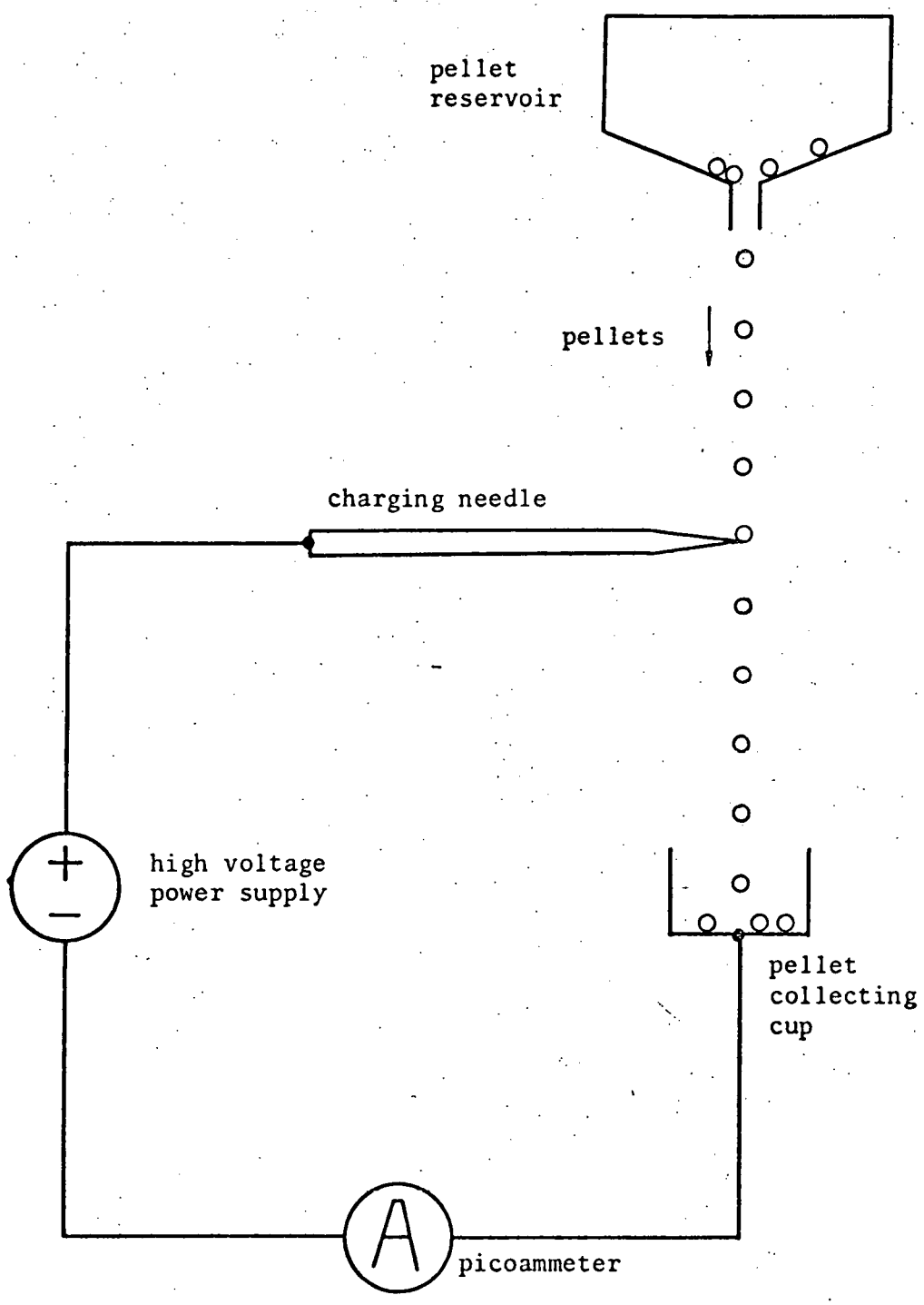

Figure 1: Faraday Cup Charge-Measuring Scheme

plates with a potential between them. If a charged pellet with constant velocity passes between the plates and its position is measured at two times, separated by a delay of t seconds, it will be deflected from its path by some distance d. From this data, the charge-to-mass ratio can be computed. It is given by

$$\frac{q}{m} = \frac{2dR}{Vt^2} \qquad (4)$$

where q is the pellet's charge, m is the pellet's mass, R is the plate separation, and V is the potential between the plates, all in mks units. The arrangement is shown in Figure 2.

The most serious problem occurs with measuring the pellet's position while between the plates. This would best be done with a camera, making a double exposure by flashing a stroboscopic lamp at a precise interval. The distance traveled could be measured and calibrated from the photograph.

The major drawback in this system involves determining when a pellet is between the plates and then automatically triggering the flash lamp. Since the pellets are quite small and moving rapidly in a variety of directions, this is indeed a difficult task. Some sort of device would be needed to detect the charged pellet before it moves between the plates,

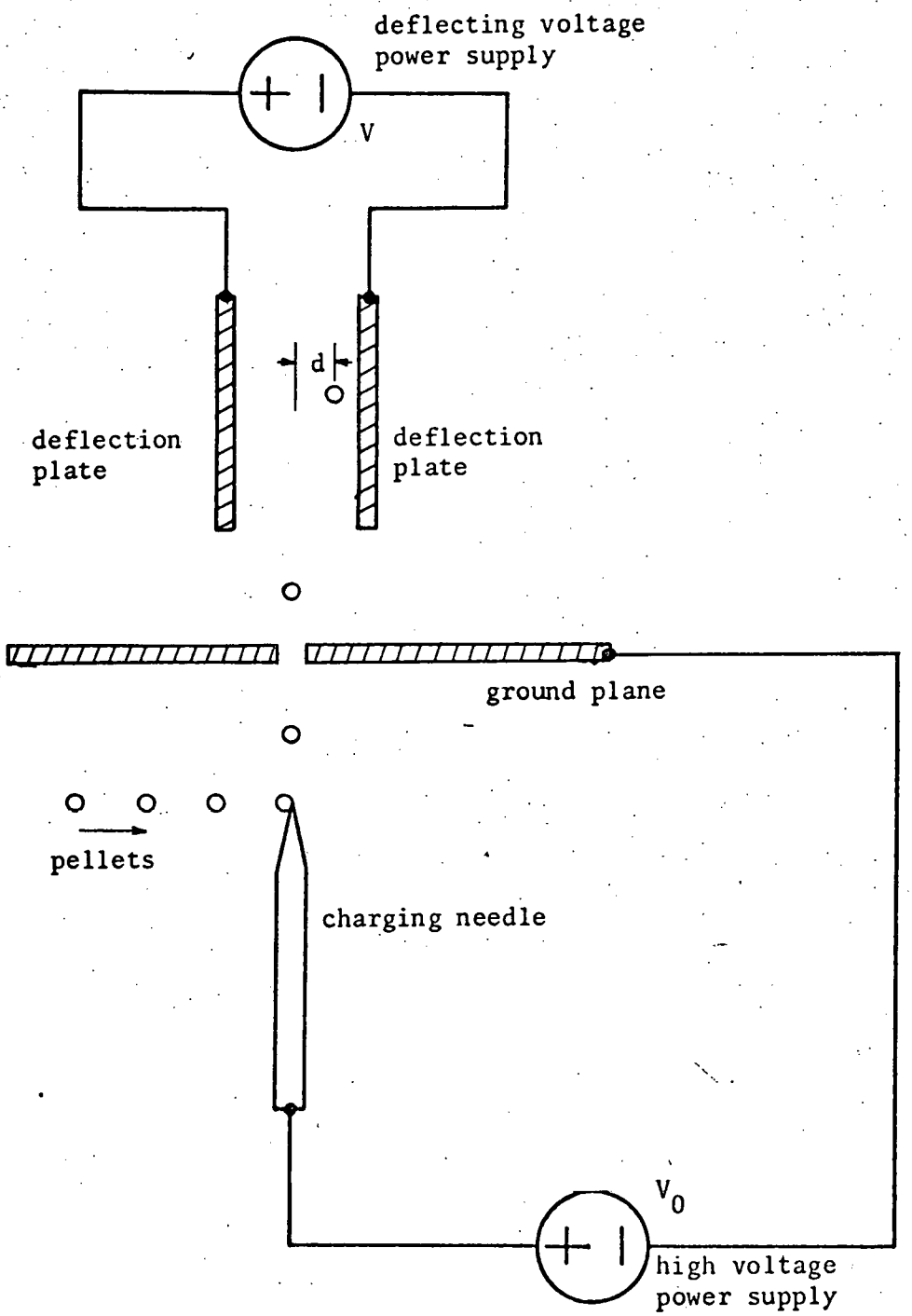

Figure 2: Pellet Deflection Charge Measuring Scheme

so it seems simpler to build a detecting device capable of measuring charge by itself, and dispense with the other apparatus. One such device is called a Faraday cage or drift-tube detector. An explanation of its operation follows.

The capacitance C of an object with respect to a reference is determined by the charge Q on it, necessary to raise it to a potential V with respect to the reference. That is,

$$C = Q/V. \qquad (5)$$

If a charge is brought near this object, it induces an image charge on it, which is equivalent to a voltage, by Equation (5). Therefore, if a charged pellet moves through a detector with a known capacitance, the charge on the pellet can be computed by measuring the voltage induced on the detector. This is the function of a Faraday cage.

It will be valuable to look at the effect the detector's shape has on the induced voltage, since the output should be made as easy to measure as possible. The ideal detector would produce no voltage until the charged pellet is entirely within its confines, then the output should be a constant voltage. When the pellet passes out of the detector, the output should again be zero. This requires that the field of the pellet should be entirely confined within the detector when the pellet is inside, and should have no effect at any

other time. This would produce a rectangular voltage pulse, as a function of time.

A metal cylinder, slightly larger than the pellet and many times longer will meet these requirements reasonably well. A compromise must be made, however, to accomodate some variation in the trajectories of the pellets, in order to prevent them from hitting the cylinder walls. If the open ends of the cylinder are a small fraction of its inside surface area, most of the pellet's field will be confined and accuracy will be good.

For a completely-confined field, a charge Q on the pellet would induce a charge -Q on the cylinder. Then, if the capacitance of the cylinder can be determined with respect to a reference, measuring the equivalent voltage with respect to the reference, and using Equation (5), the charge on the pellet can be found. In practice, the capacitance of the cylinder will be small compared to the input capacitance of the device measuring the voltage.

As an example, suppose the detecting tube is 15 millimeters long and 5 millimeters in diameter, and is surrounded by another concentric reference cylinder which is 15 millimeters long and 40 millimeters in diameter as shown in Figure 3. The outer cylinder is grounded and represents

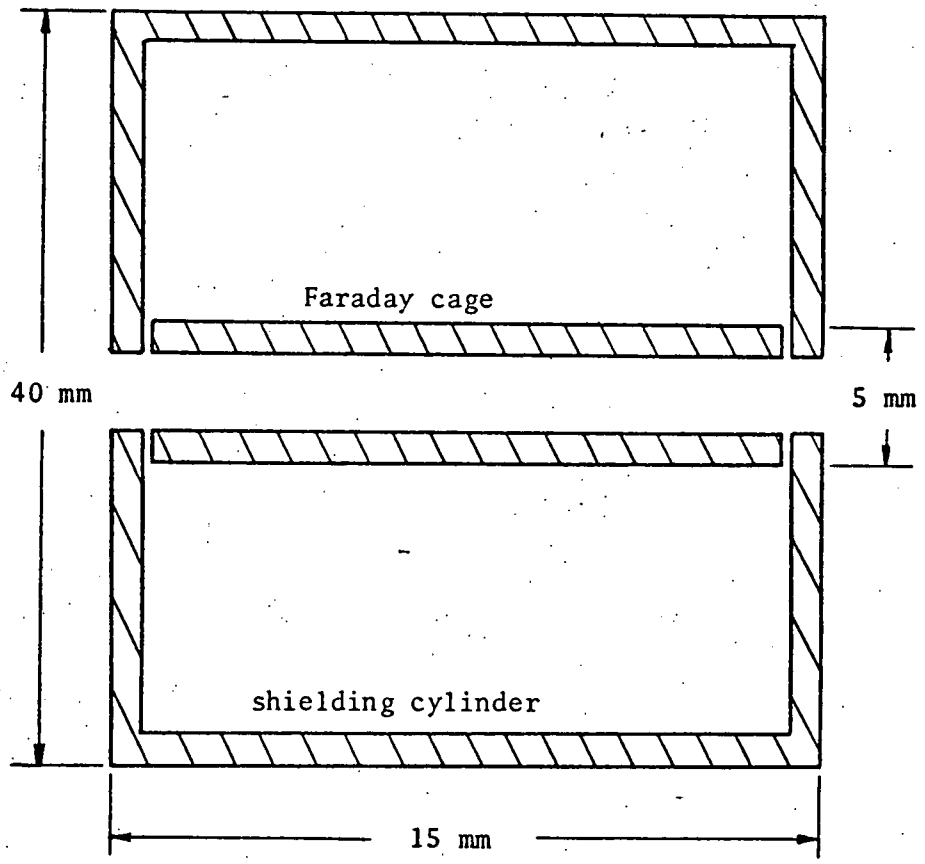

Figure 3: Faraday Cage and Shield Arrangement

a noise shield. Ignoring wall thickness and edge effects, the capacitance per unit length is given by

$$C = 2\pi\epsilon/\ell n \frac{b}{a} , \qquad (6)$$

where, in mks units, ϵ is the permattivity of the material between the cylinders, b is the radius of the outer cylinder, and a is the radius of the detecting tube, all in mks units. If ϵ is that of free space, the total capacitance of this system is 0.4 picofarads, which is small compared to the input capacitance of electronic measuring devices such as an oscilloscope. In addition, the connection between the cage and the measuring device will probably be coaxial cable to reduce noise. This adds a minimum of 10 picofarads per foot extra capacitance. In sum, the effect is to reduce the sensitivity of the Faraday cage by increasing the value of capacitance which appears in Equation (5). The remedy for this problem will be presented later.

The duration of the pulse induced on the Faraday cage can be used to compute the radius of the charged pellet passing through the tube, once the charge has been found. From the length of the pulse the velocity, v, of the pellet is computed. The energy acquired by the pellet being accelerated in a potential V_0 is qV_0; q is the pellet's

charge. Equating this electrostatic energy to kinetic energy, $1/2\ mv^2$, the radius can be expressed as

$$r = \left(\frac{3qV_0}{2\pi\rho v^2} \right)^{\frac{1}{3}} \qquad (7)$$

where ρ is the density of the pellet material. This computation will enable the charge to be related to the volume or surface area of the pellet.

The accurate measurement of the velocity will require sharp leading and trailing edges of the pulse on the detecting cylinder. The diameter of the tube cannot be very much greater than that of the pellets and still meet this requirement. Some provision must be made to ensure that at least some of the pellets have the correct trajectory to navigate the tube.

An additional problem in getting a well-shaped pulse from the detector comes from the measuring device, usually an oscilloscope. An oscilloscope has a fairly high input resistance. However, coupled with the low capacitance of the detector, the time constant of the system will be small. If it is too small, the induced pulse may leak off the cylinder before the pellet has traversed its length. Therefore, the resistance seen by the cylinder must be as high as possible.

In order to keep the sensitivity of the drift-tube detector as high as possible, the input capacitance must be kept as low as possible. This will be difficult to do if the cylinder is connected directly to the oscilloscope by coaxial cable. What is needed is a buffer amplifier mounted at the detecting cylinder in order to isolate the cylinder from the transmission line and oscilloscope.

Ideal input parameters for this amplifier are an infinite input resistance and a very low, well-known input capacitance. It must be able to drive an oscilloscope without affecting the input characteristics for a wide range of input voltage levels. It is also necessary that the amplifier be attached directly to the detector, in order to minimize the stray capacitance of extra wire, and to shield from noise.

A one-stage, simple amplifier is adequate for this application. Since the input is a very small current, the only gain necessary to meet the objectives is current gain. A suitable configuration meeting the desired parameters is the cathode follower or common collector circuit.

There are two devices which can provide the characteristics required. These are the M.O.S. field effect transistor and the electrometer vacuum tube CK5886. Both

have an input resistance in excess of 10^9 ohms and an input capacitance in the range of 2-5 picofarads. Initially, the mosfet was used as the buffer amplifier, but special considerations required that the vacuum tube be used. The design of the mosfet circuit is shown in Figure 4.

The resistors R_D and R_S were chosen to bias the transistor correctly for positive pulses. Also, their values were chosen to give unity voltage gain. This was done for convenience since large voltage gain was not needed. R_{IN} was used to try and prevent charge build-up on the gate which could eventually burn out the transistor. The input capacitance is low but uncertain by a factor of two, so C_{IN} was included and made roughly ten times (25 pF) the transistor's capacitance to insure that the value of C needed for Equation (5) is well known.

Charge build-up on the transistor's gate proved to be the undoing of this circuit. Due to the number of ions being created and accelerated away by the positive charging needle, a great deal of charge built up and quickly broke down the metal-oxide layer in the transistor, burning it out.

Rather than spending a great deal of time working on methods to prevent this destruction, a more durable amplifier was built.

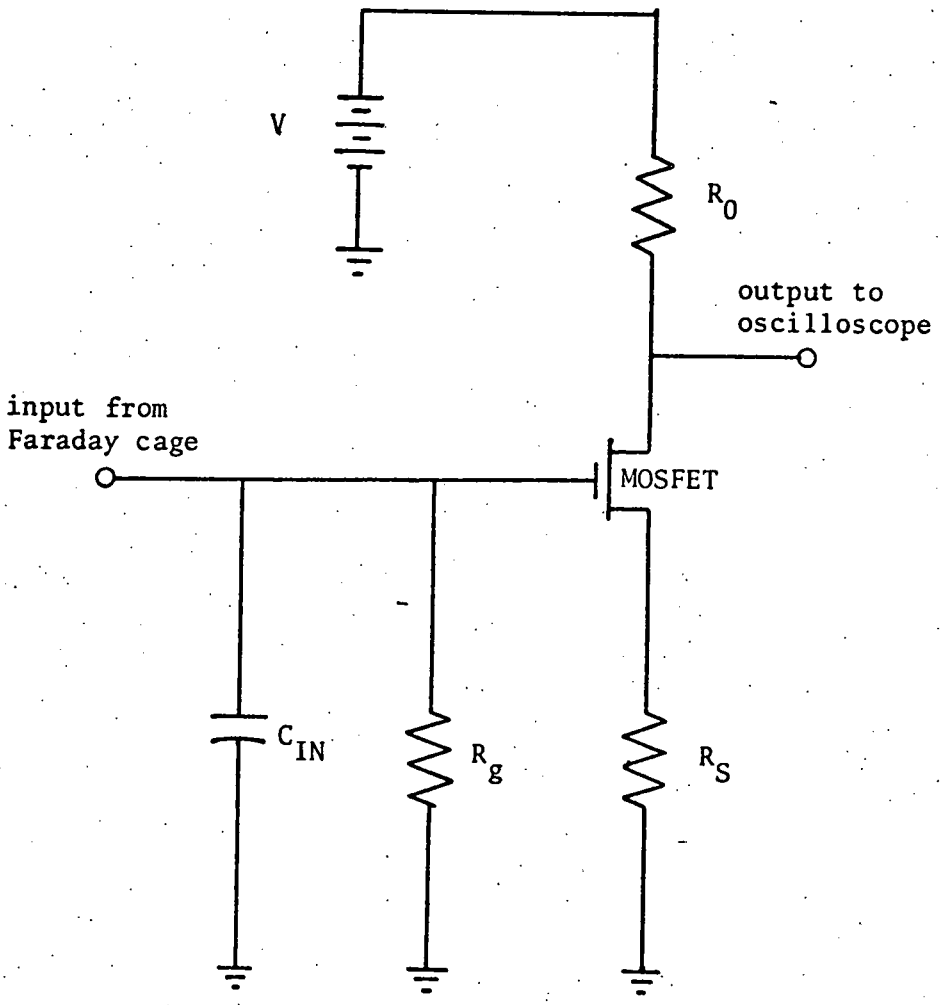

Figure 4: Transistor Buffer Amplifier

The CK5886 electrometer vacuum tube proved to be quite suitable for this application. The only detrimental effect incurred from charge accumulation on the grid involved a change in the tube's bias. With the use of a suitable grid-leak resistor, this was minimized and the input impedance was maintained at 10^9 ohms or better. The cathode-follower circuit which was used is shown in Figure 5.

The nominal input resistance for the CK5886 is about 10^5 ohms. R_{IN} reduced this to 10^9 and provided grid protection. C_{IN} served precisely the same function as its counterpart in the mosfet circuit, and had a value of 25 picofarads.

The biasing of the vacuum tube was specilized to the polarity of the expected pulse. Since positive charging was selected, a negative image charge would be induced on the detection tube. This negative charge would be pulled off the grid, causing a positive pulse on the grid. Since there is no phase shift in a cathode-follower, the output is a positive pulse. This can be seen by considering the flow of electrons off the cathode: as the grid goes positive, more electrons will flow off the cathode. This is equivalent to a positive current in the opposite direction, resulting in a positive pulse across R.

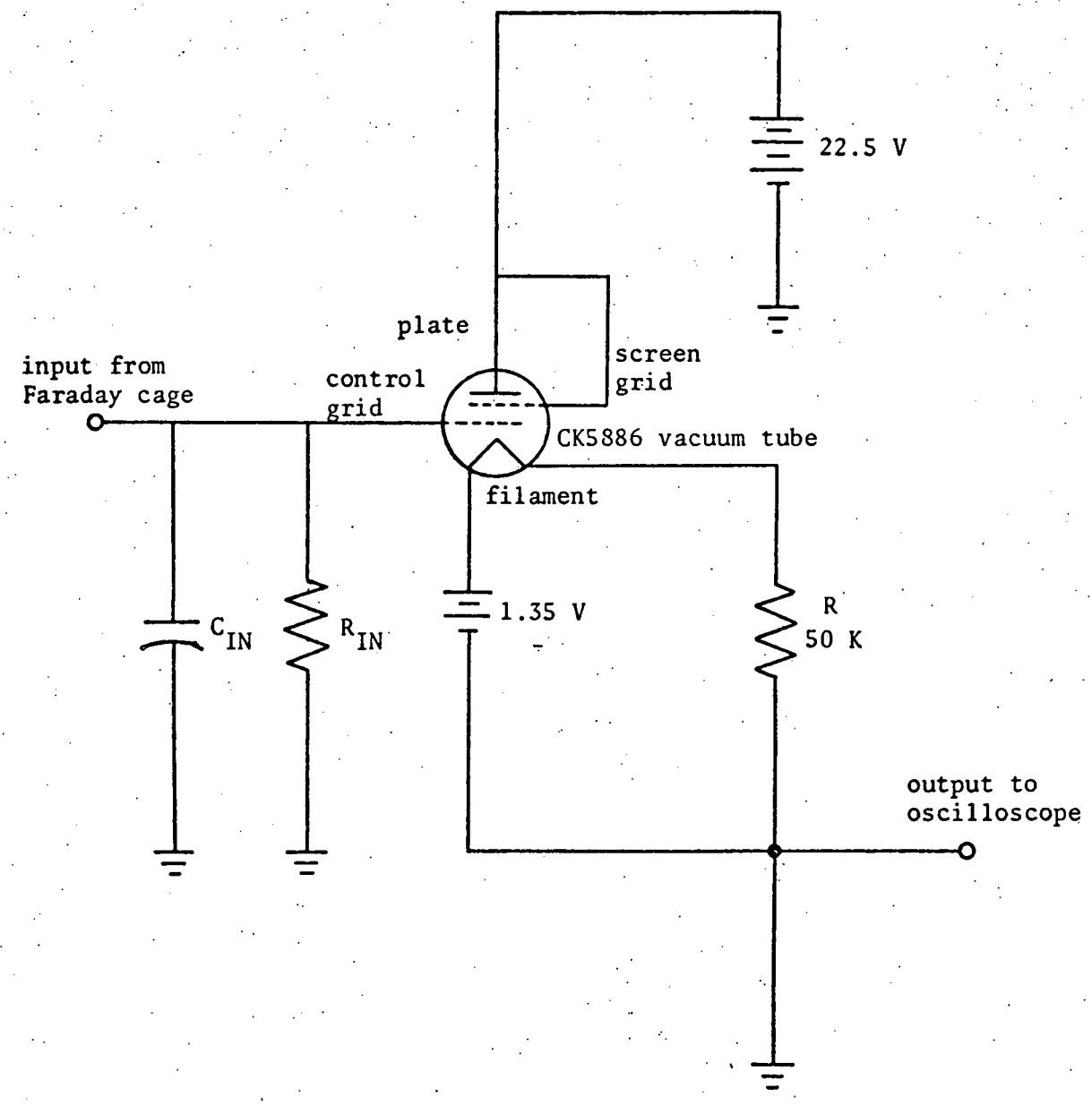

Figure 5: Vacuum Tube Buffer Amplifier

Also, if the positively charged pellet strikes the cylinder wall and transfers charge, the pulse generated across R is still positive. This is so because the electrons acquired by the pellet must flow off the grid, leaving it positive just as before. This pulse, however, will decay very slowly, with the time constant $R_{IN}C_{IN}$.

Since in both cases the output would be a positive pulse, the tube should be biased so it can best handle positive voltages on the grid. Allowance must be made to detect a wide range of voltages, since the amount of charge expected is unknown. The standard values for bias are indicated in Figure 5. These sources were batteries, remotely connected to the vacuum tube, since they were most easily left outside of the vacuum system.

These particular bias batteries resulted in a plate current of 100 microamperes, and R (50 K) was chosen to give a five volt drop. In this way the tube was biased in a fairly linear range and pulses as large as 17.5 volts could be measured.

The vacuum tube, R_{IN}, R, and C_{IN} were attached to the detector cylinder by a very short wire. This assembly was housed inside a larger cylinder which was almost completely closed on both ends. A five millimeter diameter hole was

provided to allow pellets to enter, and the detector was alligned directly behind the hole. The small cylinder was supported by a teflon stand-off, specially machined to increase the surface-leakage path length. The amplifier components were suspended from the cylinder by their electrical connections. This arrangement is diagrammed in Figure 6.

With this configuration the gain was measured as a function of frequency and signal level. The results are presented in Table 1.

With the amplifier gain, G, equal to 0.56, and the total input capacitance, C_{IN}, equal to 25 picofarads, the charge, q, on a pellet is given by

$$q = \frac{C_{IN}V}{G}, \qquad (8)$$

where V is the measured output voltage of the buffer amplifier.

The pulses were measured with a Tektronix storage oscilloscope model (549) , set to trigger and store on the leading edge of the pulses. It was then a simple matter to make a permanent record of the trace with an oscilloscope camera.

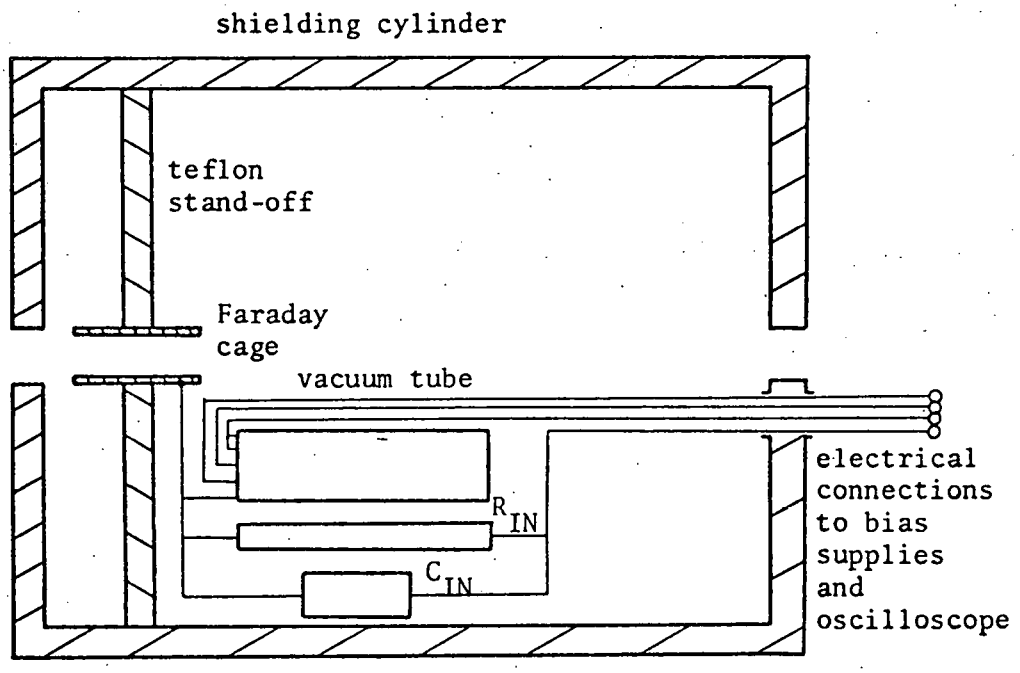

Figure 6: Arrangement of Amplifier Components and Faraday Cage Within Shielding Cylinder

Table 1: GAIN AND FREQUENCY RESPONSE OF AMPLIFIER

		Gain				
Frequency (Hertz)		10	10^2	10^3	10^4	10^5
Input Signal	50	0.56	0.56	0.54	0.48	0.24
Level (Millivolts)	500	0.56	0.56	0.54	0.48	0.24

Upper 3 dB point is 38 KHz

5. Experimental Apparatus

As discussed earlier, the process of field ionization requires a very good vacuum in order to prevent damage to the tip of the high voltage electrode. A pressure of 10^{-6} millimeters of mercury is relatively easily attained with common vacuum equipment. In this case, the charging electrode, Faraday cage, and pellet-feeding device were all enclosed in a four inch glass tee (See Figure 7). The end-plates were sealed to the glass with teflon gaskets. A 500 liter-per-minute mechanical roughing pump and a diffusion pump provided the required vacuum condition, which was measured with a thermocouple gauge and an ionization gauge.

The low-voltage supplies for the buffer amplifier were routed through the end plates with BNC vacuum feed throughs, as was the output of the amplifier. The high voltage feed-through was made by soldering a 3/4 inch quick-connect in one end-plate (Refer to Figure 8). An eight inch section of 3/4 inch pyrex glass tubing was closed on one end with a kovar seal around a 1/8 inch coaxial metal rod. The glass tube was expanded slightly near its center to prevent it from being pushed into the vacuum system by atmospheric pressure. This device provided a very long surface leakage path outside the system and a very clean surface path inside

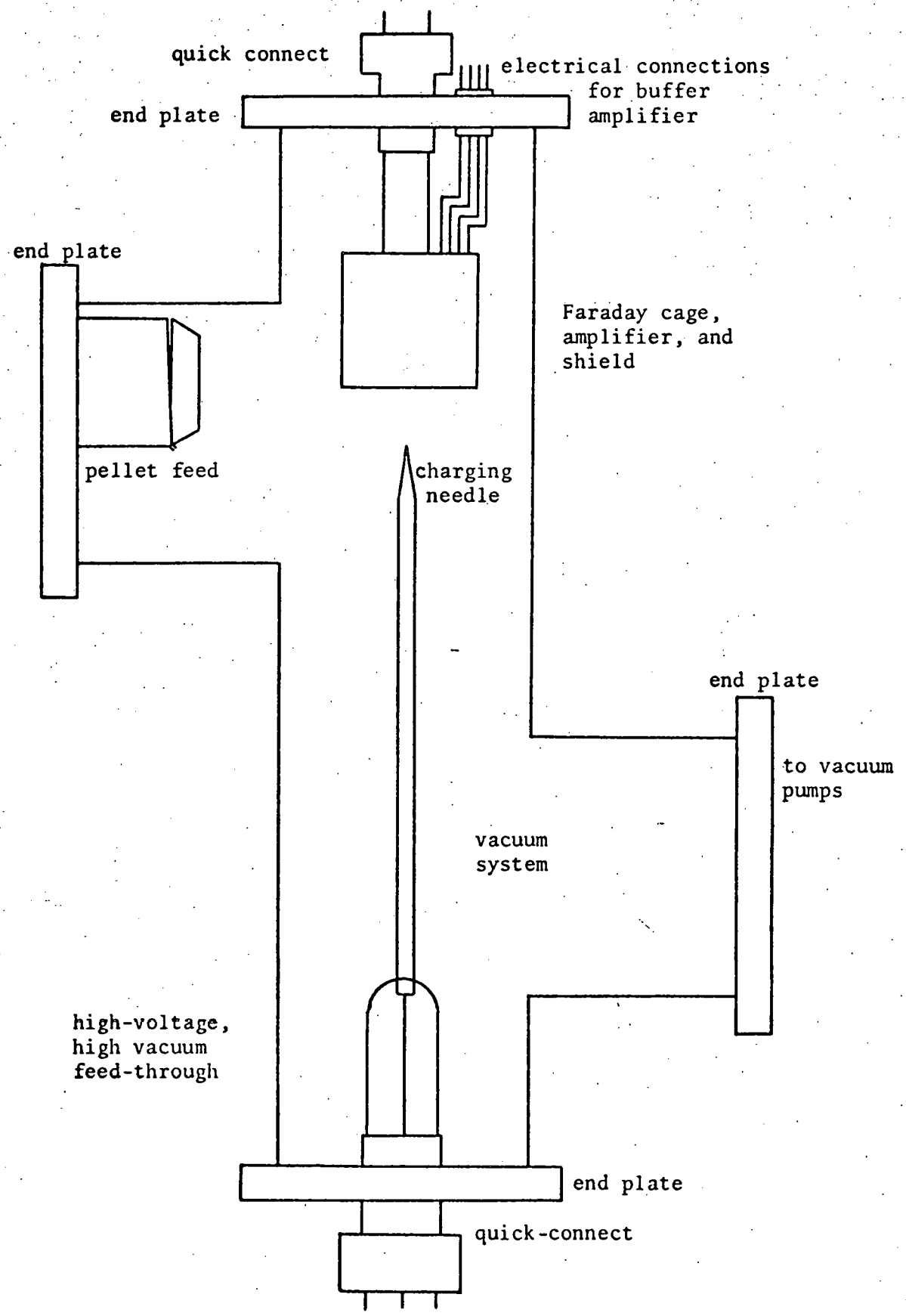

Figure 7: Layout of Components Within Vacuum System

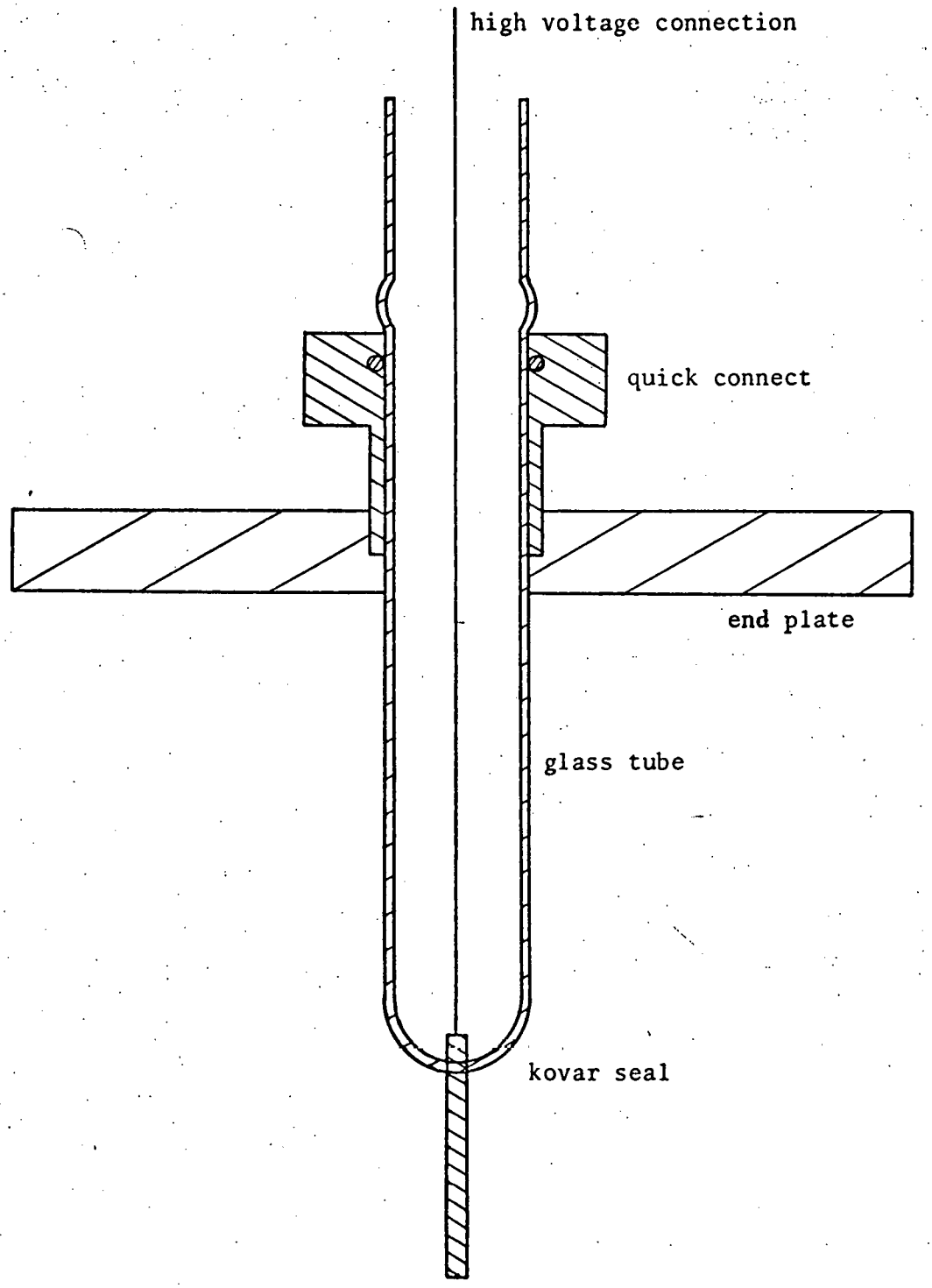

Figure 8: High Voltage, High Vacuum Feed-Through

the system.

The Faraday cage was installed on the end of a long rod directly opposite the needle. This rod extended outside the system, being sealed by a quick connect, enabling the alignment between needle and detector to be varied.

The most difficult problem to deal with in the experiment was that of feeding the polystyrene pellets to the charging electrode. Since a well-collimated, uniform stream of pellets was desirable, the most straight-forward procedure appeared to be to allow the pellets to flow out of a reservoir through a long narrow tube. However, the beads tended to form large clumps which blocked the tube. This effect did not appear to be caused by cohesion between the pellets, but rather by the polarization of many pellets due to a few charged ones. Very little charge was required to cause this, and the source of the charge was probably from the bombardment of the pellets by ions being accelerated away from the needle. A number of modifications were made to try and free the bunched pellets, but none were sufficiently successful. This led to a slightly more sophisticated feed device.

To prevent the pellets from being "pre-charged" by ions, the feed was made of metal and completely closed except for a small hole, through which the pellets were discharged

(shown in Fig. 9). The reservoir was a cylinder with an aluminum foil bottom. A speaker was mounted under the cylinder and its voice coil was glued to the foil in such a way that, when excited, the speaker vibrated the foil and agitated the pellets. The foil was inclined and funneled to the discharge hole, and by varying the amplitude of the excitation (at a resonant frequency of the system) the flow rate of the pellets could be controlled. Later, copper tape was found to withstand fatiguing and cracking better than aluminum foil. Also, the speaker was replaced by a small d.c. electric motor with an eccentric weight on its shaft. The motor was glued to the copper tape and the rotation of the weight produced vibration which was easily controlled by varying the motor's rotation rate. This system was largely immune to clogging, and was, consequently, quite reliable.

With the configuration of Figure 7, pellets were dropped onto the needle at a given rate. Various potentials were impressed on the needle and the resulting charged pellets were deflected horizontally by the grounded shield surrounding the Faraday cage. All the pellets which passed through the hole in the shield were detected and their charge and radius could be computed (provided they did not collide with the drift tube, and most did not). A detailed account of the

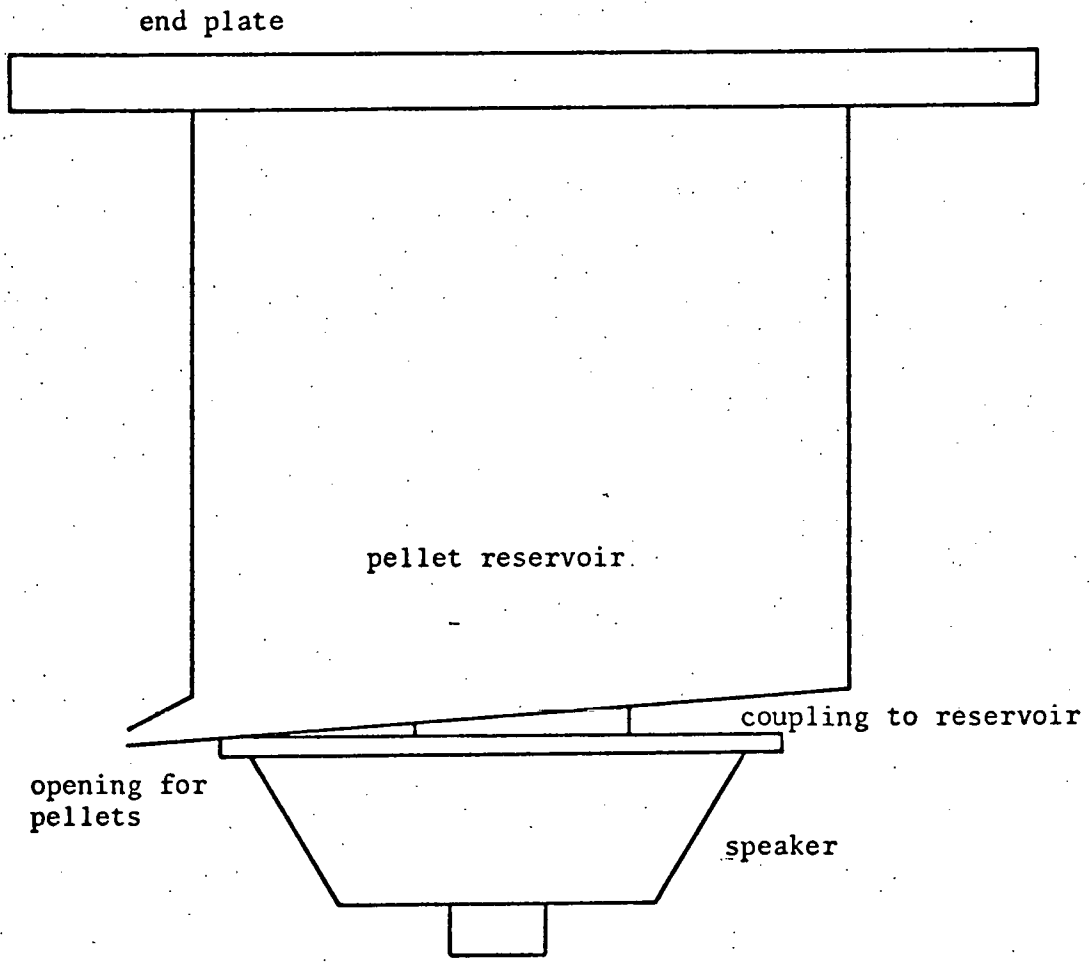

Figure 9: Pellet Feeding Device

experimental procedure and results follows.

6. Experimental Procedure

The primary objective of the contact charging experiment was two-fold: to determine the effects of various charging electrode dimensions and various charging potentials on the over-all efficiency of the charging process. The radius of the needle near the tip ranged from pellet-sized (150 micrometers) to as small as possible (less than one micrometer). The grainy nature of the tungsten wire caused it to be brittle at small radii and prone to breaking. Also, the etching process employed to produce the needles was difficult to control with small tips, sometimes resulting in needles with pitted surfaces. The electric field produced by such a tip would be a function of the detail of the surface and would vary substantially from point to point on the surface. Also the needle would tend to be eroded by field desorption (for positive potentials) since small points on the surface would produce extremely high fields, increasing the chance that atoms could be torn from the surface.

Positive charging potentials ranged from ten kilovolts to thirty kilovolts. This polarity was preferred since negative voltages could easily produce a great deal of field desorption of atoms from the surface of the pellet and

tungsten strongly resists this effect. Since destruction of the tip by the bombardment of ions from the residual gas was important, the system was operated at 10^{-6} torr and 10^{-3} torr to measure the effects.

The polystyrene pellets were spherical with radii ranging from 70 microns to 280 microns. They were kept as clean and dry as possible to minimize clumping. Throughout the experiment the pellets were allowed to fall about 10 cm before striking the needle. This distance had to be kept as large as possible to prevent charged pellets from being attracted to the grounded metal pellet feed where they would cause clumping as before. The longer free-fall meant less collimation of the stream, but a sufficient number of pellets still hit the needle close to the tip. The radius of the needle varied by roughly a factor of three along the length struck by pellets, so the field which produced the charge was uncertain by a factor of three, at the very least.

In the first trial the needle was about 150 micrometers in radius near the tip and was operated with positive potentials between ten and thirty kilovolts. The pressure in the vacuum system was 10^{-6} torr. The pellets fell in a slender cone and struck all along the last four millimeters of the needle. When the voltage was applied the needle was quickly covered with a

layer of pellets from shank to tip. The rest of the pellet stream continued to fall past the needle, with occasional collisions knocking pellets off the needle. These gaps were quickly filled by other pellets. The sticking was attributed to polarization of the pellets, since, if they were charged, they would have been repelled. When the high voltage was turned off many of the pellets clinging near the tip were rapidly ejected, as were some farther up on the shank. Most remained stuck, except on the sharpest part of the needle. Some of the pellets were obviously being slightly charged while in contact with the needle, and when the voltage was turned off, mutual repulsion forced them off the needle. The amount of charge was very small and insufficient to overcome the attractive polarization force holding the pellets on the needle, since none were seen to be accelerated horizontally towards the grounded Faraday cage shield. The shield was moved to within four centimeters of the tip but no pellets were observed to jump to the shield.

The results were the same for this needle for any positive voltage between ten and thirty kilovolts. No significant amount of charging was seen to take place with the maximum electric field strength of about 10^8 volts per meter on the tip.

For the second trial the sharpest possible needle was produced by careful etching of 0.012 inch diameter tungsten wire. Although a point of 0.1 micrometer diameter was created, it was quickly broken by vibration due to handling. The smallest point with sufficient structural integrity was about one micrometer in diameter on the end and five micrometers in diameter four millimeters from the end.

When a positive potential of twenty kilovolts was applied to this needle in a vacuum at 10^{-6} torr, charging took place readily. On the shank of the needle where the radius was over 150 micrometers, the pellets stuck just as before. However, within several millimeters of the tip they were propelled with high velocities in all directions. When viewed in a strong light the pellets could be seen as they bounced off the grounded metal end plates on the vacuum system. Although quite a number of the polystyrene beads missed the needle entirely, enough were charged to produce an occasional pulse on the Faraday cage. Most of the charged pellets were not going in the right direction to pass through both the hole in the shield and the drift tube. Charges were measured with positive voltages of twenty, twenty-five, and thirty kilovolts by taking pictures of the oscilloscope trace produced by the Faraday cage. Equation 10

allows the charge to be computed and Equation 7 gives the radius using the pulse length measured from the oscilloscope trace. A sketch of a representative pulse is shown in Figure 10, and a table showing the results of this trial is given in Table 2.

This experiment was repeated using needles with various tapers, but all with tips as sharp as possible (around one micrometer radius). All the results were virtually identical. No differences were observed with any charging potential between fifteen and thirty kilovolts while the vacuum was kept at 10^{-6} torr. However, when the pressure was increased to 10^{-3} torr, a very serious problem was encountered.

At this pressure it was not possible to increase the voltage above ten kilovolts because of large currents drawn from the power supply. At this pressure and voltage a great deal of ionization took place in the vicinity of the needle, consequently the current was greater than the rated capacity of the high voltage supply, resulting in reduced performance. This ion current had quite a surprising effect on the pellets. They fell no more than a centimeter below the feed device before they were deflected upward, away from the needle. The positive ions streaming away from the needle were striking and sticking to the pellets as they emerged from the feed. At

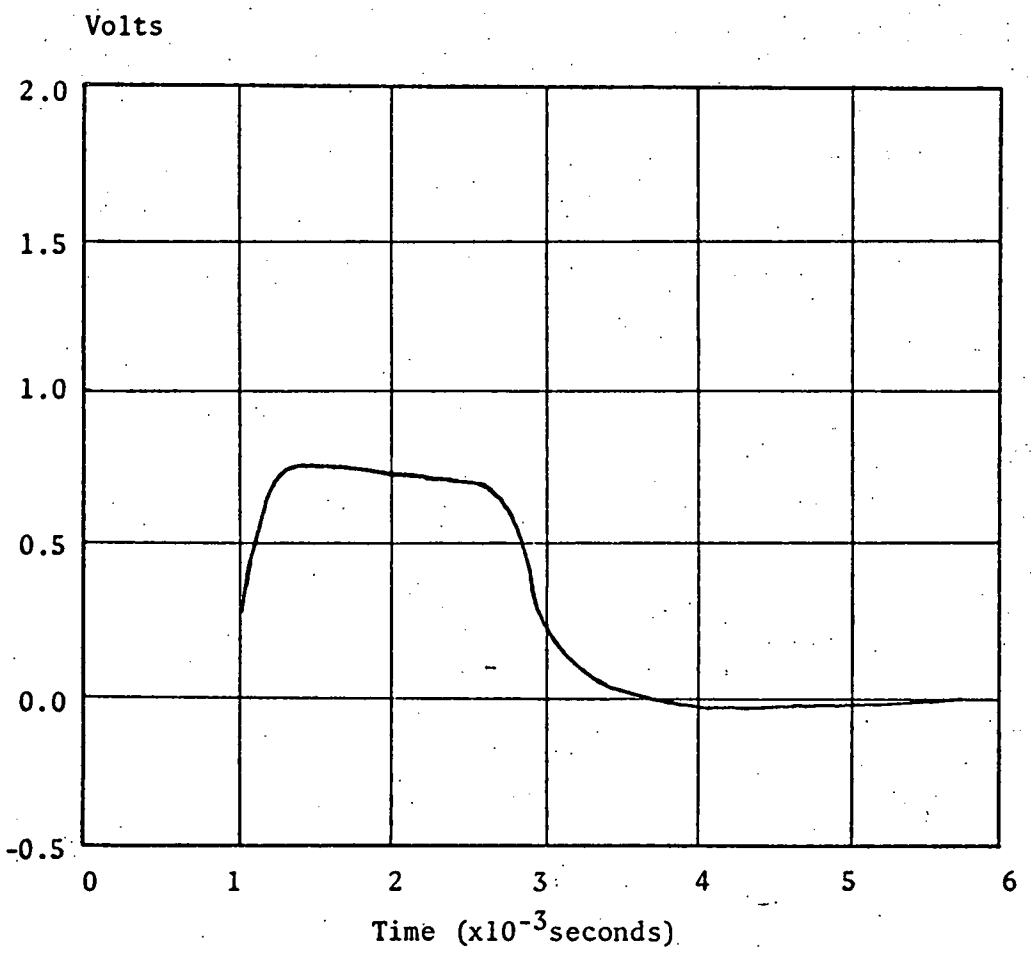

Figure 10: Sketch of Oscilloscope Trace of Representative Pulse from Faraday Cage

Charging Potential (KV)	Induced Voltage (Volts)	Pellet Velocity (M/S)	Pellet Charge ($x10^{-11}$ coulombs)	Pellet Radius ($x10^{-6}$ meters)	Charge To Mass Ratio ($x10^{-3}$ C/Kg)
	0.35	6.2	1.5	155	0.96
	0.35	10.7	1.6	109	2.9
	0.45	6.0	2.0	175	0.89
(Positive)	0.48	7.9	2.1	148	1.5
Twenty	0.52	9.4	2.3	135	2.2
Kilovolts	0.70	12.5	3.1	124	3.9
	0.85	7.9	3.8	180	1.6
	1.0	12.0	4.5	144	3.6
	1.0	7.5	4.5	197	1.4
(Positive)	0.33	7.5	1.4	144	1.1
Twenty-five	0.51	9.4	2.3	145	1.8
Kilovolts	0.76	4.7	3.4	264	0.44
	1.0	7.5	4.5	212	1.1
(Positive)	0.65	25.0	2.9	87	10.5
Thirty	0.70	10.0	3.1	164	1.7
Kilovolts					

Table 2: EXPERIMENTAL RESULTS OF CHARGING

a pressure of 10^{-3} torr there were enough ions to sufficiently charge the pellets to produce the observed radical deflection. No pellets were seen to reach the tip at all, and none were able to pass through the Faraday cage for measurement.

Operation at 10^{-3} torr also had a serious effect on the needle itself. When the system was again operated at 10^{-6} torr, using the needle which had just been used at 10^{-3} torr for a few minutes, no charging took place, even at thirty kilovolts. The pellets stuck (by polarization) all along the needle, including the tip. Since the needle might have been eroded during operation at 10^{-3} torr, it was removed and measured under a microscope. The radius was found to have increased to twenty-five micrometers at the tip, and the surface near the tip was quite rough and pitted.

The observed destruction could have been caused by the impacts of negative ions bombarding the positive tip, or by field desorption of tungsten atoms from the surface of the tip. Any roughness on the needle's surface would enhance the field locally and tend to promote field desorption, so the processes of bombardment and desorption may act in concert to blunt the needle.

The electric field at the surface of a 20 micrometer radius tip will be less than 10^{9} volts per meter when

raised to 20 kilovolts. This field was observed to produce only polarization and no charging with small polystyrene spheres and may be taken as the lower limit for contact charging of that material. In the light of this limitation, the remainder of the experiment was carried out with very sharp needles in a pressure of 10^{-6} torr.

Next, a variation in the geometry of the system was made to change the orientation of the needle with respect to the pellet stream. The last five millimeters of the tip of the needle were bent at an angle of 45 degrees with respect to the shank. The detector was placed under the tip and almost in line with the pellet stream, as shown in Figure 11.

With this arrangement, it was hoped the pellets would be polarized as they approached the needle and pulled more towards the tip than before. The higher field strength at the tip might then produce greater charge on the pellet. The Faraday cage was placed below the needle to see how well the direction of flow of the pellets could be maintained after they struck the needle, which would be useful information if the pellets were expected to be traveling at high velocity prior to impact.

With an operating pressure of 10^{-6} torr and a positive charging potential of twenty kilovolts, the pellets were

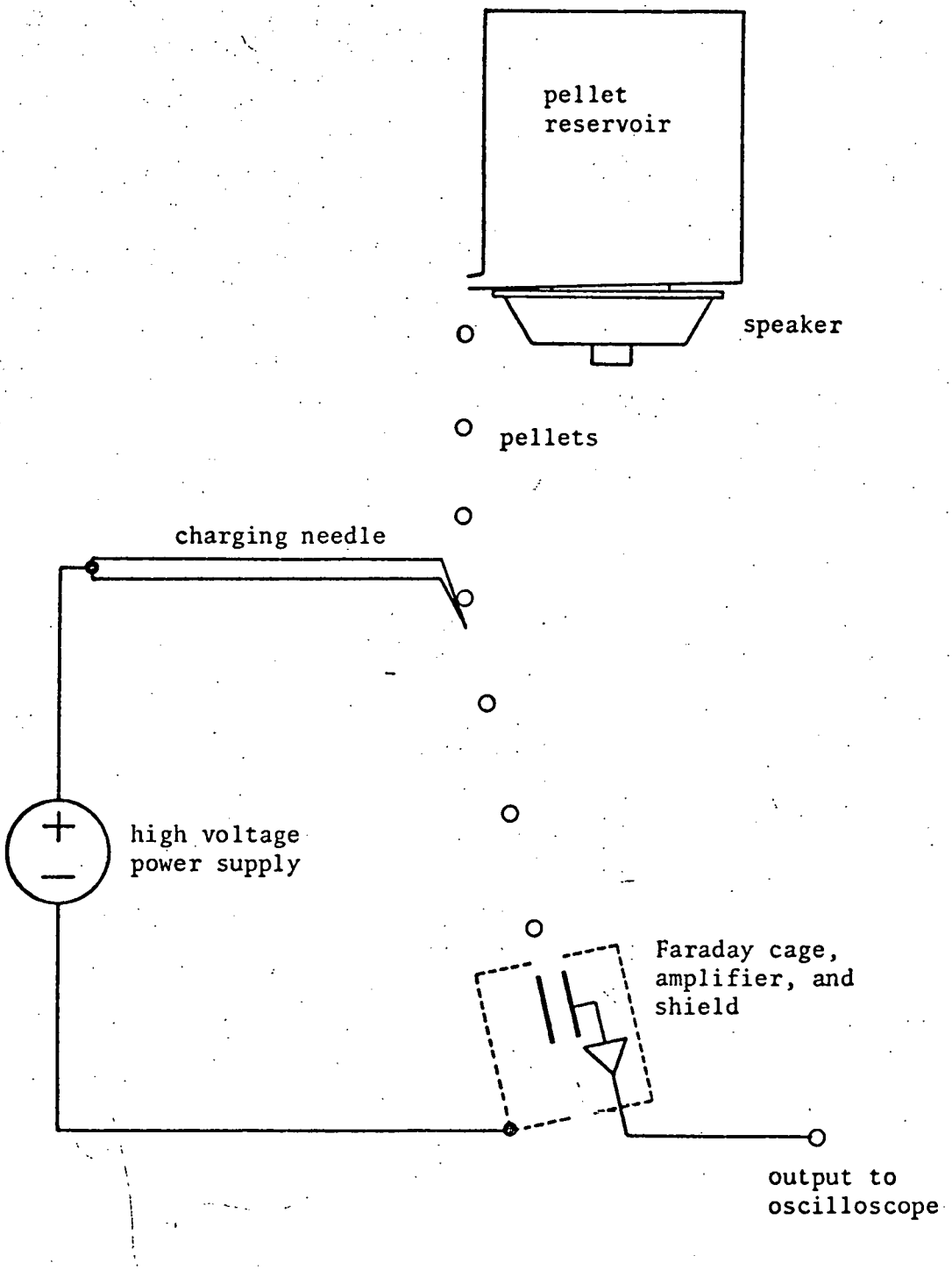

Figure 11: Alternate Arrangement for Pellet Deflection and Charge Measurement

charged much the same as before. Some difficulty was encountered with charge measurement since only a little deflection was required to allow a pellet to enter the Faraday cage, but few could pass through without striking the walls. The vast majority of the pellets made contact and transfered their charge, which leaked off slowly. Results from this test were substantially the same as previous results, such as those in Table 2, although similar data (for charge and radius) was difficult to collect because of the alignment problem. The number of pellets striking the cylinder could be decreased some by placing the cylinder directly under the tip, but the problem of false triggering by slightly charged pellets or by pellets striking the walls caused most of the "good" pulses to be obscured.

When judged by the relative uniformity of results operation at a high vacuum with a very sharp needle was considered as yielding adequate information about the charging process. In addition, experience with higher pressures and with blunter needles pointed up some of the limitations of a contact charging system.

7. Analysis of Data

Regardless of the geometric arrangement used, when pellets were successfully charged, the amount of charge varied

by no more than a factor of three between maximum and minimum. The electric field which produced the charge was uncertain by perhaps an order of magnitude, since it was impossible to have the pellets strike the tip in exactly the same place every time. Also, the field at the surface of the needle was not well known because the geometry made it difficult to calculate, and more importantly, surface irregularities could have tremendously enhanced the field around rough spots. Furthermore, the latter effect was something of a function of time, especially at higher pressures, since the needle was subject to bombardment by ions and to field desorption of material from the surface of the tip.

The data from one experiment was used, along with equations 7 and 8, to calculate the radius and charge for each charged pellet measured, as shown in Table 2. The experiment was operated at three different voltages, with a one micrometer radius tip, and a pressure of 10^{-6} torr. Less data was taken at higher voltages because of the increased possibility of damaging the needle. The mass of the pellets was calculated using 1.2 grams per cubic centimeter as the density of polystyrene.

The information in Table 2 shows no apparent relationship between the charging voltage and the resultant charge.

Figure 12 is a plot of charge versus radius, and there appears to be a trend towards higher charge for larger radii. The charge-to-mass ratio is plotted as a function of radius in Figure 13, and it shows a definite decrease for increasing radii. Although the relationship is not at all strong, the amount of charge on a pellet seems to be roughly proportional to the surface area (See Figure 14). The amount of deviation in the data certainly cautions against this conclusion, but in general it can be stated that the charge-to-mass ratio will go down for larger radii.

The data collected for 25 and 30 kilovolt positive potentials shows little difference from that at 20 kilovolts. It is known from the results with less sharp needles that the field needed to produce significant charging must be greater than approximately 10^9 volts per meter. These results indicate that once a threshold level of field strength is reached, the amount of charge for a given-sized pellet does not depend significantly on the field strength. This is undoubtedly related to the distances required for tunneling to occur.

As was suggested earlier, tunneling will probably be confined to the surface of the pellet very near the needle. The field inside the pellet will be strongly reduced by the

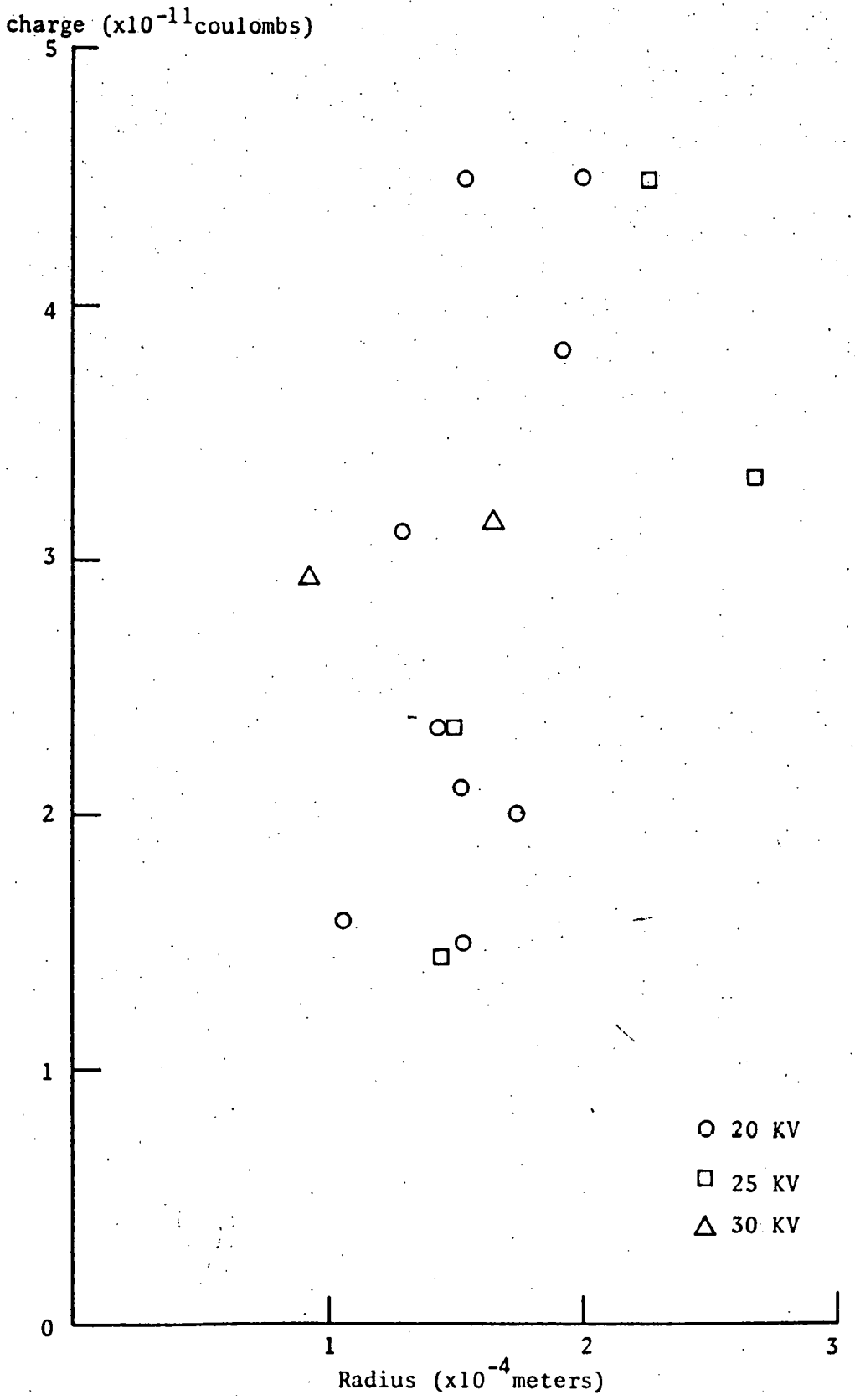

Figure 12: Charge Versus Radius

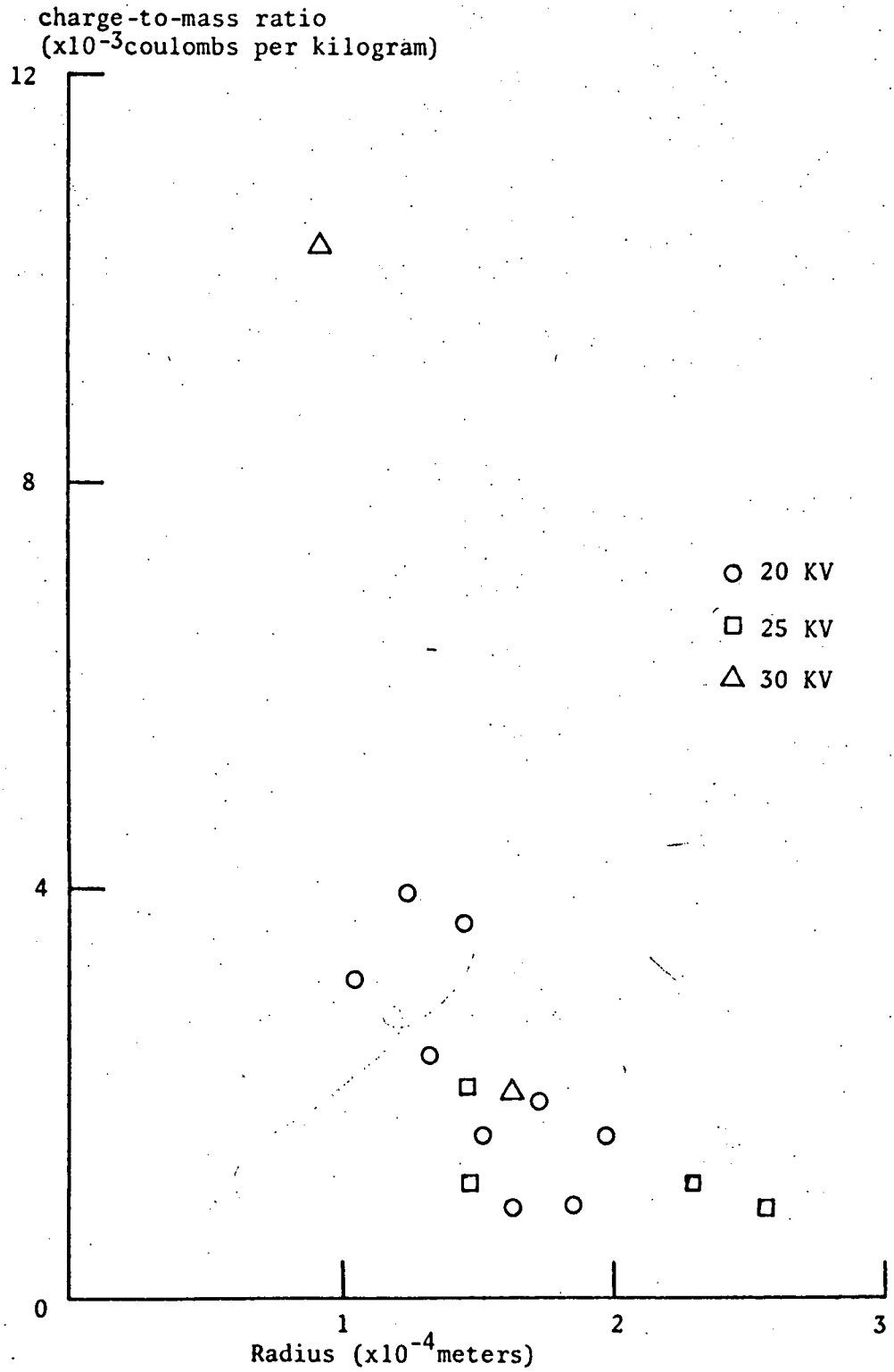

Figure 13: Charge-To-Mass Ratio Versus Radius

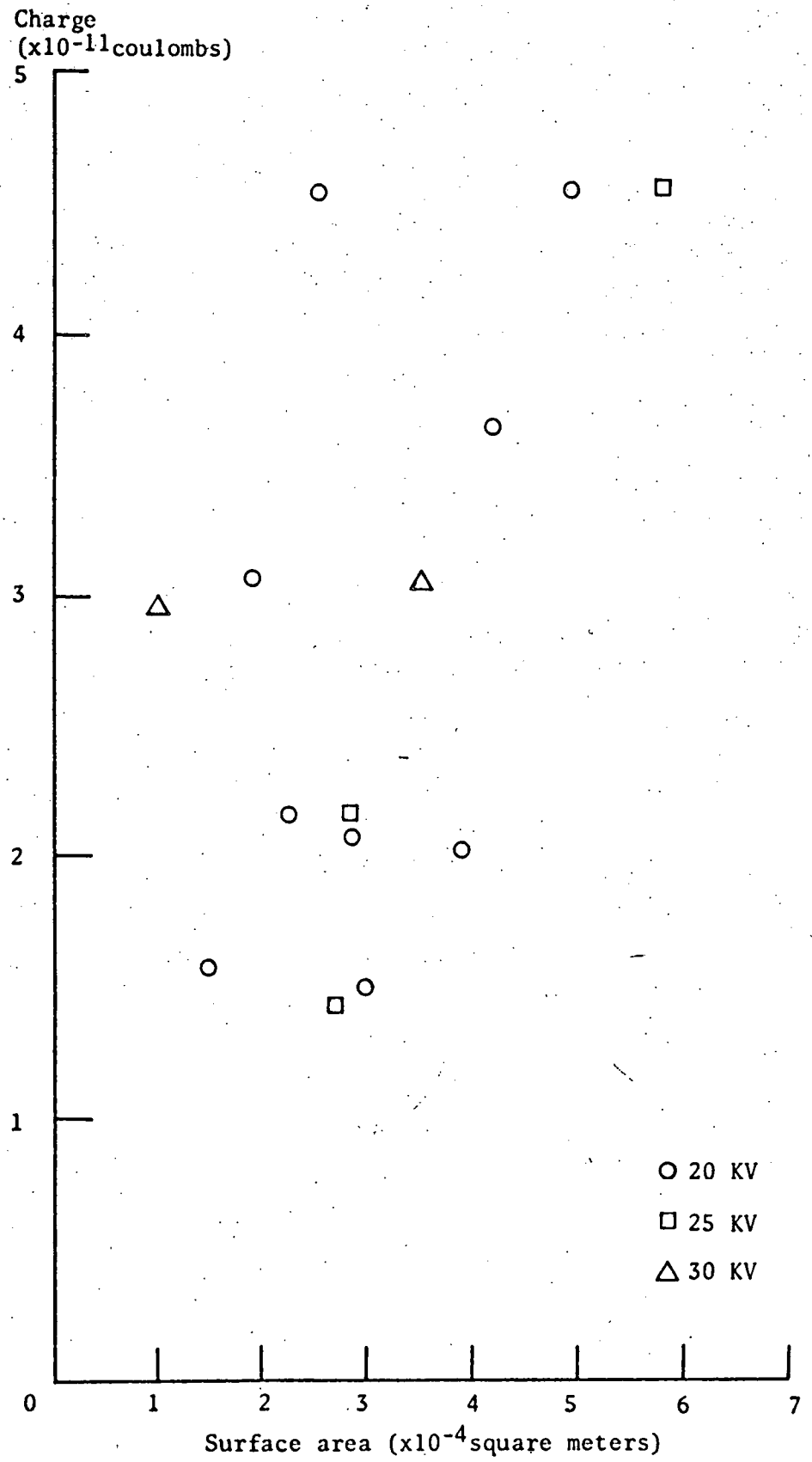

Figure 14: Charge Versus Surface Area

polarization field and the field produced by the transferred charge, and will not be sufficient for significant charging. Therefore, once the field is strong enough to cause tunneling at the point of contact, a stronger field will produce very little more charging in that area and could possibly heat and vaporize pellet material if breakdown occurs.

Breakdown is an electron avalanche effect which takes place when an atom is ionized and the resulting electron is given enough energy to ionize other atoms by collisions. Very quickly, the material's insulating properties are lost, large currents result, and a great deal of heating can occur. If breakdown occured during charging it could vaporize pellet material.

Another limitation to charging is also possible; that of electrostatic repulsion. It could be that, once the pellet has reached a certain amount of charge, it is repelled by the strong field at the needle's surface. It is not likely that this is a dominant factor, however, since more massive pellets would be repelled less easily, and therefore, should be more highly charged. The experimental results indicate little support for either case, as indicated in Figure 15.

One very important factor observed during the course of this experiment is the effect on the needle of the surrounding

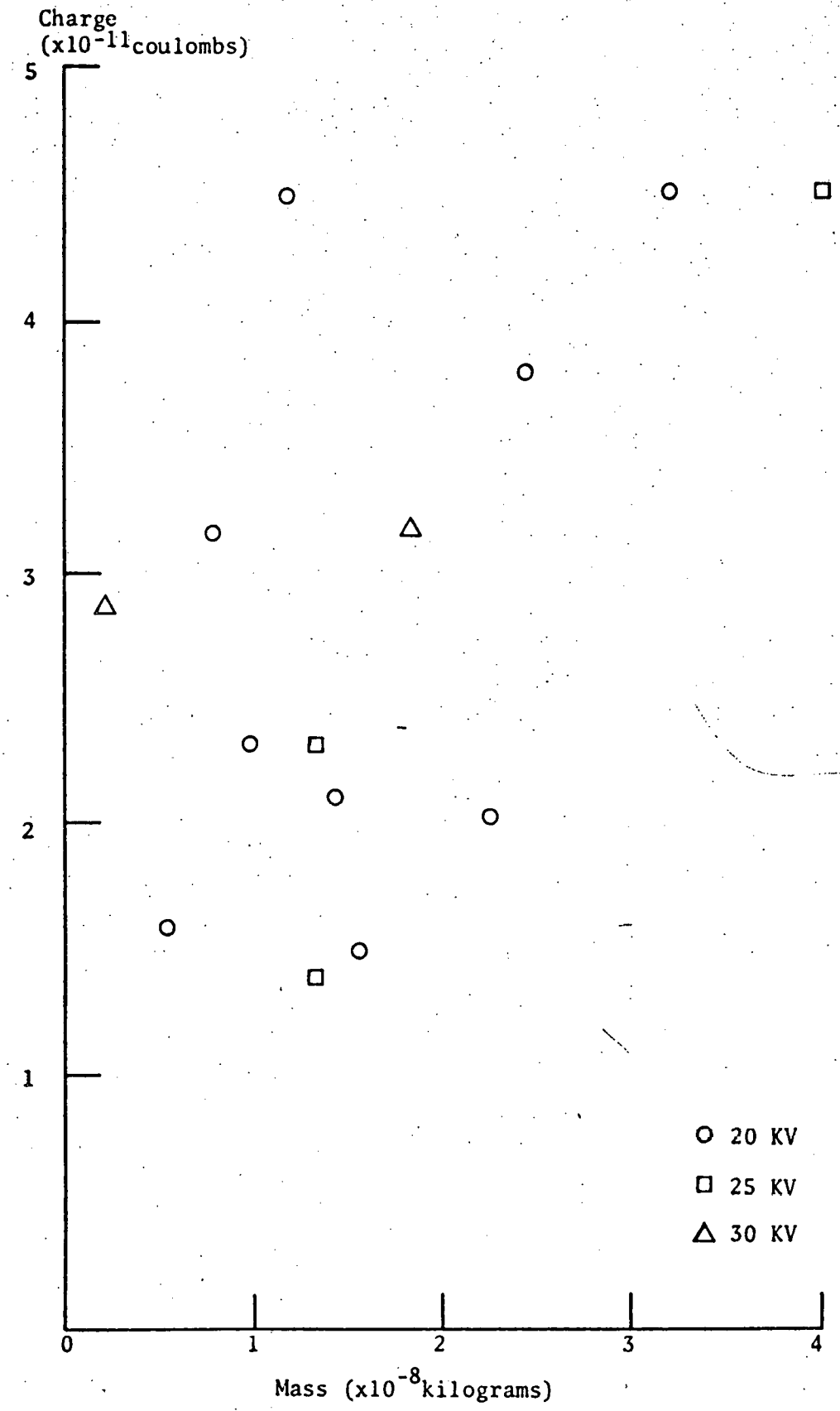

Figure 15: Charge Versus Mass

gas. While the system is operated at a pressure of 10^{-6} torr very little, if any, destruction of the tip is observed, but when the pressure is increased to 10^{-3} torr the needle is rapidly etched to a uselessly large diameter. Furthermore, at 10^{-3} torr ions streaming away from the needle completely deflect the pellets from the needle. Both effects indicate it is imperative that the pressure be kept as low as possible. Alternatively, these problems would be minimized by pulsing the high voltage on for only short intervals. The rate of polystyrene pellets striking the needle in this experiment is much too random to lend itself to this method, since the number of charged pellets would be drastically reduced along with the chance of measuring one with the drift-tube detector.

An additional difficulty must be surmounted in order to measure charged pellets at 10^{-3} torr pressure. Because the atmosphere is readily ionized, the high voltage power supply must produce very low ripple on its output. This ripple is transmitted by the ionized gas and produces a ripple on the output of the Faraday cage. The power supply used in this experiment is rated at 0.5% rms ripple per milliamp of output current. When the system is operated at 10^{-3} torr the current is generally about five milliamps. At this current, the

maximum output voltage attainable is ten kilovolts. This produces a maximum ripple of 250 volts rms. The signal impressed on the Faraday cage can reach ten volts and completely obscure any pulse induced by a pellet passing through the cylinder.

It is clear that the best results are obtained with the sharpest possible needle in the highest possible vacuum. Low vacuums (10^{-3} torr) lead to dull needles and charge measuring problems.

8. Conclusions

Within the limitations imposed by the materials and the nature of the experiment, contact charging has been shown to produce significant positive charge on small polystyrene spheres. The field strength at the charging needle's surface must be greater that 10^{9} volts per meter and optimum performance was achieved with tips of radii of about one micrometer raised to twenty kilovolts. For needles of practical sharpness, slight charging was observed with potentials below fifteen kilovolts, and little variation in the amount of charge was seen for potentials between twenty and thirty kilovolts. The onset of appreciable electron tunneling can be assumed to occur for the value of field strength cited above.

During the course of the experiment it was determined that operation at pressures near 10^{-3} torr were unsatisfactory for a variety of reasons; the principal ones being tip destruction by negative ion bombardment, premature pellet deflection due to positive ion accumulation on the pellets, and power supply interference with the Faraday cage charge measuring device. With the system working in a pressure of 10^{-6} torr these problems were avoided to a great degree.

The pellets used throughout the experiment were made of polystyrene with a density of 1.2 grams per cubic centimeter. The radii computed from the data ranged from 87 to 264 micrometers in radius with an average of 160. The computed charges ranged from 14 to 45 picocoulombs with an average of 29 picocoulombs. The best charge to mass ratio produced was 10.5×10^{-3} coulombs per kilogram, with an average value of 2.4×10^{-3}. While there was considerable spread in the data, the results were more consistent than might have been expected in view of the unknown nature of the electric field. on the needle's surface.

All charging was done with the tip at a positive potential, in order to prevent certain damage to the pellets from field desorption of material from their surfaces. For the same reason tungsten was choosen for the needle material

because of its very high resistance to field desorption. For good vacuums (10^{-6} torr) very little blunting of the needle was observed.

To predict the performance of the contact charging technique when used with materials other than that used here may be misleading, but it is probable that the results would be much the same, since it should be possible to produce a sufficiently intense electric field to initiate charging in a wide variety of materials. With improvement in high voltage insulation and better vacuums, charging potentials somewhat higher than those used here would be possible, resulting in higher fields and improved prospects for contact charging. Although most materials should be chargeable the amount of charge will be limited by the geometry of the pellet and needle, and by the requirements of field ionization between them.

V. A TECHNIQUE FOR PRODUCING UNIFORM CHARGED DROPS OF CRYOGENIC LIQUIDS

See the Appendix for a paper which has been written on this subject.

VI. AN APPARATUS FOR PRODUCING UNIFORM SOLID SPHERES OF HYDROGEN

See the Appendix for a paper which has been written on this subject.

VII. WORK CURRENTLY UNDER WAY

A. Extruder

A hydrogen extruder has been under construction and is nearing its completion. The principal features of the extruder being incorporated into its construction are as follows. Hydrogen gas is initially cooled down to liquid nitrogen temperature in the pre-cool heat exchanger which employs liquid nitrogen as the coolant. As a next step, the cold hydrogen gas is fed into the final heat exchanger, in which the liquid helium, used as the coolant, solidifies the hydrogen. Finally, the solid hydrogen is forced out of a small hole in the final heat exchanger into a vacuum chamber, of which an elaborate control on both the temperature and pressure is maintained so as to facilitate the extrusion process. The idea is to create a thermodynamic environment in which hydrogen is easily extrudable through a simple adjustment of the pressure of the feeding hydrogen gas.

When completed (which should happen in the near future), the extruder will be used to test the maximum charge that can be maintained on solid hydrogen. By placing in the hydrogen being extruded a tungsten needle which is raised to a high potential, we will be charging the hydrogen either positively (via field ionization) or negatively (via field emission) depending on the polarity of the needle. In either case, the limit on the charging of solid hydrogen will be investigated. The limits can occur due to one of two possible effects. One, the hydrogen may emit ions or electrons

when its surface charge becomes too large, or the solid hydrogen may shatter into small particles if its tensile strength is exceeded. The purpose of this experiment will be to determine which effect limits the charge on hydrogen and what the maximum charge is.

Since the extruded hydrogen pellets are already in solid form, one may, without worrying about destroying them due to possible shocks, try to accelerate the pellets gas-dynamically under different physical conditions such as varying acceleration nozzle dimensions, temperatures of the gas, etc. With the completed hydrogen extruder, we will investigate the maximum acceleration on a hydrogen pellet that can be achieved in practical sense.

B. Electron Beam Acceleration

If a frozen hydrogen pellet is placed in an electron beam, the results are similar to that obtained when a pellet is injected into a plasma. That is, the surface of the pellet is heated and the pellet begins to ablate away. However, in the electron beam the ablation will occur only on one side of the pellet. The result is that there is a net momentum transfer to the pellet, accelerating it.

To test this concept an electron beam is being constructed. Electrons are being accelerated out of a hollow cathode discharge. At the present time a pulsed beam of about 100 amp, 5 KeV and 1 cm diameter is being produced. Pellets from an existing pellet generator will be injected into this beam for the acceleration experiments.

C. Plasma Gun Accelerator

Plasma accelerators have been used to accelerate particles for micometeorite simulation[10]. These experiments have been done using pellets with much higher evaporation temperatures than hydrogen. The pellets were also attached to a membrane which was ruptured by the discharge. The pellets could be accelerated to a velocity of greater than 10^6 cm/sec. We are designing experiments to see if hydrogen pellets can be accelerated using this technique without using the membrane which is inappropriate for the repetition rates needed for refueling fusion reactors. The plasma gun is essentially used to create a high velocity gas flow which in turn accelerates the pellet.

We have constructed a power supply system consisting of about 50 μf of 20 kV capacitors and a trigger circuit using a spark gap. The system is ready to produce a discharge. It is planned to try the system first with plastic pellets and then with hydrogen pellets.

VIII. EVALUATION OF ELECTROSTATIC ACCELERATION

In order to evaluate electrostatic acceleration, two quantities must be known: the maximum charge which can be placed on a pellet and the accelerating voltage. As an accelerating voltage, we will assume that 10^7 volts is available from, for example, a tandem van de Graff machine. With this assumption Table 7.1 gives the charge necessary to

accelerate two different sized pellets to various velocities. These charges would be reduced if some kind of linear accelerator could be built to accelerate the pellet to higher velocities.

As indicated in the section on contact charging, it was possible to charge plastic pellets of about 100 μm radius to about 10^{-11} Coulomb. If a hydrogen pellet could be charged to the same extent, it could be accelerated to about 10^5 cm/sec by a 10 MV accelerator. The limit to the total charge which can be placed on a hydrogen pellet appears to be the tensile strength of solid hydrogen. Stetsenko et al.[11] measured the tensile strength of solid hydrogen and found it peaked at about 2-4° K at a value of about 50 g/mm^2. If we set this equal to the electric stresses, we get an electric field of 3.4×10^8 V/m. Assuming this value of surface field, we get the results in Table 7.2.

In summary, electrostatic acceleration has the possibility of accelerating hydrogen pellets smaller than 100 μm to velocities greater than a rotating arm. If larger sized pellets are needed, the velocities are reduced by the square root of the radius. One possible scheme would be to use charged pellets together with an electron or ion beam. The charge would prevent the beam electrons or ions from depositing their energy into the pellet as heat. All the energy lost by the beam would go into the kinetic energy of the pellet.

REFERENCES

1. H. Shelton, C. D. Hendricks, Jr., and R. F. Wurcker, J. Appl. Phys., 31, 7 (1960).

2. A. Y. H. Cho, J. Appl. Phys., 35, 9 (1964).

3. K. Kim and R. J. Turnbull, J. Appl. Phys., 47, 1964 (1976).

4. J. P. Woosely, M. S. Thesis, University of Illinois (1976).

5. C. D. Hendricks, Jr., J. Colloid Sci., 17, 3 (1962).

6. Lord Tayleigh, Phil. Magazine, 14, 184 (1882).

7. R. Gomer, Field Emission and Field Ionization, Harvard Univ. Press, Massachusetts (1961).

8. E. W. Muller, Phys. Rev., 102, 3 (1956).

9. Holt, Foundations of Plasma Dynamics, Macmillan, New York (1965).

10. E. B. Igenbergs, E. L. Shriver, and D. W. Jex, Acta Astronautica, 1, 1337 (1974).

11. Yu. E. Stetsenko, D. N. Bolshutkin, and L. A. Indam, Sov. Phys. Solid State, 12, 2958 (1971).

SPHERICAL SOLID HYDROGEN PELLET INJECTION EXPERIMENTS ON ORMAK

K. Kim, R. J. Turnbull
Department of Electrical Engineering
University of Illinois
Urbana, Illinois 61801

R. J. Colchin, C. A. Foster, S. Milora
Oak Ridge National Laboratory, Oak Ridge, Tennessee
United States of America

December 3, 1976

Abstract

In order to test the feasibility of refueling fusion reactors, solid hydrogen spheres, both of 70 μm diameter at a speed of 93 m/sec and of 210 μm diameter at 100 m/sec, have been injected into the ORMAK Tokamak. The injection was in the tangential direction, and each of the 210 μm pellets, for example, represented an approximate ½% increase in the ORMAK plasma density. Light bursts from the pellet-plasma interaction were monitored by a phototube and by a fast movie camera. The principal experimental results are the lifetimes and ablation rates of the injected pellets, and the time-dependent spatial distribution of the neutral ablation cloud. The measured lifetimes are 380 μsec for the 70 μm pellets and 850 μsec for the 210 μm pellets, which represent, respectively, a radial penetration into the plasma of 2.5 cm and 6 cm. The data on the lifetime and ablation rate have been compared with a relevant theoretical model[1] with good agreement.

1. INTRODUCTION

Conceptual designs of future fusion power reactors based on Tokamak concept will require a long sustained burn cycle time.[2] The plasma in the Tokamak is initially created by breaking down a gas pre-fill. It is then heated by a combination of ohmic heating from the induced current in the plasma and high energy neutral-beam injection to finally reach the ignition temperature for fusion reaction.[3] Once the ignition conditions are met, the energetic alpha particles released from the deuterium-tritium fusion reaction can balance out the energy loss which occurs from the plasma to the reactor walls via particle diffusion. The end result is a self-sustaining fusion reaction which will then last for the remainder of the burn cycle. The particle confinement time, however, is only a small fraction of the burn time,[2] and as a result of this the plasma would very rapidly become depleted of the fuel ions, resulting in the cessation of the self-sustained fusion reaction long before the end of the burn cycle. In order to overcome this drawback one must, therefore, replenish the lost fuel ions with fresh ones by injecting fuel particles into the Tokamak plasma during the burn cycle of the reactor operation. Since a long sustained burn cycle is essential for a favorable (economical) power balance in the Tokamak type fusion systems, the task of refueling becomes of utmost importance in realizing a successful fusion power reactor of the Tokamak type.

As for the actual methods of refueling, there have been proposed in the past a few different fuel injection schemes.[4] One such method is to inject fuel into the outer edge of the plasma and rely on its inward diffusion to the central plasma core where the burn is occurring. This method, however, may result in an inversion of the desired density profile of the

plasma. Noting that the burn takes place in the central portion of the plasma where the density and temperature are the highest, this particular fueling scheme must therefore be considered inadequate. In general, one requires that an adequate fueling method be such that the fuel is injected deeply into the burning core of the plasma. Closely related to this requirement are the difficulties involved in injecting the fuel particles deeply into the reactor core which arise due to the magnetic field which confines the plasma, the large size of the plasma, the intense electron and ion fluxes, and the energy balance requirements which are inherent in a power producing reactor. High energy neutral-beam injection, for example, is not considered to be a viable refueling scheme from energetics point of view because it does not meet the kind of power economy requirements which are necessary for a practical fueling device.

Injection of macroscopic pellets composed of fuel elements, on the other hand, seems to offer the chance to meet all these refueling requirements, thus rendering itself the right to be the most promising refueling scheme proposed thus far.[5] Most of the future Tokamak power reactors have incorporated this refueling scheme into their conceptual designs.[2]

Investigation on how far a pellet will penetrate into the plasma through the intense electron and ion fluxes comprises a very complicated theoretical problem because any successful solution to the problem will require a thorough understanding of the complex ablation dynamics which the injected fuel pellet must undergo as it traverses the plasma.

A theoretical investigation on the pellet ablation in the plasma was initiated by Spitzer et al. in 1954.[6] Since then, the investigation has been reconsidered by Rose in 1968,[7] Gralnick in 1973,[8] and more recently by Parks et al.[1]

Experimentally, the only work which has any remote bearing on this

investigation has been that of Jørgensen et al.[9] In their experiment, they fired a rotating plasma device which had the ion and electron energies, respectively, of 500 eV and 10 eV around an extruded 250 μm diameter hydrogen cylinder. After the plasma discharge which lasted 5 μsec, the remains of the pellet were trapped and measured. Photographs of the pellet ablation cloud were obtained during the plasma discharge. Their conclusion was that the energy carried away per ablating hydrogen atom is 0.05 eV as opposed to the sublimation energy of 0.005 eV/atom. These results, however, are not directly applicable to the presently considered problem of pellet ablation because it is the effects of the ion energy flux on the pellet that they were measuring, not of the electron flux which is in fact responsible for the ablation of the pellet in the Tokamak plasma.

In this paper we describe an experiment which represents the first pellet injection experiment performed on a Tokamak. Solid hydrogen spheres both of 70 μm diameter at the speed of 93 m/sec and of 210 μm diameter at 100 m/sec were injected into the ORMAK plasma during the steady state portion of the plasma discharge.

Two of the prime motivations of this experiment are as follows: first, we are interested in establishing some sort of scaling law for the lifetime of an injected fuel pellet as a function of the size and speed of the pellet as well as the temperature and density of the plasma into which the fuel pellet is injected. This information is a must in making a realistic assessment on the feasibility as well as the requirements of the pellet injection refueling scheme. Secondly, by injecting pellets of known size and speed into a plasma and by observing them as they interact with the plasma, one might be able to determine such important parameters as the density and temperature of the given plasma. We are interested in

investigating this possibility.

In Section 2 we present a brief description of the experiment along with the equipment and diagnostic tools that we employed for specific measurements. The results of the experiment are then discussed in Section 3 and compared with a relevant theoretical model[1] in Section 4. The final section is for the concluding remarks and suggestions for future experiments.

2. DESCRIPTION OF THE EXPERIMENT

A schematic diagram of the experimental set-up which was employed for the present pellet injection experiment is shown in Fig. 1. Solid hydrogen pellets of a predetermined size were produced by the pellet generating apparatus.[10] A desired number of pellets were then selected out, and accelerated via gas dynamic drag to a speed of the order of 100 m/sec. The pellet generator was connected to the ORMAK via an injection tube which was attached to a port normally used for neutral beam injection experiments. The ORMAK is a Tokamak device with a minor radius of 25 cm, central plasma density of the order of 3×10^{13} cm^{-3}, central electron temperature of 1 KeV, and central ion temperature of 200 eV without neutral-beam injection heating. No neutral beam heating was done during the pellet injection experiments. Details on the ORMAK machine can be found elsewhere.[11] The opening of a miniature solenoid-operated gate valve which is part of the injection tube was timed relative to the ORMAK plasma discharge so that the pellets would arrive at the plasma during the quasi-steady-state portion of the discharge. The pellets were injected tangentially to the plasma. On the way to the plasma the pellets passed through a hole in the center of an observation mirror. The mirror was used to reflect the light resulting from the pellet-plasma interaction to a separate port on the side of the injection tube. The light output resulted from the interaction of the plasma with the neutrals ablated off the pellet. This light output was monitored using either a photomultiplier tube or a high speed movie camera, and was used to determine the lifetime as well as the ablation rate of the injected pellet in the plasma. The phototube was used in conjunction with an interference filter which passed the H_α hydrogen line at 6563 Å. The camera (Wollensak WF2

FASTAX II) was fitted with a telephoto lens and was capable of taking 16000 frames/sec. The size of the pellets was measured optically and their speed was determined by measuring the time delay between the opening of the shutter and the beginning of the light pulse from the pellet-plasma interaction. The shutter-to-plasma distance was measured to be about 2.93 m. In addition, the usual diagnostic tools such as the microwave interferometer, the double Langmuir probe, and the laser-Thompson scattering diagnostics were used to determine the plasma conditions as well as to monitor possible changes in the plasma density and temperature during the arrival of the pellets.

3. PRESENTATION OF DATA

A typical pellet injection H_α signal monitored by the photomultiplier tube is shown at the top in Fig. 2, along with a delayed signal on an expanded time scale at the bottom. The two signals in the middle represent, respectively, the line-averaged central and mid-point electron densities of the ORMAK plasma. Except on the expanded trace at the bottom of Fig. 2 where the horizontal axis has a time unit of 1 msec, all the time scales are in 10 msec. Concentrating on the full H_α signal at the top, we see a large H_α light output during the first few milliseconds of the ORMAK discharge, which results from the initial breakdown of the hydrogen gas pre-fill. The steady-state portion of the trace which immediately follows this is a result of the H_α output from the plasma particles refluxing off the liner of the torus and re-entering the plasma. The injection of hydrogen pellets into the ORMAK plasma triggers a sharp increase in H_α output, and appears as a series of sharp peaks on the trace about 40 msec after the ORMAK discharge. The small peaks of random size are caused by fragments of the full-sized hydrogen pellets, whereas the large peaks of constant height and breadth, which appear on the trace repeatedly and consistently, result from the whole 210 μm diameter hydrogen pellets.

The time coordinates of these sharp peaks allow us to measure the speed of the pellets. A detailed information on the lifetime as well as on the ablation rate of the injected pellets in the plasma may be obtained from the expanded H_α trace at the bottom of Fig. 2. Summarized in Tables I and II are the data on the lifetime from a number of injection runs along with a set of relevant plasma parameters for each shot. Table I contains the data obtained with the pellets of 70 μm diameter and Table II with the pellets of 210 μm diameter.

It is seen from the tables that the average lifetime of a 70 μm diameter hydrogen pellet traveling at about 93 m/sec in the plasma is approximately 380 μsec, whereas the lifetime of a 210 μm diameter pellet at the speed of 100 m/sec is approximately 850 μsec. In terms of the radial penetration into the plasma, these lifetimes represent, respectively, a penetration depth of 2.5 cm and 6 cm.

By overlapping on the same figure the data points on the ablation rate collected from different injection runs, one may deduce the characteristic behavior of the ablation rate as a function of time of a solid hydrogen pellet injected into the plasma. Figure 3 contains such information for a 210 μm diameter solid hydrogen pellet injected at a speed of 100 m/sec. As is represented by the solid line in Fig. 3, the ablation rate starts off slowly, then increases quickly to reach its maximum, and finally drops off almost suddenly to zero due to the fact that there is no more solid hydrogen pellet left to be ablated. Once again, the average lifetime is seen to be about 850 μsec.

The spatial extent of the neutral ablation cloud (as monitored by the light output resulting from the pellet-plasma interaction) as well as its evolution in time are made more visual by the movie pictures taken with the fast movie camera described in the foregoing. Figure 4 is one such picture. No filters were used in taking this picture, although the film is only sensitive to visible light. The six bright spots appearing consecutively in six frames as a whole show the life of a 210 μm diameter hydrogen pellet being ablated in the ORMAK plasma. It is clearly seen in this picture that the spatial extent of the neutral ablation cloud increases very rapidly with time until it dies out at the end because of no more available ablation source. This particular aspect of pellet ablation seems to represent the actual ablation dynamics as is confirmed by the H_α

trace shown, for example, by the bottom picture of Fig. 2. Each picture frame in Fig. 4 represents approximately 140 μsec in time as may be determined from a curve provided with the fast movie camera manual, thus giving rise to 840 μsec for the lifetime of the 210 μm diameter pellet.

Because of the current which exists in the plasma, a solid hydrogen pellet injected into the plasma would have to be exposed constantly to a higher electron flux on one side. This means that there would be more ablation of hydrogen from one side, and therefore, that the injected pellet would, instead of following a straight trajectory, be pushed radially outwards as the pellet traverses inside the plasma. It is interesting that the vestige of this happening is seen in Fig. 4.

The pellet speed can also be determined from the movie picture by measuring the physical distance on the film from the beginning of the ORMAK discharge to the set of bright spots, and then by converting the distance into real time to find the time delay between the pellet leaving the injection shutter and arriving at the plasma. The shots 10,240A and 10,242A in Table I and the shot 15,036 in Table II constain such data.

By doing a detailed micro-densitometer reading of Fig. 4, one may also extract quantitative information on the time evolution of the spatial extent of the neutral ablation cloud. The result shown in Fig. 5 is derived from this analysis. Note from Fig. 5 that at its maximum the size of the neutral ablation cloud is about one hundred times as large as the size of the pellet being ablated.

4. COMPARISON WITH THEORY

Among the experimental results which were presented in Section 3, the data on the lifetime and ablation rate are specifically subject to direct comparison with approximate theoretical values. The theory to be employed for this comparison is the one on an ablating solid hydrogen pellet in a plasma developed recently by Parks et al.[1] The essential features of this theoretical model are as follows: neutral molecules evaporate from the pellet as a result of its elevated surface temperature to instantly form a quasi-steady neutral ablation cloud around the pellet. The incident electron energy flux is then shielded by this ablation cloud, with most of the flux going into the neutral ablation cloud accelerating, heating, and ionizing it. As a result, only a small fraction of the incident electron energy flux reaches the surface of the pellet, raising its surface temperature to a point where the energy flux at the pellet surface is in balance with the energy lost through vaporization. The vaporization rate, in turn, determines the total integrated neutral gas cloud density.

One of the principal results derived from the model is that the pellet lifetime, τ_p, varies as: $\tau_p \sim T_e^{-1.71} n_e^{-1/3} r_{po}^{5/3}$, where T_e, n_e and r_{po} are, respectively, the temperature, density of the plasma, and the initial pellet radius.

In the detailed analysis of the pellet ablation dynamics, the temperature and density profiles of the transonic gas flow are further approximated by assuming that the Mach number of the flow is equal to its asymptotic value, 1.89, everywhere in the cloud.[12] This guarantees that the momentum in the gas flow is conserved in the asymptotic sense. One of the results derived from this approximate analysis, that can be tested directly against the present experiment, is that of the ablation rate of a hydrogen pellet in a plasma.

In what follows we make a brief comparison of these theoretical predictions, both on the ablation rate and on the lifetime, with the present experimental results.

To begin with, we note that both the steady-state electron temperature and density profiles of the ORMAK plasma are represented, respectively, by a smooth parabola with its maximum at the center. This enables us to approximate each of the actual temperature and density profiles near the edge of the ORMAK plasma by a straight line. The equation of this straight line is then determined by measuring the actual values of either the temperature or the density at a few pre-designated points in the ORMAK plasma. In this way the electron temperature and density at the final point of penetration of an injected hydrogen pellet are found, for example, for the case of a 210 μm diameter pellet injected at a speed of 100 m/sec to be about 75 eV and $3 \times 10^{12}/cm^3$.

The theoretical values of both the ablation rate and the lifetime have been calculated based on these profiles of the electron temperature and density for the ORMAK plasma.

In Fig. 6 is presented a comprehensive comparison between the experimental and theoretical values of the ablation rate. The results are for the 210 μm hydrogen pellets injected into the ORMAK plasma at a speed of 100 m/sec. The solid line is the theoretical predictions and the circles are the experimental data collected from a number of different injection runs. It is clear from this figure that there exists an excellent agreement between the theory and the experiment.

Using the same profiles for the ORMAK plasma, the lifetime of a 210 μm solid hydrogen pellet injected into the ORMAK at 100 m/sec can also be calculated from the theory. The resulting lifetime is 854 μsec and is

again in excellent agreement with the experimental value, which is 850 μsec.

We therefore conclude safely that at least at such electron temperatures and densities as those encountered by the injected hydrogen pellets during the current experiment, the theoretical model of Parks et al.[1,12] accurately accounts for the actual ablation dynamics of a hydrogen pellet in a plasma.

5. CONCLUSIONS

In this report, we have described an experiment in which solid hydrogen spheres were injected into the ORMAK Tokamak to investigate the feasibility of refueling fusion reactors. Solid hydrogen spheres, both of 70 μm diameter at a speed of 93 m/sec and of 210 μm diameter at 100 m/sec, were injected into the ORMAK plasma in the tangential direction, and were observed to last, respectively, for 380 μsec and 850 μsec. In terms of a radial penetration into the plasma, these lifetimes of the pellets represented, respectively, a penetration depth of 2.5 cm and 6 cm. The ablation rates of the injected pellets in the plasma were also measured along with the time-dependent spatial distribution of the neutral ablation cloud.

The data on the lifetimes and ablation rates were compared to a recent theoretical model of Parks et al.[1] with excellent agreements. This has led us to believe that the theory of Parks et al. accounts for the actual ablation dynamics which the injected hydrogen pellets underwent as they traversed the ORMAK plasma, at least, to the points of their penetration where the electron temperature and density of the ORMAK plasma were, respectively, about 75 eV and $3 \times 10^{12}/cm^2$ in the case of 210 μm pellets, and far less in the case of 70 μm pellets.

REFERENCES

1. PARKS, P. B., TURNBULL, R. J., FOSTER, C. A. (To be published).
2. DAVIS, J. W., KULCINSKI, G. L., Nucl. Fusion 16 (1976) 355.
3. FURTH, H. P., Nucl. Fusion 15 (1975) 487.
4. MILLS, R. G., Editor, Princeton Plasma Physics Lab. Report MATT-1050 (1974).
5. TURNBULL, R. J., Trans. Am. Nucl. Soc. 23 (1976) 38.
6. SPITZER, L., GROVE, D. J., JOHNSON, W. E., TONKS, L., WESTENDROP, W. F., Report NYO-6047, USAEC (1954).
7. ROSE, D. J., Culham Laboratory Technology Division Memorandum No. 82 (1968).
8. GRALNICK, S. L., Nucl. Fusion 13 (1973) 703.
9. JØRGENSEN, L. W., SILLESEN, A. H., ØSTER, F., Plasma Physics 17 (1975) 453.
10. FOSTER, C. A., KIM, K., TURNBULL, R. J., HENDRICKS, C. D. (To be published in the Review of Scientific Instruments).
11. BERRY, L. ET AL., Proc. 5th Intl. Conf., Tokyo, IAEA, 1 (1975) 101.
12. MILORA, S., ORNL-TM-5776 (In preparation).

LIST OF FIGURES

LIST OF TABLES

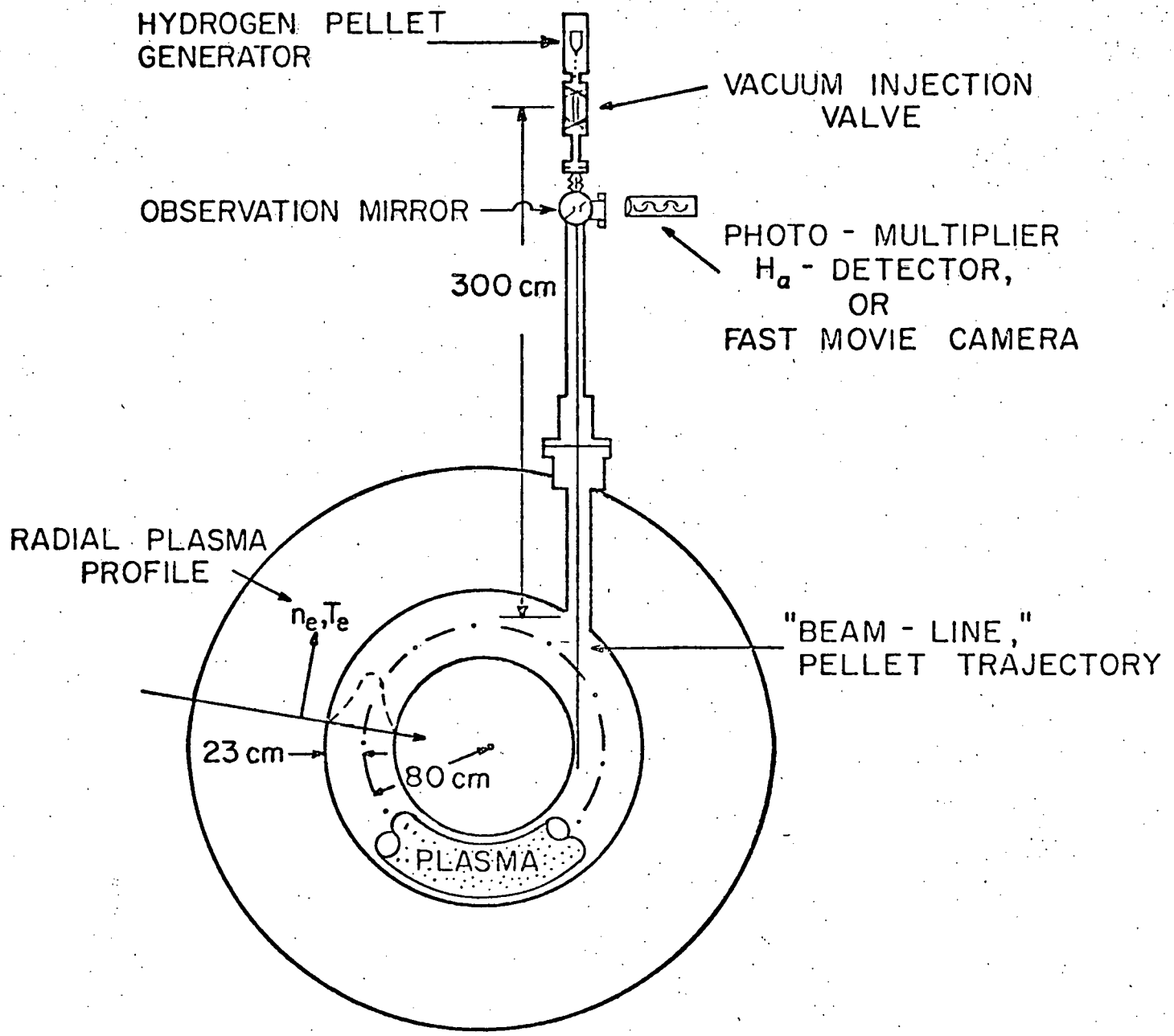
HYDROGEN PELLET GENERATOR
VACUUM INJECTION VALVE
OBSERVATION MIRROR
PHOTO - MULTIPLIER
H_α - DETECTOR,
OR
FAST MOVIE CAMERA
300 cm
RADIAL PLASMA PROFILE
n_e, T_e
"BEAM - LINE,"
PELLET TRAJECTORY
23 cm
80 cm
PLASMA

Figure 1

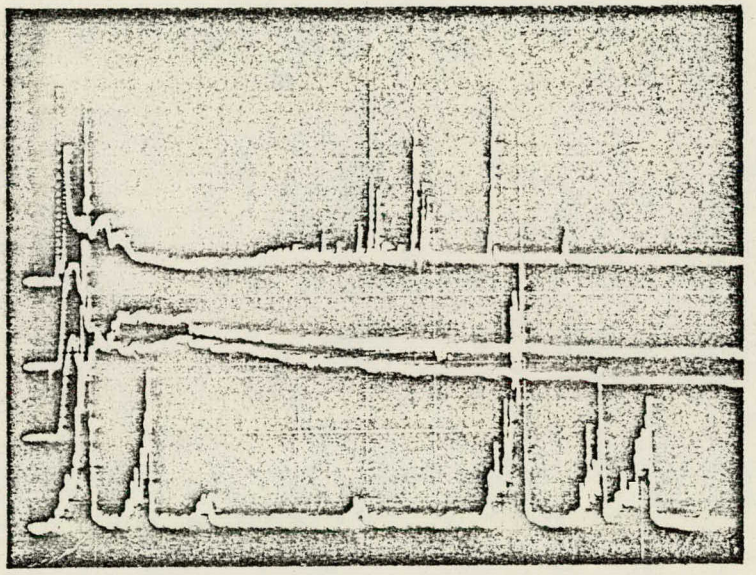

Figure 2

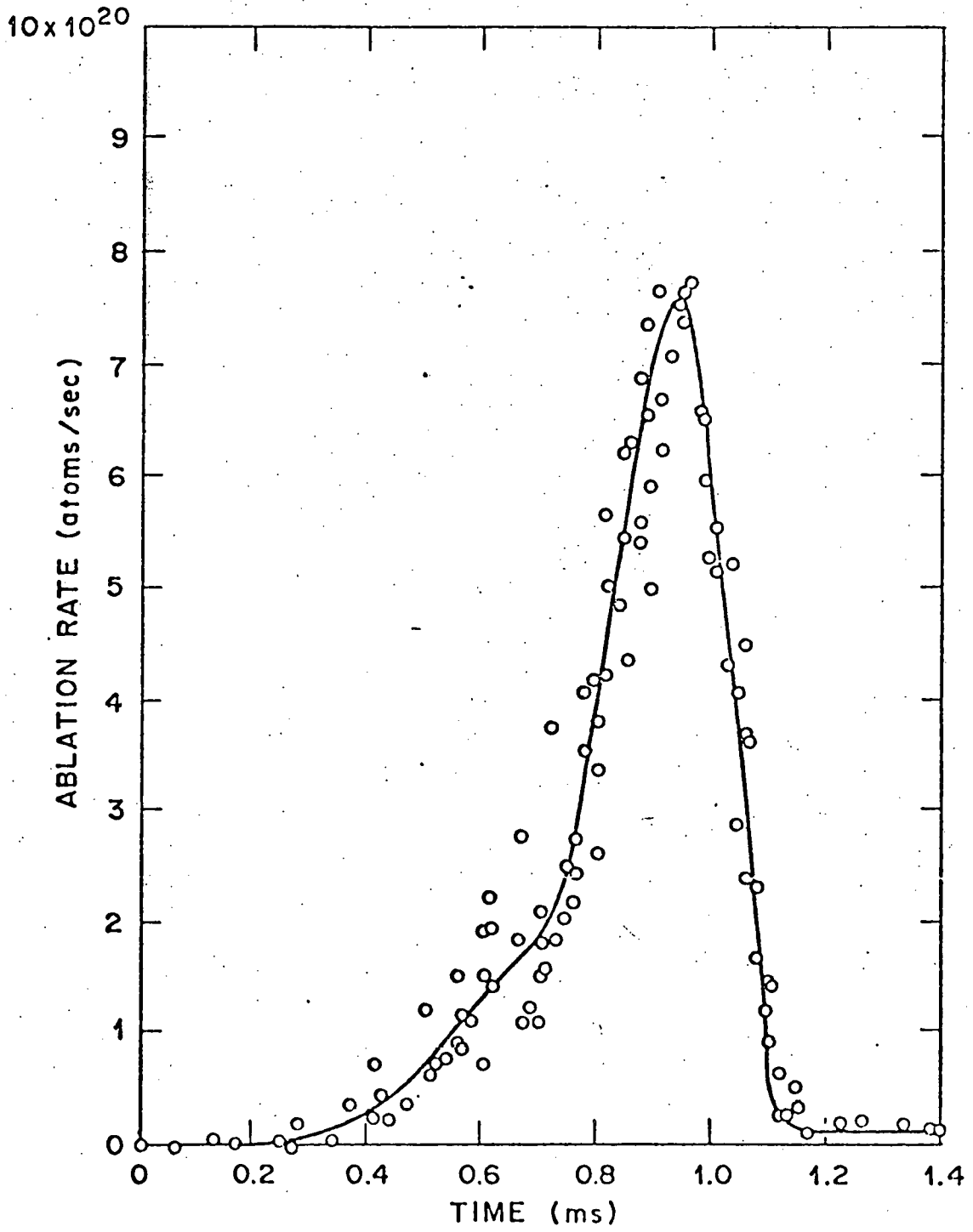
10 x 10^20
9
8
7
6
5
4
3
2
1
0
ABLATION RATE (atoms/sec)
0
0.2
0.4
0.6
0.8
1.0
1.2
1.4
TIME (ms)

Figure 3

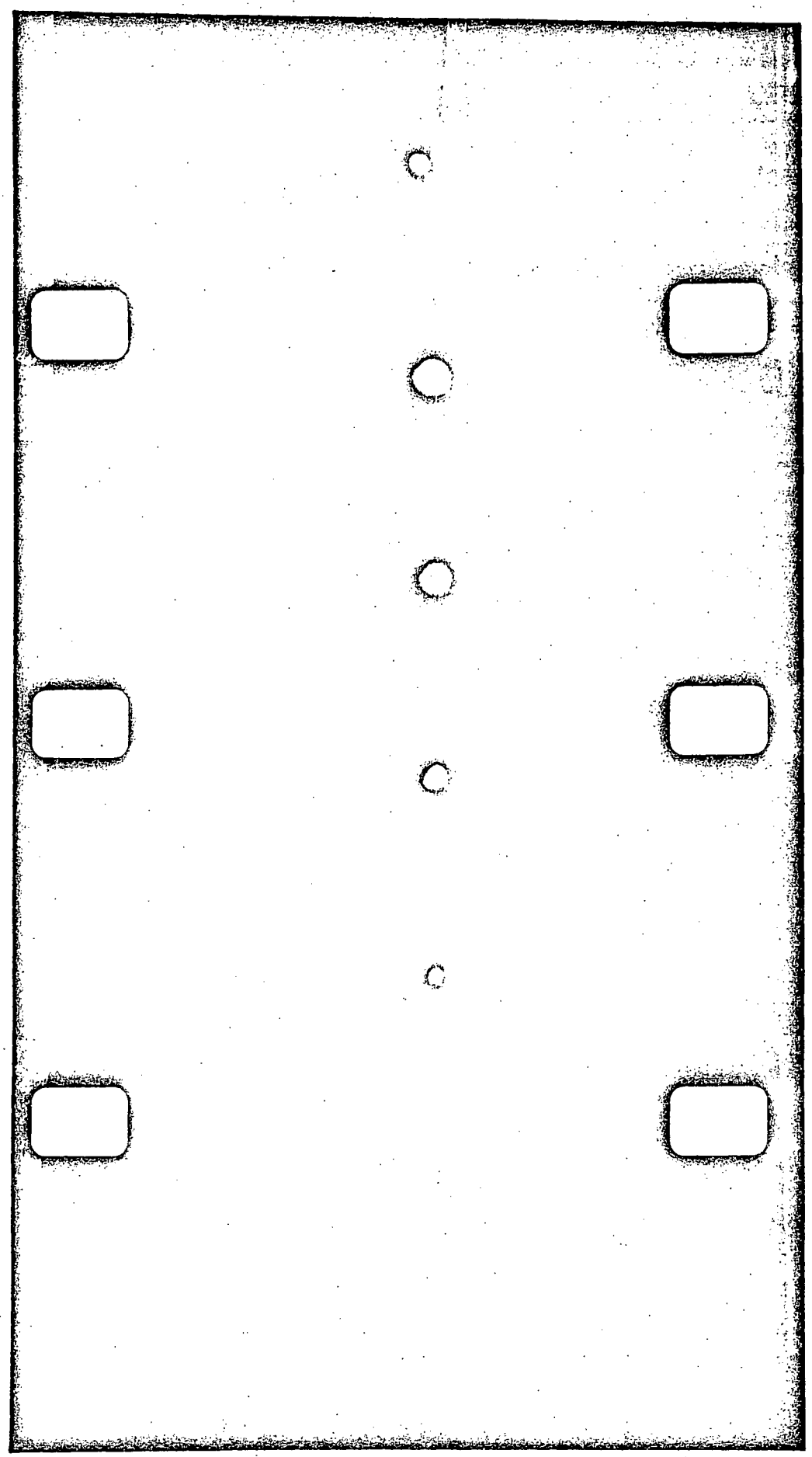

Figure 4

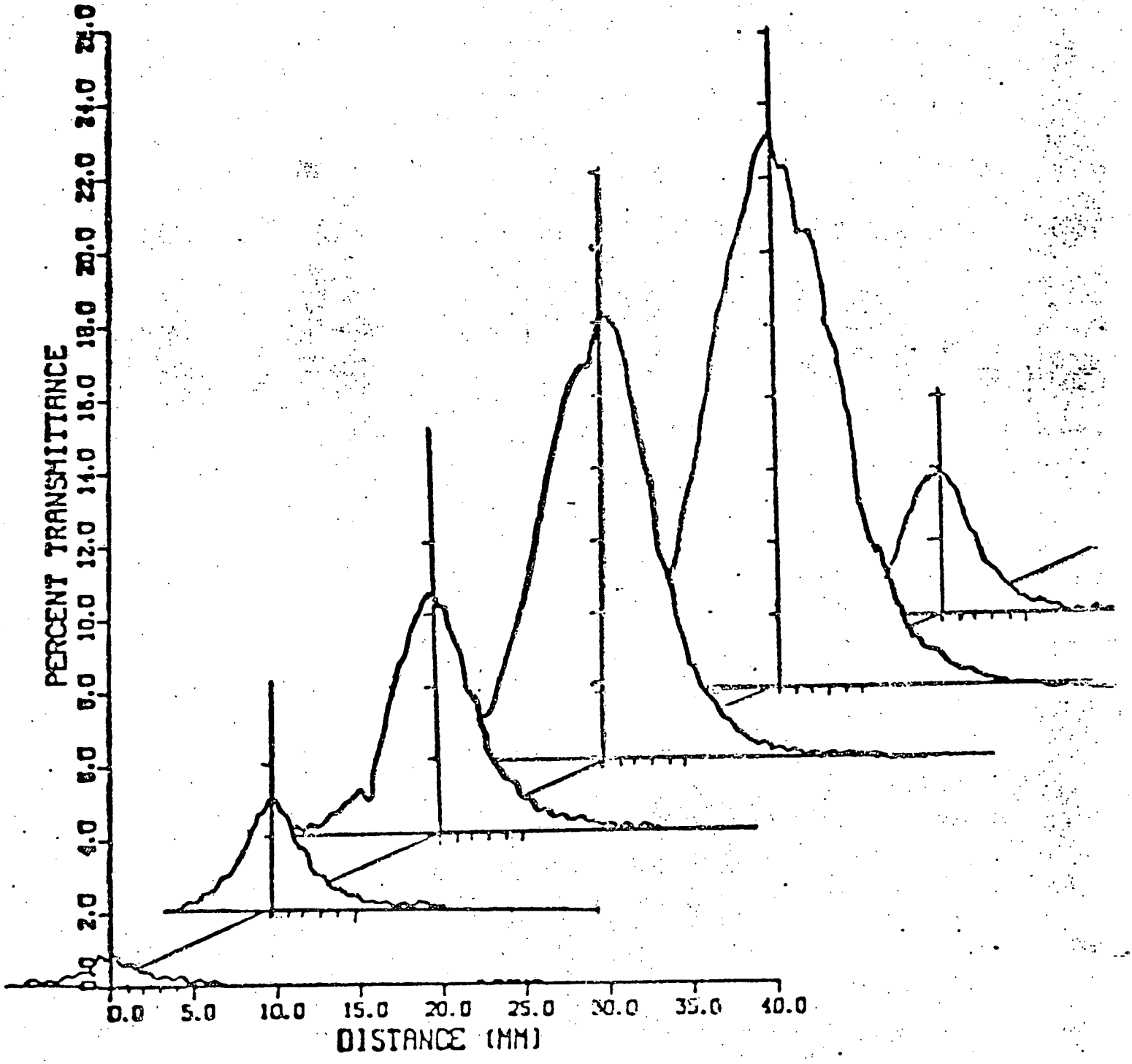
PERCENT TRANSMITTANCE
0.0
2.0
4.0
6.0
8.0
10.0
12.0
14.0
16.0
18.0
20.0
22.0
24.0
0.0
5.0
10.0
15.0
20.0
25.0
30.0
35.0
40.0
DISTANCE (MM)

Figure 5

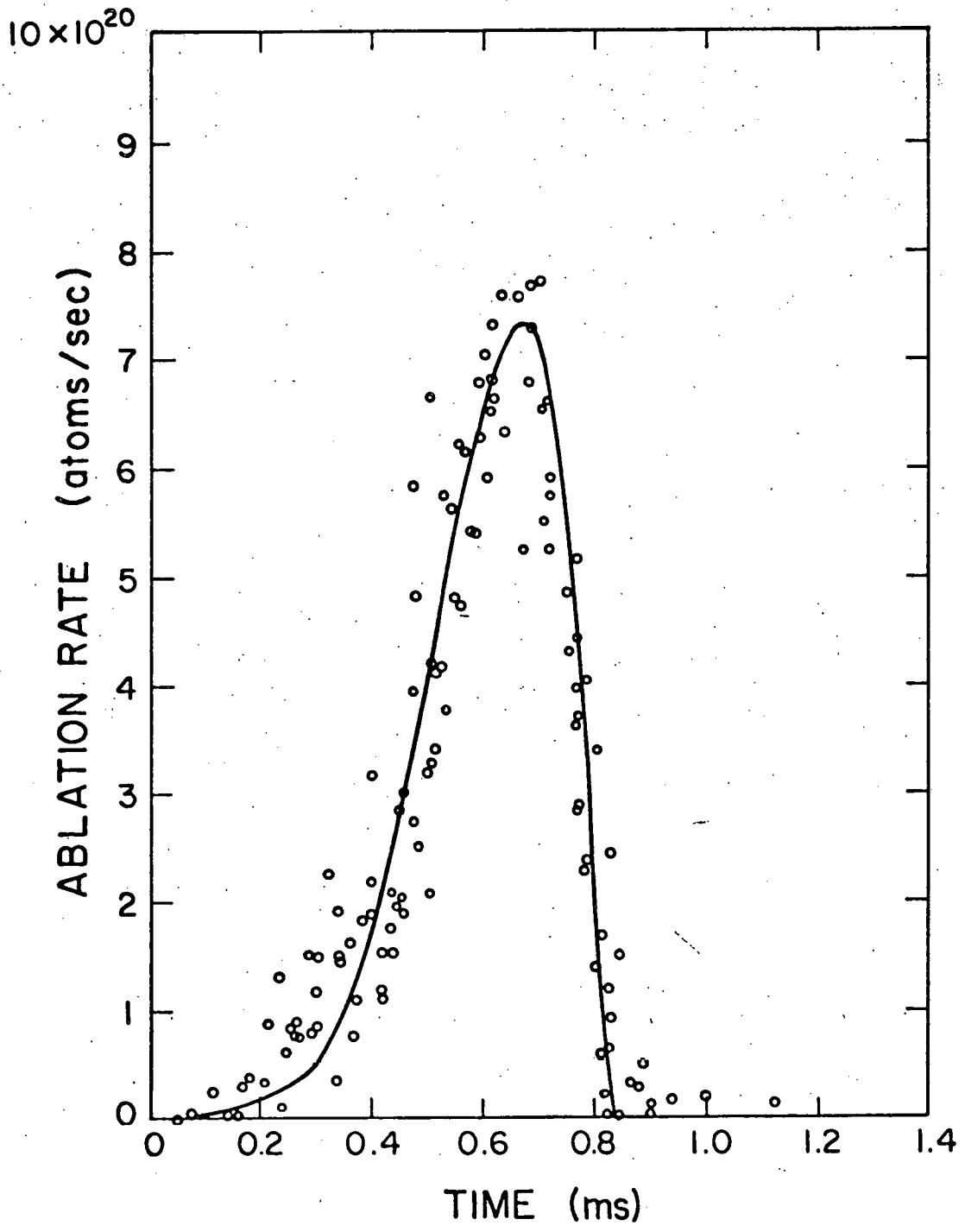
10×10^20
9
8
7
6
5
4
3
2
1
0
ABLATION RATE (atoms/sec)
0
0.2
0.4
0.6
0.8
1.0
1.2
1.4
TIME (ms)

Figure 6

SHOT #	PELLET #	PLASMA DENSITY	PLASMA CURRENT	MHD TYPE	PELLET VELOCITY	PELLET LIFETIME
10086	1	2.04×10^{13}	103KA	A	91 m/s	450 μsec
10150	1	1.28×10^{13}	119KA		91	447
10200	1	2.07×10^{13}	122KA		91	435
10222A	1	2.3×10^{13}	120KA	B	103	494
10222A	2	2.3×10^{13}	120KA	B	91	482
10226A	1	2.0×10^{13}	120KA	B	103	364
10260A	1		120KA	A	94	399
10260A	2		120KA	A	85	364
10240A-FASTAX		1.5×10^{13}	120KA	A	94	>300
10242A-FASTAX		1.4×10^{13}	120KA	A	84	>268

TABLE I

DATA FROM PELLET INJECTION EXPERIMENTS ON ORMAK

(PELLET RADIUS = 105 μm ; PELLET SPEED = 100 m/s)

ORMAK SHOT #	PELLET #	PLASMA DENSITY 30 ms / 45 ms	PLASMA CURRENT (kA)	TOROIDAL FIELD (kG)	PELLET LIFETIME (μs)
15025	1	$1.32 / 0.88 \times 10^{13}$	61	11.3	780
15026	1	NA	61	11.2	660
15027	1	NA	61	11.2	890
15027	2	NA	61	11.2	970
15029	1	1.26 / 1.14	60	11.3	840
15030	1	1.42 / 1.05	61	11.3	900
15031	1	1.54 / 1.10	61	11.2	850
15037	1	1.47 / 0.98	61	11.2	920
15045	1	1.19 / 0.96	61	11.4	845 *

AVE. 850 μs

TABLE II

A MODEL FOR THE ABLATION RATE OF A SOLID HYDROGEN PELLET IN A PLASMA

By

Paul B. Parks*, Robert J. Turnbull, and Christopher A. Foster**
Department of Electrical Engineering
University of Illinois at Urbana-Champaign
Urbana, Illinois 61801

ABSTRACT

It is shown that the ablation of a solid hydrogen pellet subject to a plasma is likely to produce a quasi-steady dense neutral gas cloud. The total integrated density of the cloud is such that the plasma electrons lose essentially all their energy in the cloud. The electron energy flux is degraded by inelastic collisions and elastic backscattering with the neutral molecules, providing local heating and acceleration of the neutral gas. Only a small fraction of the energy flux reaches the surface of the pellet, raising the pellet's surface temperature to a point where the energy flux at the pellet's surface is in balance with the energy lost through vaporization. The vaporization rate, in turn, determines the total integrated neutral gas cloud density.

The scaling laws derived from the model indicate that the pellet lifetime varies as: $\tau_p \sim T_e^{-1.71} n_e^{-1/3} r_{po}^{5/3}$, where τ_p is the lifetime of the pellet and T_e, n_e, and r_{po} are the electron temperature, density of the plasma, and initial pellet radius, respectively.

A good agreement is found between this model and the ORMAK pellet injection experiment.

*Present address: General Atomic Company,
San Diego, California 92138

**Present address: Oak Ridge National Laboratory
Oak Ridge, Tennessee 37830

I. INTRODUCTION

The possibility of using small frozen deuterium-tritium pellets to refuel fusion reactors was first conceived by Spitzer and Tonks [1] in the early days of fusion research. Their main idea was that the preservation of the self-shielding by the ablation cloud ions and electrons against free spherical dispersal by means of self-consistent fields created by motion of the ionized cloud across the magnetic field would increase the pellet lifetime. Later Rose [2] introduced the idea that a high β magnetic bubble caused by the pressure of the charged particles in the ablation cloud would be formed around the pellet, thereby diverting the incoming electron flux around the pellet, enhancing its lifetime. In contrast to Rose's balloon model, Chang [3], using a "magnetic nozzle" model, concluded that the shielding becomes more effective when the β of the ablation cloud is low. Recently, Gralnick [4], [5] postulated that an ionizing vaporization front is driven into the pellet by the hot incident reactor electrons and the resulting cold ablation plasma absorbs energy from the electrons, thereby reducing the ablation rate of the pellet.

Generally speaking, the above models have all assumed a high degree of ionization of the ablation cloud surrounding the pellet. If we consider present day and proposed Tokamaks, it appears that the amount of ionization will be negligible within a few pellet radii of the pellets' surface. Since this is where the shielding is most pronounced, a neutral ablation model should be used to calculate the pellet lifetimes.

The model we propose is that the molecules are ablated off the pellet as neutrals. The resulting neutral cloud then undergoes an expansion away from the pellet. The incoming plasma electrons are slowed down by the neutral cloud, reducing the energy flux to the pellet and thus increasing its lifetime.

Quasi-steady state conditions are assumed. It will be shown later that all problems of fusion interest allow the quasi-steady state assumptions.

The plasma electron energy provides a thermal energy source to the ablation cloud. Some of this energy goes into the kinetic energy of the ablation cloud with the remainder going into increasing the temperature of the cloud. The cloud molecules are thus continuously accelerated as they move away from the pellet surface. The dynamics are illustrated in Fig. 1a.

In Section II we deal with some overall considerations related to the problem. In Section III a self-consistent solution to the ablation rate is obtained by deriving a simple energy transport equation for electrons slowing down and scattering in molecular hydrogen of arbitrary density. The results of this section are then applied in Section IV where the dynamics of the phase transition are developed. In Section V an approximate solution is found for the heating and expansion of the ablation cloud.

Scaling laws are presented in Section VII which relate the ablation rate and the lifetime to the initial pellet radius and plasma electron temperature and density. A comparison with the existing experimental evidence for the lifetime of a pellet injected into a plasma is made and good agreement between theory and experiment is found.

II. GENERAL CONSIDERATIONS

When a pellet is subject to plasma, it is bombarded by electrons, ions, and radiation. If the electron and ion temperatures are equal, the electron energy flux is the dominant form of energy transport to the pellet since the ratio of the electron-to-ion energy flux is $\sqrt{m_i/m_e}$ (where m_i and m_e are the masses of the ions and electrons, respectively). It can, indeed, be shown that the ions are found to be even less effective than the electrons since

their ranges are shorter by a factor of $\sim m_e/m_i$. The pellet and its surrounding ablation cloud are transparent to the hard thermal radiation in the plasma. In addition, this radiation is several orders of magnitude less than the electron energy flux [2]. Therefore, the plasma electrons are the primary energy carriers to the pellet.

With the above in mind, the pellet ablation process may be described as follows: electrons strike the surface of the pellet, causing vaporization. The freshly formed vapor - hereafter referred to as the "ablation cloud" - consisting of neutral molecules flows away from the surface of the pellet in a more or less spherical manner. The density of the ablation cloud, $\rho(r)$, falls by *at least* r^{-2} for a spherical expansion. Because of the rapid decrease in density of the vapor for a spherical expansion and the fact that the vapor flow velocity is significantly greater than the pellet surface recession speed, a situation arises such that the establishment of the neutral vapor cloud occurs in a time scale which is almost negligible compared to the time for the pellet's radius to change appreciably. The pellet will therefore vaporize at a rate determined by its *instantaneous* radius and the instantaneous external energy flux. This consideration admits the use of a "quasi-steady" approximation.

In all subsequent analyses, the pellet's motion through the plasma will be neglected for two reasons. First, the mean free path of the electrons in the plasma is much larger than the pellet's radius. Further, the velocity of the pellet is highly subsonic with respect to the plasma ions and electrons. Therefore a shock layer which would divert plasma from the surface of the pellet does not develop ahead of the pellet. This consideration sets the present problem apart from typical problems in atmospheric re-entry. The pellet's motion plays a part only insofar as the plasma parameters such as

temperature and density vary along the pellet trajectory.

Fortunately for a wide class of plasma conditions the gradients in the energy flux as seen by the pellet as it moves through a nonuniform plasma are weak enough to satisfy the quasi-steady approximation for the pellet ablation process. A semiempirical qualification for the above statement to be valid is given by:

$$\left| \frac{d\ln q_o}{dx} \frac{V_p}{\overline{v(r)}} r_p \right| << 1 \qquad (1)$$

where $d\ln q_o/dx$ is the logarithmic change in the external (unattenuated) electron energy flux, q_o, along the pellet's trajectory, V_p is the velocity of the pellet, and $\overline{v(r)}$ is the average flow velocity of the ablation cloud. If V_p is of order 10^4 - 10^6 cm/sec and $\overline{v(r)} \simeq 10^5$ cm/sec, then Eq. (1) is easily satisfied. Therefore a quasi-steady state model will be used throughout the remainder of this paper.

The incident electrons interacting with the neutral ablation cloud partition their energy into basically four processes [6]: the loss to primary ionization threshold from which secondary electrons result; the energy of the secondary electrons; dissociative ionization from which only low energy atoms emerge unable to produce more ions; and finally, discrete-state excitations. Reference [6] gives the partition of the incident electron energy into these various processes.

The cross sections for direct ionization of H_2 into e - H_2^+ pairs is over an order of magnitude larger than the dissociative ionization in which case H^+ results [7].

The H_2^+ ions can undergo several subsequent reactions. The most efficient reaction is dissociative recombinations with thermalized secondary electrons in the ablation cloud. Energetic H atoms arise which thermalize rapidly in

the ablation cloud. As shown in Section VII, Eq. (41) the ablation cloud has a temperature of about 1 eV even for fusion plasma conditions. For electrons of 1 eV the dissociative recombination cross section is quite large $\sim 6.4 \times 10^{-16}$ cm [8], [9]. The product $\langle \sigma v \rangle_{recombination}$ is about an order of magnitude higher than $\langle \sigma v \rangle_{ionization}$ by incident electron impact. Clearly the density of thermalized primary electrons and secondary electrons is much higher than the incident electrons density in the ablation cloud. Thus recombination of the H_2^+ ion is very fast. There are two additional but less important processes competing for the H_2^+ ion. The first is dissociation by incident electron impact creating both hard H^+. The cross section for this process is $\sim$ 2 times the e - H_2 ionization cross section for incident electron energies $\gtrsim$ 500 eV [10]. Finally the H_2^+ ion can undergo an exothermic ($\sim$ 1.6 eV) reaction with H_2 forming hard H_3^+ [11]. From these processes most of the energy which went into ionization eventually goes into heating of the ablation cloud.

The discrete-state excitation leads eventually to heat also. This is because collisions between the neutrals in the ablation cloud under most conditions occur in a time scale much shorter than the time for the excited molecules or atoms to re-emit by spontaneous emission. Therefore, the excitation energy is distributed among the ablation species as an additional kinetic energy of the molecules.

Therefore, we expect that nearly all of the incident electron's energy (including secondary electrons) is degraded into thermal energy of the ablation cloud. It is this heating which drives the flow outward. At some point in the flow the molecules have reached a distance at which point most of them have become ionized by electron impact as described above. We call this distance the "ionization radius,". An estimate of the ionization radius denoted by

r_I, can be obtained as follows. Let v(r) be the gas-dynamic flow velocity of the ablation cloud at a radial distance r from the center of the pellet. Without treating recombination, r_I can be estimated according to:

$$\int_{r_p}^{r_I} \frac{dr}{v(r)} = \tau_{ei} \qquad (2)$$

where r_p is the pellet radius, and τ_{ei} is the lifetime of a neutral molecule against electron ionization. As shown in Section VII, Table I, r_I/r_p is quite large even for plasmas characteristic of present day or near term Tokamak reactors [12].

From the above, if $r_I/r_p \gg 1$, justification is given to the mechanism of continuous absorption of the electron energy flux in the predominately neutral portion of the ablation cloud near the surface.

Since as will be shown in Section VII a large fraction of the incident electron energy flux is absorbed in the ablation cloud the average incident electron energy has been degraded enough so that by the time the electron strikes the pellet surface, it has an effective range in the solid on the order of a micron or less even for energetic plasmas. Heat is developed in a thin layer underneath the surface and is conducted back to the surface and simultaneously into the interior of the pellet. The part conducted back to the surface sustains the vaporization. The velocity of heat transport into the interior of the pellet after a time t is of the order $\left(\frac{\alpha}{t}\right)^{1/2}$ where $\alpha = .003\ cm^2/sec$ is the thermal diffusivity for liquid hydrogen [13]. (The term α for the liquid instead of the solid phase is taken here because conduction in the solid could only raise the interior temperature up to the triple point.) For example, for a pellet of radius 300 μm subjected to a plasma with T_{eo} = 2000 eV and $n_{eo} = 4 \times 10^{13}\ cm^{-3}$ the lifetime is 26 μs and

the surface regression speed is $\approx 10^3$ cm/sec. Taking $t \sim 26$ μs, $\left(\frac{\alpha}{t}\right)^{1/2}$ = 10 cm/sec. It is concluded that the heat conduction does not permit an adequate outlet of heat into the pellet interior. Thus, it is insignificant in the energy balance at the surface, other than maintaining a relatively thin layer of heated solid or liquid near the surface at a temperature which is determined by the evaporation rate.

Concomitant to the vaporization and neutral vapor-shielding is the possible charging of the pellet and its dense ablation cloud resulting in an electrostatic shielding effect as first suggested by Spitzer [1]. In Spitzer's model the negative equilibrium potential on the pellet is such that the incident electron and ion currents to the pellet just balance. Gralnick [4] showed however, that the ions should be stopped by the pellet's ablation cloud whereas the electrons of course penetrate. The model presented here is in agreement with this claim.

In light of this, we feel that the incident electron current must be balanced by the "returning" scattered and degraded electrons which are almost entirely deposited throughout the neutral ablation cloud. These returning electrons set up electric fields in the ablation cloud. The numerous short ranged secondary electrons which are created by primary electron impact and undergo subsequent thermalization will attempt to suppress these electric fields to the extent of their mobility in the dense ablation cloud. (The ions are relatively immobile in the frame of the flow.) This suppression of the field can be countered by the rapid dissociative recombination processes so as to drain off these secondaries. The net effect of the above events could lead to a negatively charged ablation cloud.

The negative charging of the pellet is possible also. Recently Sorensen [14] has found that without a surface charge the secondary electron emission

coefficient for solid deuterium $\varepsilon < 1$ for incident electron energies above $\sim$ 500 eV. The charging aspect of the pellet ablation problem deserves further study. Pellet charging is neglected in this paper.

Because of the extremely low degree of ionization in the ablation cloud near the pellet, the influence of the magnetic field on the expansion of the ablation cloud is also not considered in this study. Its presence does, however, direct the electrons as they slow down and scatter in the cloud, and concurrently introduces an anisotrophy to the heating of the ablation cloud. This anisotrophy will at least be partially accounted for in this study.

III. TRANSPORT OF PLASMA ELECTRONS THROUGH THE NEUTRAL ABLATION CLOUD

Many authors have studied the transport of electrons through matter [15]-[17]. For our purposes, an analytic transport model of the electron energy flux at any given point in the ablation cloud is needed. The model will be coupled with the gas-dynamic motion of the ablation cloud. The model should include the physical effects of large angle backscatter and cumulative small angle scatterings of electrons on hydrogen as well as slowing down in a non-uniform background density.

Plasma electrons encountering the pellet's ablation cloud lose energy through inelastic processes such as ionization and excitation of the neutral hydrogen molecules and simultaneously undergo elastic scattering. The electrons, which are traveling along the magnetic field lines, have a spectrum of pitch angles with respect to the magnetic field. In progressing a distance along a field line threading the cloud, electrons with large pitch angles will scatter and slow down more than those with small pitch angles. In the inelastic collisions the direction of the electrons can be assumed to be unaltered because the differential scattering cross section is so strongly

peaked at small scattering angles [18] i.e., the electrons lose energy but essentially continue on with the same pitch angle. In an elastic collision the electron's pitch angle changes, but its energy does not change appreciably due to the small electron to molecule mass ratio.

In the following derivation for the transport of the electron energy flux, we assume that the electrons stick to the field lines. This means that a "pencil beam" of electrons which are contained within an elemental flux tube, threading the ablation cloud, remain in that flux tube. Inherent in this assumption is that the electron gyro-radius must be much less than the pellet radius so that the neutral cloud density variation transverse to the magnetic field can be neglected. For example, if the magnetic field strength is 50 kG then this assumption becomes $6.6 \times 10^{-5} \sqrt{T_{eo}}/r_p << 1$, where T_{eo} is the electron plasma temperature in eV, and r_p is the pellet radius in cm. This almost always holds for combinations of plasma temperatures and pellet radii of interest. For simplicity, only those electrons which are headed towards the pellet (forward flux) are considered. Electrons which are turned around (backward flux) by elastic collisions are no longer considered because their contribution to the total energy flux is small; the "double backscattering" process reduces their energy to essentially zero.

Let us consider the energy flux of electrons moving towards the pellet within an elemental flux tube threading the ablation cloud. From Fig. 1b 's' denotes the coordinate along any given flux tube. Assuming Maxwell-Boltzman statistics apply for the plasma electrons far away from the pellet which have temperature T_{eo} and density n_{eo} then the unattenuated electron energy flux q_o, is

$$q_o = \frac{n_{eo}\bar{V}_{eo}}{4} \cdot E_o \qquad (3)$$

where $v_{eo} = \sqrt{\frac{8kT_{eo}}{\pi m_e}}$ and $E_o = 2kT_{eo}$.

As an approximation, the distribution of electrons is replaced with an equivalent mono-energetic flux of electrons with average energy E_o. Assuming that these mono-energetic electrons lose their energy continuously as they enter the ablation cloud, a relation between the distance an electron travels along a flux tube and its energy is given by

$$\frac{dE}{ds} = \frac{n(s)L(E)}{< \cos \theta >} \tag{4}$$

where n(s) is the density of neutral hydrogen molecules and L(E) is the energy dependent loss function. The $< \cos \theta >$ term in Eq. (4) accounts for the average pitch angle which if weighted with an assumed isotropic distribution is approximated by 1/2.

Pitch angle scattering removes electrons from the forward flux. Let $\sigma_B(\theta,E)$ be the cross section for electrons removed (backscattered) by suffering a single elastic collision which sends an electron with initial *pitch angle* θ and energy E anywhere into the domain $(\pi/2,\pi)$ (see Fig. 2). $\sigma_{MS}(E)$ is the cross section for scattering considering cumulative small angle elastic collisions which lead to a total mean square deflection of $\simeq 90°$. The derivations of $\sigma_B(\theta,E)$ and $\sigma_{MS}(E)$, which follow in the Appendix make use of the differential elastic scattering cross section, $\frac{d\sigma(\xi)}{d\Omega}$, based on the Born approximation [18]. They are then adjusted to reflect the experimentally determined values for the total elastic scattering cross section [19].

The forward particle flux, $\phi(s)$, of these mono-energetic electrons along a flux tube is governed by the following equation:

$$\frac{d\phi(s)}{ds} = \phi(s)n(s)\hat{\sigma}_T[E(s)] \tag{5}$$

where $\hat{\sigma}_T[E(s)]$ is the energy dependent effective elastic scattering transport cross section. Again, approximating the pitch angle distribution by its average value, $\hat{\sigma}_T(E)$ is defined as

$$\hat{\sigma}_T(E) = 2\,\sigma_{MS}(E) + 2\int_0^{\pi/2} \sin\theta\;\sigma_B(\theta, E)d\theta \qquad (6)$$

The boundary condition on Eq. (5) is $s \to \infty$, $\phi \to \frac{n_{eo}\bar{v}_{eo}}{4}$.

The differential form of the forward electron energy flux $q(s) = \phi(s)E(s)$ is simply

$$\frac{1}{q}\frac{dq}{ds} = \frac{1}{\phi}\frac{d\phi}{ds} + \frac{1}{E}\frac{dE}{ds} \qquad (7)$$

Substituting Eq. (5) into Eq. (7) and making a variable change with the help of Eq. (4) we have after integration,

$$q(s) = q_o\,\frac{E(s)}{E_o}\,\exp\left[-\int_{E(s)}^{E_o} 1/2\hat{\sigma}_T(E')\,L(E')^{-1}dE'\right] \qquad (8)$$

where E(s) is given according to

$$1/2\int_{E(s)}^{E_o} dE'L(E')^{-1} = \int_s^{\infty} n(s')ds' \qquad (9)$$

Since the density of the ablation cloud is expressed in terms of the radial coordinate r we replace s by r in Eqs. (4)-(9). This is justified since it can be easily shown geometrically that the total integrated cloud density from $s = \infty$ up to any spherical surface r along any two given flux tube "1" and "2" is equal to within a few per cent. (Refer to Fig. 1b.)

The electron loss function, L(E), used in the above expressions, has been studied extensively for molecular hydrogen by Miles et al. [20], who obtained accurate semi-empirical cross sections for the discrete excitation, ionization, and dissociation processes. In this way L(E) can be constructed

from a knowledge of the various individual cross sections which characterize the inelastic collisions. Miles fitted L(E) to a versatile expression which is accurate down to 20 eV, viz.,

$$L(E) = \frac{a_o z}{2R_e}\left[\left(\frac{E}{A}\right)^{\Omega} + \left(\frac{E}{B}\right)^{M} + \left(\frac{E}{C}\right)^{\Lambda}\right]^{-1} \quad \text{ev - cm}^2 \tag{10}$$

where $a_o = 6.514 \times 10^{-14}$ cm^2eV^2, R_e is the Rydberg energy (13.6 eV), and $z = 3.6$. The constants are:

$$A = 100 \text{ eV}, \; B = 60.0 \text{ eV}, \; C = 48.87 \text{ eV}$$

$$\Omega = .823 \;, \; M = -.125 \;, \; \Lambda = -1.938 \; .$$

Using the results in Appendix A, $\hat{\sigma}_t(E)$ is computed from Eq. (6). The results were fitted to a convenient form, viz.,

$$\sigma_t(E) = \begin{cases} \dfrac{\sigma_1}{E^p} - \dfrac{\sigma_2}{E^r} & E \geq 100 \text{ eV} \\ \\ \dfrac{1.1 \times 10^{-14}}{E} & E \leq 100 \text{ eV} \end{cases} \tag{11}$$

where $\sigma_1 = 8.8 \times 10^{-13}$, $\sigma_2 = 1.62 \times 10^{-12}$, $p = 1.71$, $r = 1.932$, and E is in electron volts.

Fig. 3 illustrates $E\hat{\sigma}_t(E)$ and L(E) vs. energy. The comparable effects of scattering and slowing down on the total energy flux degradation are shown.

IV. SURFACE ABLATION DYNAMICS AND THE INTEGRATED CLOUD THICKNESS

Electrons which have made their way through the ablation cloud deposit their energy to the pellet's surface. The surface temperature is raised, which induces vaporization of H_2 molecules. Let q_o be the unattenuated electron energy flux far away from the pellet ($r \to \infty$), and q_1 the degraded

energy flux just at the pellet's surface ($r = r_p$). The fraction, f_H, of the energy flux, q_1, which goes into heat at the pellet surface giving rise to the elevated surface temperature and the phase transition can be shown to be

$$f_H = 1 - \frac{1}{W_o(E_1)} \tag{12}$$

where E_1 is the average final energy of the electron which strikes the pellet surface; I, the ionization threshold for products of H_2^+, 15.42 eV; and $W_o(E_1)$, the incident energy E_1 divided by the total number of ion-electron pairs which are produced as the electrons slow down completely. For cases when E_1 is greater than 200 eV, $f_H = .576$. The mean radiative lifetime for excited H_2 molecules is on the order of 10^{-9} sec, [21] and the mean free path for line radiation is about 400 Å [22] in liquid or solid H_2. Because the average range of an electron at the pellet surface is on the order of a few microns the excitation radiation is absorbed. A similar argument can be applied to the secondary electrons created in the heated layer.

Eq. (12) assumes that no dissociative recombination of the newly created $e - H_2^+$ pairs occurs in the liquid heated layer on the pellet's surface. It is not clear whether one can apply the previously mentioned recombination coefficient for thermalized electrons in a low temperature liquid or solid ($\sim$ 20-30° K). In this sense, f_H as given by Eq. (12) is actually a lower limit. Since more than half of the incident energy to the pellet surface appears to go into heat and since the energy needed to vaporize a molecule is more than three orders of magnitude less than the energy needed to ionize it, we conclude that only a very small number of molecules (< .1 percent) leave the surface in an ionized state. It is for this reason that we conclude that the ablation cloud is predominantly neutral near the pellet surface.

Because of the spiraling of the electrons around the magnetic field lines, the actual energy flux falling upon the pellet surface is reduced by not more than 1/2 of its value in the case with no magnetic field, depending upon the ratio of the pellet radius to the average gyro-radius of the electron with energy E_F striking the pellet. A detailed analysis of this effect has been studied and for most cases of interest f_B, the energy flux entering the pellet normalized to the case where no magnetic field is present and a Maxwellian distribution of electrons is assumed at the surface of the pellet is found to be about .5 - .6 [23].

With the above considerations in mind, the energy balance at the pellet surface in the steady state can be shown to be given by:

$$q_1 f_H f_B = \rho_o \dot{r}_p \left[\frac{U_s}{m_{H_2}} + \int_{T_o}^{T_s} C_p(T) dT \right] \tag{13}$$

where U_s is the sublimation energy, (.01 eV/molecule), m_{H_2} is the mass of a hydrogen molecule, T_s is the pellet surface temperature, T_o the pellet interior temperature ($\simeq$ 10 - 12° K), ρ_o, the solid (or liquid) density, and $\dot{r}_p$ the rate of change in the pellet radius. $C_p(T)$ is the heat capacity at constant pressure. For solid hydrogen $C_p(T) \simeq C_o T^{3/2}$; for liquid hydrogen $C_p(T) \simeq C_1 + C_2 T$ [24]. Without consideration of reradiation from the surface Eq. (13) is similar to other standard forms regarding surface ablation; for example, the ablation of meteors in the upper atmosphere, [25], [26].

The specific enthalpy content of the heated surface layer, $\int_{T_o}^{T_s} C_p(T) dT$, becomes comparable to U_s/m_{H_2} when T_s is above $\simeq$ 20° K.

At the completion of bond rupture at the surface, the vapor just created is at cryogenic temperatures and has a total specific enthalpy $h_{t_1} = h_1 + \frac{V_1^2}{2}$, which must be equal to the specific enthalpy content of the

heated surface layer. If ideal gas law behavior is assumed, i.e. $h_1 = \frac{\gamma k T_1}{(\gamma-1)m_{H_2}}$, then

$$\int_{T_o}^{T_s} C_p(T)dT = h_{t_1} = \left[\frac{1}{(\gamma-1)} + (\tfrac{1}{2})M_1^2\right] \frac{\gamma k T_1}{m_{H_2}} . \qquad (14)$$

Here γ is the ratio of specific heats and M_1 is the Mach number for the initial vapor flow. Eq. (14) glues the connection between the surface temperature, vapor temperature, and initial Mach number of the flow.

Conservation of mass at the pellet surface, assuming $\dot{r}_p \ll v_1$ is simply

$$\rho_1 v_1 \simeq \rho_o \dot{r}_p \qquad (15)$$

where ρ_1 is the ablation cloud density just at the surface in g/cm^3 and the velocity v_1, of the flow just at the pellet surface is:

$$v_1 = M_1 \sqrt{\frac{\gamma k T_1}{m H_2}} \qquad (16)$$

Typical ablation cloud temperatures near the pellet are low ($\simeq$ .02 - .1 eV). At these temperatures hydrogen molecules have only translational and rotational energies [27]. For this reason we take $\gamma = 7/5$.

The surface temperature, T_s, is in turn, coupled to the rate of vaporization. From kinetic theory [28] the flux of molecules leaving the pellet surface is equal to the rate at which molecules would strike the surface from its saturated vapor pressure as if the surface were in equilibrium with its vapor at temperature T_s. Since in equilibrium not all molecules which strike the surface recondense the striking rate must be multiplied by a condensation coefficient, $\alpha(T_s)$, which is the fraction of molecules which are not reflected upon striking the surface of the liquid or solid.

Assuming that none of the molecules leaving the surface return and recondense, then the flux of molecules from the surface is

$$\frac{\rho_1 v_1}{m_{H_2}} = \frac{P_v(T_s)\alpha(T_s)}{\sqrt{2\pi m_{H_2} kT_s}} \tag{17}$$

where

$$P_v(T_s) = P_o \exp \frac{-A}{T_s} + BT_s \tag{18}$$

is the saturated vapor pressure for liquid or solid H_2 [13] at a temperature T_s. The constants P_o, A, and B are 4.841×10^7 dynes/cm^2, 108.7 K and .0907 K^{-1} respectively. The condensation coefficient $\alpha(T_s)$ is not known for hydrogen, but is taken to be unity here, as with most other insulators [29].

The energy flux and average electron energy at the pellet surface, q_1 and E_1, respectively, depend on the total integrated ablation cloud thickness from Eqs. (8) and (9). It will be convenient to form the dimensionless quantities $\xi = r/r_p(t)$, and $y(\xi) = \frac{\rho(r)}{\rho_1}$. Using the above relations the following expressions for q_1 and E_1, at $\xi = 1$, are

$$q_1 = q_1 \frac{E_1}{E_o} \exp - \left[\int_{E_1}^{E_o} < \cos \theta > \hat{\sigma}_t(E')L(E')^{-1} dE' \right] \tag{19}$$

where $q_o = \frac{n_{eo} v_{eo}}{4} \cdot E_o$ is the unattenuated electron energy flux, and

$$\int_{E_1}^{E_o} < \cos \theta > \frac{dE'}{L(E')} = \frac{\rho_1}{m_{H_2}} r_p(t) \int_1^\infty y(\xi) d\xi = \frac{\rho_1}{m_{H_2}} r_p(t)\Gamma \tag{20}$$

By making use of Eqs. (10) and (11) for L(E) and $\hat{\sigma}_t(E)$ respectively the integrations in Eqs. (19) and (20) can be easily carried out. In Eq. (20) a "shape factor" $\Gamma = \int_1^\infty y(\xi) d\xi$ has been defined which indicates the magnitude

of the gradient in the ablation density profile; the total integrated cloud thickness in cm^{-2} is $\frac{\rho_1}{m_{H_2}} r_p \Gamma$. A necessary condition for quasi-steady state is that this quantity be finite. This is always true for spherical flows in vacuo since the velocity of such flows either increases without bound (for instance with heat addition) or approaches a limiting value as in polytropic flows ($p = p^{\gamma}$) cf [30]. As an example, it is easy to show that an adiabatic expansion in spherical geometry has a normalized density, $y(\xi)$, given implicitly as:

$$\frac{1}{\xi 4} = y^2 \left[\left(\frac{\gamma + 1}{\gamma - 1} \right) - \frac{2}{(\gamma - 1)} y^{\gamma - 1} \right] \tag{21}$$

in which case $\Gamma = .570$ for $\gamma = 7/5$.

The expansion of the ablation cloud is not a free or adiabatic expansion. Therefore in our case the determination of the shape factor Γ must be made in connection with the ablation cloud heating by incident electron energy deposition.

V. EVALUATION OF THE SHAPE FACTOR Γ

Given pellet radius $r_p(t)$, electron plasma density n_{eo} and temperature T_{eo}, then the energy and mass balance Equations (13) and (15) with the equations for the energy flux at the pellet surface (19) and (20) and the additional Equations (14), (16), and (17) constitute a set of seven coupled algebraic equations with nine unknowns -- $\dot{r}_p$, T_s, ρ_1, v_1, T_1, M_1, q_1, E_1, and the shape factor Γ. Two additional equations are needed to close the system. These are the two relations for M_1 and Γ which depend upon the ablation cloud heating by the incident electrons. In this way a self-consistent solution for the pellet lifetime can be found by solving the above set of equations for $\dot{r}_p$ for a given instantaneous pellet radius r_p, plasma density,

n_{eo}, and temperature, T_{eo}. We must now turn to the problem of the heating up of the ablation cloud and its quasi-steady expansion. By including this important effect the dimensionless density profile, $y(\xi)$, may be obtained which is then used to obtain the shape factor, Γ, in terms of the quantities T_1 and r_p.

Qualitatively the hydrodynamic motion of the heated flow can be described as follows: heating predominates near the surface of the pellet where absorption of the energy flux is strongest, whereas further away from the pellet radial expansion predominates over heating. It is then possible for the ablation cloud to be accelerated up to a sonic radius where heating and expansion work exactly balance and then pass over into the supersonic range where the gas is still receiving heat but it is spent mostly on the kinetic energy of the flow.

Rather than solve the equations exactly we chose to make another approximation at this point. The flow will be assumed to be sonic everywhere. This approximation then allows the remaining equations to be solved easily. The justification for this approximation is that the shape factor and the pellet lifetime are not strong functions of the velocity of the flow.

The magnetic field imposes an anisotrophy on the volumetric heat source, denoted by $S_v(r)$, in the spherically expanding ablation cloud. We average the volumetric heat source term, S_v, over a spherical shell of volume $4\pi r^2 dr$. As pointed our earlier, the energy flux passing through a spherical surface is reduced by f_B over the non-magnetic case. From Fig. 1b it can easily be seen that

$$< s_v(r) > = f_B Q \frac{dq}{dr} = (r_g << r_p) 1/2Q \frac{dq}{dr} \qquad (22)$$

where Q represents the fractional energy loss of the incident electrons which heats up the ablation cloud. As mentioned in Section II, Q will be close to

one for a highly collisional ablation cloud for any electron energy. Expressing Eq. (8) for q(r) in differential form and with the help of Eq. (4) results in

$$\frac{dq(r)}{dr} = n(r)q(r)\left[\frac{L(E(r))}{<\cos\theta>_{E(r)}} + \hat{\sigma}_t(E(r))\right] \tag{23a}$$

$$= \frac{\rho(r)}{m_{H_2}} q(r)\Lambda(E(r)) \tag{23b}$$

where $\Lambda(E(r))$ in Eq. (23b) is an effective "energy flux cross section." If G is the instantaneous ablation rate in g/sec, then the mass and energy conservation equations neglecting heat conditions for the steady spherically-symmetric ablation cloud are the following:

$$\rho v r^2 = \rho_1 v_1 r_p^{\ 2} = \frac{G}{4\pi} = \text{constant} \tag{24}$$

$$\frac{1}{r^2}\frac{d}{dr}\left[r^2\rho v\left(\frac{\gamma p}{(\gamma-1)\rho} + 1/2v^2\right)\right] = f_B \frac{\rho}{m_{H_2}} q(r)\Lambda(r) \tag{25}$$

since $r^2\rho v$ is constant then Eq. (25) can be expressed as

$$\frac{d}{dr}\left[\frac{\gamma p}{(\gamma-1)\rho} + 1/2v^2\right] = \frac{f_B q(r)\Lambda(r)}{m_{H_2} v(r)} \tag{26}$$

As a first approximation to the source term on the right-hand side of Eq. (26) scattering is neglected so that $q(r) = \frac{q_o}{E_o} E(r)$, (constant particle flux), and $\Lambda(r) = \frac{L(E(r))}{<\cos\theta>_{E(r)}}$ (note that this approximation is made only in the cloud heating equation and not in the pellet energy flux equation). Let $L(E(r))$ be constant and equal to $L(E_o)$. Since $\frac{\gamma p}{\rho} = \frac{\gamma kT}{m_{H_2}} = C^2$, where C is the local speed of sound, then with the above approximations Eq. (26) becomes

$$\frac{d}{dr} v(r)^2 \left(\frac{1}{2} + \frac{1}{(\gamma-1)M^2}\right) = \frac{f_B Q}{<\cos\theta>} \frac{q_o L(E_o)}{E_o m_{H_2} v(r)} \tag{27}$$

With Q(r) = 1 then solution of Eq. (27) yields:

$$v(\xi) = \sqrt{\frac{\gamma k T_1}{m_{H_2}}}\, M(\chi(\xi-1) + 1)^{1/3} \tag{28}$$

$$T(\xi) = T_1(\chi(\xi-1) + 1)^{2/3} \tag{29}$$

$$y(\xi) = \frac{\rho(\xi)}{\rho_1} = \xi^{-2}(\chi(\xi-1) + 1)^{-1/3} \tag{30}$$

The pressure, $p(\xi)$, is then

$$p(\xi) = \frac{\rho_1 k T_1}{m_{H_2}}\, \xi^{-2}(\chi(\xi-1) + 1)^{1/3} \tag{31}$$

where χ is defined as

$$\chi = \frac{3}{16} \frac{m_{H_2}^{1/2}}{(\gamma k T_1)^{3/2}} \frac{n_{eo} v_{eo} L(E_o) Q r_p}{\left(\frac{M^3}{2} + \frac{M}{(\gamma-1)}\right)} \tag{32a}$$

for M = 1 this is

$$\chi = .068 \frac{n_{eo} v_{eo} L(E_o) r_p(t) Q}{(T_1)^{3/2}} \tag{32b}$$

Defining $a = (\chi-1)^{1/3}$, the expression for the shape factor, Γ, is from Eqs. (20) and (30)

$$\Gamma = \begin{cases} 3/4 \text{ if } \times = 1 \\ \dfrac{\chi}{(\chi-1)} \left[\left| \dfrac{\pi}{2a\sqrt{3}} \right| + \dfrac{1}{6a} \ln\left[\dfrac{(a+1)^2}{a^2-a+1}\right] - \dfrac{1}{a\sqrt{3}} \arctan\left[\dfrac{2-a}{a\sqrt{3}}\right] - \dfrac{1}{\chi} \right] \text{ if } \chi \neq 1 \end{cases} \tag{33}$$

For the expression in Eq. (32b) the units for $L(E_o)$ are eV - cm^2 and T_1 is in °K. Aside from the external plasma parameters, Γ is a function of

the instantaneous pellet radius, r_p, and the temperature, T_1, of the ablation cloud just at the pellet's surface ($\xi = 1$).

VI. RESULTS OF THE SONIC APPROXIMATION AND COMPARISON WITH EXPERIMENT

With the expression for Γ as a function of T_1 and $\dot{r}_p$ and with $M = 1$, the aforementioned set of equations is now closed. $\dot{r}_p$ is found for an initial pellet radius r_{po} by solving the set of simultaneous equations numerically. By incrementing the pellet radius a new r_p is found and so forth. In this way the lifetime for the pellet to decrease to 5 percent of its original value (99.987 percent vaporized) can be computed. The lifetimes for typical pellet radii and uniform plasma parameters are illustrated in Figs. 4a and 4b.

In order to compare our model with the recent pellet injection experiment performed on the ORMAK Tokamak [31], the pellets' motion through the varying plasma conditions is taken into account in the calculations of the lifetime. The experimental lifetime of 35 μm radius pellets moving 100 M/sec into ORMAK was about 380 μsec whereas the theoretical prediction is 381 μsec. For 210 μm pellets moving at the same speed the experimental lifetime is 850 μsec and the theoretical calculation gives 820 μsec . Reference 31 gives a detailed description of these experiments and calculations.

VII. SCALING LAWS AND THE IONIZATION RADIUS

From Figs. 4a and 4b, one observes that the lifetime of the pellet is not a strong function of the plasma density; furthermore, the lifetime is a much stronger function of the pellet's initial radius than the obvious linear relationship. These results are not surprising in light of certain central implications of this model. This becomes evident upon making simplifying approximations to the foregoing derivations, leading to scaling laws for the

ablation cloud temperature and the pellets' lifetime in terms of r_p, n_{eo}, and T_{e0}.

The pellets' surface temperature, T_s, is a slowly varying function of the ablation rate since only a small change in T_s produces a very large change in the ablation rate (see Eqs. (17) and (18)). Further, in order for the vapor pressure relation in Eq. (18) to be meaningful the surface temperature must be below the critical point temperature for hydrogen (33° K). At this temperature the ablation rate is, from Eq. (17), 4.24×10^{25} molecules/sec/cm^2, which corresponds to a surface regression speed, $\dot{r}_p = 2 \times 10^3$ cm/sec. However, the surface temperature does not determine the ablation rate for energy fluxes strong enough to cause this regression speed. Instead the ablation cloud controls the ablation rate. In other words, even though we cannot apply the surface conditions above the critical temperature this model is still valid. In fact, at a surface temperature of 33° K the surface conditions are almost totally insignificant because of the almost complete absorption of the electron energy flux in the ablation cloud. The following example illustrates this point clearly. An H_2 pellet of radius 320 μm subjected to a plasma with temperature and density 3 KeV and 3.5×10^{13} cm^{-3} respectively has a lifetime of 12.33 μs; indicating a surface temperature $\sim$ 33° K. The external energy flux to the pellet is $q_o = 1.92 \times 10^{26}$ eV/cm^2 - sec. From Eq. (13) it is shown that the ratio of the energy flux at the pellet surface, q_1, to the external energy flux, q_o, is $\frac{q_1}{q_o} \approx \frac{U_s \rho_o \dot{r}_p}{q_o m_{H_2}} = .0023$. This indicates that the ablation rate is not sensitive to the energy balance at the pellet surface, nor the details of the phase transition. Essentially what this means is that the ablation cloud controls the dynamics of pellet evaporation.

From the nature of the pellet ablation dynamics a scaling law for the ablation rate can be found. Since T_s is slowly varying for a wide range of

ablation rates, T_1 and v_1 may be taken to be constant in what follows. Assuming an average value for L(E), then from Eq. (20) one has

$$(E_o - E_1) = 2\, L(E_o)\, \frac{\rho_1}{m_{H_2}}\, r_p \Gamma(r_p, T_1) \tag{34}$$

Neglecting scattering for simplicity then from Eq. (19) and Eq. (34) the energy flux at the pellet surface is given as

$$q_1 = q_o \left[1 - \frac{2\rho_1}{m_{H_2}} \frac{r_p L(E_o) \Gamma(r_p, T_1)}{E_o} \right] \tag{35}$$

Neglecting the heat capacity effect in Eq. (13), then with Eq. (35) and Eq. (15) the surface regression speed is

$$\dot{r}_p = \left(\frac{1}{\rho_o / m_{H_2}} \right) \left\{ \frac{q_o}{\frac{U_s}{f_H f_B} + \frac{2 q_o r_p \Gamma(r_p, T_1) L(E_o)}{v_1 E_o}} \right\} \tag{36}$$

Here again, the insensitivity of the boundary conditions at the pellet surface is apparent. The first term on the left hand side of the denominator in the above equation contains the sublimation energy U_s. This term can be neglected in comparison with the term on its right provided that:

$$\frac{v_1 E_o U_s}{2 f_H f_B q_o r_p \Gamma L(E_o)} = \frac{2 v_1 U_s}{f_H f_B n_{eo} v_{eo} r_p \Gamma L(E_o)} \equiv \varepsilon_h << 1 \ . \tag{37}$$

For instance, in keeping with the above example where T_{eo} = 3 KeV, n_{eo} = 3.5×10^{13} cm^{-3}, r_p = 320 μm; $L(E_o) = 2.91 \times 10^{-16}$ eV - cm^2, $\Gamma(r_p, T_1)$ = .20, $v_1 = 4 \times 10^4$ cm/sec, ε_h = .0137. The implication is as follows: when ε_h is large, e.g., low plasma density or small pellet radius, the ablation rate is primarily controlled by the conditions at the pellet surface since the ablation cloud is very "thin". Increasing the energy flux, in particular the electron density, increases the surface regression rate. Thus, the total ablation cloud

thickness increases up to a point where it is limited by the electron range which is strongly dependent on the plasma temperature. At this point ϵ_h is very small, so that the role of the ablation cloud dominates the ablation rate. U_s is negligible, as if $U_s \to 0$. This also implies that the electron energy flux at the pellet surface, q_1, is negligible since

$$\frac{4\pi r_p^2 q_1}{\frac{U_s}{m_{H_2}}} \quad \underset{\substack{\lim U_s \to 0 \\ q_1 \to 0}}{=} \quad G = 4\pi \rho_o r_p^2 \dot{r}_p: \ G \text{ is finite} \tag{38}$$

Provided Eq. (37) is fulfilled, Eq. (36) also predicts that increases in plasma density even further have little effect on the ablation rate. Physically, this is because a denser ablation cloud would result if the ablation rate were increased. This cannot be so since the electrons would not even reach the pellet surface; they are already "range limited". The effect of the plasma density is important in the sonic approximation insofar as the heating of the vapor and hence the shape factor Γ is affected, i.e., increased heating reduces the shape factor Γ or "tapers" the ablation cloud more because the flow velocity increases. Thus, in order to maintain the "range limited" thickness the pellet ablates at a slightly faster rate upon increase of plasma density in order to compensate.

Increases in the pellet radius cause the total integrated thickness of the ablation cloud to increase proportionally because the distance required in order for the ablation cloud density to fall to any given value is increased.

Therefore, to maintain "range limited" conditions, the gas density at the pellet surface, ρ_1, hence the surface regression speed, must decrease accordingly, giving rise to the $\sim r_p^{-1}$ dependence of $\dot{r}_p$ in Eq. (36).

The "range limited" concept is similar in principle to Krokhin's self-matched regime where the optical thickness of materials heated by intense laser light tends to remain at a constant value throughout the course of heating. In our case, though, the pellets' radius, in a manner of speaking, determines the "optical thickness".

The value of χ, given by Eq. (32) is in practically all cases of interest much larger than unity; and the dominant term in Eq. (33) is the first term on the right-hand side in the brackets. Thus, $\Gamma \sim \chi^{-1/3} \sim v_1 \, m_{H_2}^{-1/6} Q^{-1/3} n_{eo}^{-1/3} L(E_o)^{-1/3} T_{eo}^{-1/6}$, which when substituted into Eq. (36) gives the following scaling laws for $\dot{r}_p$, pellet lifetime; τ_p, and ablation cloud temperature one pellet radius away from the surface, $T_{(\xi=2)}$

$$\dot{r}_p = 6.29 \times 10^5 \frac{Q^{1/3} n_{eo}^{1/3} T_{eo}^{7/6}}{r_p^{2/3}} \frac{1}{L(E_o)^{2/3}} \frac{1}{n_o M_o^{1/3}} \text{ cm/sec} \quad (39)$$

$$\tau_p = \frac{\int_o^{r_{po}} r_p^{2/3} dr_p}{\Gamma_{po}^{2/3} \dot{r}_p (r=r_{po})}$$

$$= .867 \frac{r_{po}^{5/3} L(E_o)^{2/3} n_o M_o^{1/3}}{Q^{1/3} n_{eo}^{1/3} T_{eo}^{7/6}} \text{ μsec} \quad (40)$$

$$T_{(\xi=2)} = 1.88 (r_p n_{eo} Q)^{2/3} T_{eo}^{1/3} L(E_o)^{2/3} M_o^{1/3} \text{ eV} \quad (41)$$

Here $n_o = \frac{\rho_o}{m_{H_2}}$ is the solid molecular number density, T_{eo} is in eV, r_p in cm, and M_o is the molecular mass of the pellet in amu. D_2 and T_2 pellets have slightly higher number densities and molecular masses, providing a small but noticeable increase in lifetimes over H_2 pellets. Note, also the strong dependence of τ_p on the pellet radius and the weak dependence on the plasma

density in accordance with the above description of the ablation dynamics. We point out further, that the scaling laws are independent of the velocity of the ablation cloud at the pellet surface, v_1. This reinforces our conclusions that the surface conditions play an insignificant role in the ablation dynamics for small ε_h.

The small inverse effect the plasma temperature has on the ablation cloud temperature T_a can be shown by expressing L(E) in the limit of high energy, i.e., $L(E) \propto \frac{1}{E^{.832}}$. Therefore, $T_a \propto T_{eo}^{-.215}$. This inverse effect is due to the fact that the *production* of vapor outweighs the additional heating: a slightly cooler ablation cloud results.

By approximating the local Mach number in the flow, M(r), by a constant M=1 we have underestimated the ablation cloud temperature near the pellet (where we expect subsonic flow) by a factor of $\sim M(r)^{2/3}$ (see Eqs. (29) and (32)).

For example, if $n_{eo} = 4 \times 10^{13} cm^{-3}$, $T_{eo} = 5000$ eV, $r_p = .03$ cm, then from Eq. (41) $T_{(\xi=2)} = .152$ eV. If we take $M_{\xi=2)} = 1/2$ then $T_{(\xi=2)} = .240$ eV. One should expect the actual temperature near the pellet to be higher than that in the sonic approximation because according to Eq. (28) the flow velocity $\sim M(r)^{2/3}$. This means that the flow actually expands slower and hence spends more time heating up. However the ablation rate as given by the sonic approximation should not differ to much from reality. This is because the flow velocity has likewise been underestimated in the supersonic portion of the ablation cloud. Therefore the sonic approximation overestimates the thickness of the ablation cloud in this region.

At this point we can establish reasonable grounds for the credibility of the quasi-steady approximation. In order for quasi-steady conditions to prevail, the fractional change in pellet radius must be small in the time for the ablation cloud to be fully developed (at least over a pellet radius). If

this is true then the expression for τ_p given by Eq. (40) is valid. Let us define a characteristic time for the ablation cloud to be fully developed as $\tau_{ablation}$, where

$$\tau_{ablation} = \frac{r_p}{V_{(\xi=2)}} = \frac{r_p}{\sqrt{\frac{\gamma k T_{(\xi=2)}}{m_{H_2}}}} \tag{42}$$

In this amount of time the pellet's radius changes by δr_p where

$$\frac{\delta r_p}{r_p} = \frac{\dot{r}_p \tau_{ablation}}{r_p} = \frac{\dot{r}_p}{\sqrt{\frac{\gamma k T_{(\xi=2)}}{m_{H_2}}}} \tag{43}$$

Using the scaling laws Eq. (39) and Eq. (41) in the above expression we find

$$\frac{\delta r_p}{r_p} \sim \frac{E_o}{n_o L(E_o) r_p} \sim \theta \frac{Re}{r_p} \tag{44}$$

where Re is the range of an incident unattenuated plasma electron in the solid pellet of molecular number density n_o. It is not surprising that $\delta r_p / r_p$ should depend only on the range of the incident electron in the solid. This is because more material is needed to shield the pellet from electrons with larger ranges. If the range becomes too large, a point is reached where there is not enough material in the pellet to produce a fully developed ablation cloud. Pushed to the extreme, one can imagine ranges so large that volumetric heating of the pellet takes place, in which case the time scales for pellet disassembly and gas-dynamic expansion are the same. For most plausible combinations of pellet radii and plasma temperatures, $\delta r_p / r_p$ is indeed quite small. On the basis of these results, it is concluded that the quasi-steady model is

reasonably good. Thus, the pellet lifetime, τ_p, given by Eq. (40) is meaningful. The neglect of heat conduction in the ablation cloud can be justified on the basis of the scaling laws. For H_2 gas the thermal diffusivity in Cgs units is $\alpha = 3 \times 10^{19} T^{1/2} n^{-1}$ [28] where T is in eV and n is the number density (cm^{-3}). The characteristic velocity of heat transport in the ablation cloud in a characteristic distance δ is $v_H \sim \left(\frac{\alpha v}{\delta}\right)^{1/2}$ where v is the flow velocity. Thus $v/v_H \sim 6.4 \times 10^{6} \left(\frac{1}{Mn\delta}\right)^{1/2}$ where M is the local Mach number of the flow. For all cases of interest $v/v_H << 1$ so that heat conduction is ignorable. In fact this is true even near the pellet where M and δ decrease and n increases quite rapidly (see Eq. (30)).

Finally, an aposteriori justification for the large fraction of neutral molecules in the ablation cloud can be given at this point. The "ionization radius" r_I defined in Eq. (1) can be obtained by first assuming that τ_{ei} is constant everywhere in the ablation cloud and is equal to $\tau_{ei} = \left(\frac{n_{eo}\sigma_{ei}(E_o)\bar{v}_{eo}}{4}\right)^{-1}$. Here $\sigma_{ei}(E)$ is the cross section for ionization of H_2 by electron impact [20]. Substituting the flow velocity $v(\xi)$ from Eq. [28] into Eq. [1] yields after integration

$$\xi_I = \frac{r_I}{r_p} = \frac{1}{\chi}\left[\frac{2\chi v_1 \tau_{ei} + 1}{3rp}\right]^{3/2} + \frac{\chi-1}{\chi}. \qquad (45)$$

For typical parameters and pellet sizes in the domain where our model is valid, ξ_I is given in Table I. It is interesting to point out that at the ionization radius the temperature of the ablation cloud using Eq. (29) and Eq. (45) is given by $T_I \sim .037 \frac{< L(E_o) >}{\sigma_{ei}(E_o)} \cong 2.5$ eV independent of r_p, n_{eo} and T_{eo}. This result is close to the temperature 2.02 eV that Gralnick [4] obtained for the ablatant just at the pellet surface where in his analysis complete ionization of the surface takes place.

At this point one can discover whether or not the ionized portion of the ablation cloud has enough pressure to create a $\beta = 1$, or "magnetic bubble", under CTR conditions, as Rose [2] predicts. A reasonable criterion for this to occur would be that the pressure in that ablation cloud at the ionization radius, P_I, be greater than or equal to the imbedded magnetic field pressure $B^2/8\pi$ in the plasma. The ablation cloud pressure at the ionization radius, P_I, can be found by eliminating ρ_1 in Eq. (31) with the help of Eq. (15) and Eq. (39), viz.,

$$P_I = \frac{9.6 \times 10^{-8} L(E_o)^{4/3} T_{eo}^{13/6} n_{eo}^{7/3} r_{po}^{4/3}}{Q^{2/3}} \text{ dynes/cm}^2 \qquad (46)$$

For typical plasma parameters characteristic of EPR designs [34], $T_{eo} = 1.5 \times 10^4$ eV, $n_{eo} = 1.8 \times 10^{14}$ cm^{-3}, and B = 37 kG. For an H_2 pellet with $r_{po} = .3$ cm, ($\tau_p = 25$ μs), $\xi_I = 8.5$, and $\frac{p_I}{B^2/8\pi} = .16$. This means that a magnetic bubble as postulated by Rose will probably not form as also suggested by Chang [3]. The plasma in the ablation cloud at the ionization radius is still highly collisional, in fact $\omega_{ci}\nu_{ii}$ is much less than one but will increase further away from the pellet as the temperature in the ablation cloud is continually increasing and the density decreasing. This leads us to believe that a spherical expansion prevails at least in the vicinity of the pellet where almost total absorption of the incident electron energy flux takes place.

VIII. CONCLUSION

From the foregoing analysis as a whole it follows that the most important role in the solid hydrogen-plasma interaction is that nearly total shielding of the pellet by its own neutral ablatant occurs through the establishment of a dense ablation cloud. The integrated cloud density is largely determined by

the pellet size and governs the ablation rate by maintaining a "range limited" cloud thickness. Above plasma densities of 10^{13} cm^{-3} the exact details of the boundary conditions at the pellet surface become immaterial except possibly in determining T_1 which is used in the determination of Γ.

Because of the large ionization radius compared to the pellet size and the very low temperature of the ablatant ($\leq$ .1ev.) if $T_e < 5$ KeV., $n_e < 5 \times 10^{13}$ cm^{-3} we do not expect the magnetic field to alter the "spherical" expansion near the pellet where shielding is most effective.

The model gives a good agreement with the recent pellet injection experiment performed on the ORMAK Tokamak. Hopefully other experiments will be performed using larger pellets and faster injection speeds so that the scaling laws for the pellet lifetime and surface regression speed can be tested over a wide range of plasma densities and temperatures.

TABLE I. IONIZATION RADIUS NORMALIZED TO PELLET RADIUS FOR NEUTRAL ABLATION CLOUD AS A FUNCTION OF PLASMA TEMPERATURE AND DENSITY

($\xi_I = r_I/r_p$)

	ξ_I					
T_{eo}	$n_{eo} = 10^{13}\ cm^{-3}$		$n_{eo} = 5 \times 10^{13}$		$n_{eo} = 1 \times 10^{14}$	
(ev.)	$r_p = .02$	$r_p = .05$	$r_p = .05$	$r_p = .1$	$r_p = .1$	$r_p = .2$
200	333	134	27.4	14.2	7.57	4.28
500	414	166	34	17.5	9.1	5.05
1000	635	255	51.7	26.4	13.7	7.35
5000	1282	513	103	52	26.6	13.8

APPENDIX

DERIVATION OF $\sigma_B(\theta,E)$ AND $\sigma_{MS}(E)$

In this appendix the backscattering cross section, $\sigma_B(\theta,E)$, introduced below Eq. (4) is determined. A polar coordinate system (see Fig. 2) is imposed such that the z-axis is orientated along the magnetic field and points in the direction of the pellet. The velocity vector, $\vec{V}$, of the electron before the collision lies in the xz plane and has a pitch angle θ (after collision its velocity is $\vec{V}'$ and it has a new pitch angle θ') and scatters through an angle ξ with respect to $\vec{V}$. $|\vec{V}| \simeq |\vec{V}'|$. The solid angle into which which the electron is scattered is $\sin\theta'\, d\theta'\, d\phi'$; therefore a differential scattering cross section for scattering from θ to θ', 0 to ϕ' is

$$\frac{d\phi(\xi)}{d\Omega} \sin\theta'\, d\theta'\, d\phi' \tag{A1}$$

whence it follows that an effective differential scattering cross section for scattering from θ to θ' anywhere in the annular strip $2\pi \sin\theta'\, d\theta'$ becomes

$$P(\theta,\theta') \sin\theta'\, d\theta' = \int_0^{2\pi} \frac{d\sigma(\xi)}{d\Omega} \sin\theta'\, d\theta'\, d\phi' \tag{A2}$$

Equation (A2) is now a "pitch angle" differential scattering cross section. To evaluate Eq. (A2), the Euler relation is invoked, viz.,

$$\cos\xi = \cos\theta \cos\theta' + \sin\theta \sin\theta' \cos\phi' \tag{A3}$$

The expression for the differential elastic scattering cross section for electrons on hydrogen [18] is given by

$$\frac{d\sigma(\xi)}{d\Omega} = \frac{\sigma_o[2 + 2\varepsilon(1 - \cos\xi)]^2}{[1 + 2\varepsilon(1 - \cos\xi)]^4} \tag{A4}$$

where $\sigma_o = \frac{4\pi^4 m_e^2 e^4 a_o^4}{h^4}$; the dimensionless energy of the electron, $\varepsilon = E \Big/ \left(\frac{2\pi^2}{m_e a_o^2}\right)$; and a_o and E are the Bohr radius and electron energies in ergs, respectively. Substituting Eq. (A3) into Eq. (A4) and Eq. (A4) into Eq. (A2), one has, after some rearrangement,

$$P(0,0')\sin\theta'\,d\theta' = \sigma_o \sin\theta'\,d\theta' \int_0^{2\pi} \frac{A^2 + 2AB\cos\phi + B^2\cos^2\phi}{[C + B\cos\phi]^4}\,d\phi \tag{A5}$$

where

$$A = 2 + 2\varepsilon - 2\varepsilon\cos\theta\cos\theta'$$

$$B = 2\sin\theta\sin\theta'$$

$$C = A - 1 \,. \tag{A6}$$

Since $C^2 > B^2$, then $\int_0^{2\pi} \rightarrow 2\int_0^{\pi}$, and Eq. (A5) can be integrated to obtain

$$P(\theta,0')\sin\theta'\,d\theta' = \frac{\sigma_o \pi}{(C^2 - B^2)^{7/2}} \cdot \{2A^2C^3 - 8AB^2C^2 + 3A^2B^2C - 2AB^4 + B^2C^3 + 4B^4C\} \cdot \sin\theta'\,d\theta' \,. \tag{A7}$$

Inspection of Eq. (A7) shows that as $\theta \rightarrow 0$, $P(0,\theta') \rightarrow 2\pi\sigma_o \frac{d\sigma(\theta')}{d\Omega}$ because $\xi \rightarrow \theta'$.

The backscattering cross section for electrons with initial pitch angle θ and dimensionless energy ε is given by

$$\sigma_B(\theta,\varepsilon) = \int_{\pi/2}^{\pi} p(\theta,\theta')\sin\theta'\,d\theta' = \int_{-1}^{0} P(\mu,\mu')\,d\mu' \,. \tag{A8}$$

So,

$$\frac{\sigma_B(0,c)}{\sigma_o\pi} = A_o I + \left[\frac{1}{5c}\left(\frac{1}{\Delta} - \frac{1}{a^{5/2}}\right) - \frac{b}{2c}\, I\right] A_1 \qquad (A9)$$

$$+ \left[\frac{-1}{4\Delta c}\left(1 + \frac{3b}{10c}\right) + \frac{3b}{40c^2 a^{5/2}} + \frac{1}{c}\left(\frac{a}{4} + \frac{3b^2}{16c}\right) I\right] A_2$$

$$+ \left[\frac{1}{\Delta c}\left(\frac{1}{3} + \frac{2a}{15c} + \frac{b}{24c} + \frac{b^2}{80c^2}\right) - \frac{1}{a^{5/2}c^2}\left(\frac{2a}{15} + \frac{b^2}{80c}\right) - \frac{1}{c^2}\left(\frac{3ab}{8} + \frac{b^3}{32c}\right) I\right] A_3$$

$$+ \left[\frac{1}{\Delta c}\left(\frac{-1}{2} - \frac{3a}{8c} + \frac{b}{12c} - \frac{19ab}{240c^2} + \frac{b^2}{96c^2} + \frac{b^3}{320c^3}\right) + \frac{1}{a^{5/2}c^3}\left(\frac{19ab}{240} - \frac{b^3}{320c}\right)\right.$$

$$\left. + \frac{1}{c^2}\left(\frac{3a^2}{8} + \frac{3ab^2}{16c} - \frac{b^4}{128c^2}\right) I\right] A_4 + \left[\frac{1}{\Delta c}\left(1 + \frac{4a}{3c} - \frac{3b}{4c} + \frac{8a^2}{15c^2} - \frac{19ab}{48c^2}\right.\right.$$

$$\left. + \frac{b^2}{8c^2} - \frac{11ab^2}{160c^3} + \frac{b^3}{64c^3} + \frac{3b^4}{640c^4}\right) - \frac{1}{a^{5/2}c^3}\left(\frac{8a^2}{15} + \frac{3b^4}{640c^2}\right)$$

$$\left. + \frac{1}{c^3}\left(\frac{-15a^2b}{16} + \frac{5}{32}\frac{ab^3}{c} - \frac{3b^5}{256c^2}\right) I\right] A_5$$

where

$$a = 1 + 4\varepsilon + 4\varepsilon^2\mu^2,\quad c = 4\varepsilon^2\ ,$$

$$\Delta = (a - b + c)^{5/2}$$

$$b = -(4\varepsilon\mu + 8\varepsilon^2\mu),\quad \mu = \cos\theta,\quad \ell = 2(1 + \varepsilon),\quad \beta = 2\varepsilon\mu\ .$$

$$A_o = 2\ell^5 - 6\ell^4 + 6\ell^3 - 2\ell^2 + 4\varepsilon^2(1-\mu^2)[-4\ell^3 + 10\ell^2 - 5\ell - 1] + 64\varepsilon^5(1-\mu^2)^2$$

$$A_1 = -10\ell^4\beta + 24\ell^3\beta - 18\ell^2\beta + 4\ell\beta + 4\beta\varepsilon^2(1-\mu^2)[12\ell^2 - 10\ell + 5] - 64\varepsilon^5\mu(1-\mu^2)^2$$

$$A_2 = 20\ell^3\beta^2 - 36\ell^2\beta^2 + 18\ell\beta^2 - 2\beta^2 + 4\varepsilon^2(1-\mu^2)[-12\ell\beta^2 + 10\beta^2 + 4\ell^3 - 10\ell^2 + 5\ell + 1] - 128\varepsilon^5(1-\mu^2)^2$$

$$A_3 = -20\ell^2\beta^3 + 24\ell\beta^3 - 6\beta^3 + 4\varepsilon^2\beta(1-\mu^2)[4\beta^2 - 12\ell^2 + 10\ell - 5] + 128\varepsilon^5\mu(1-\mu^2)^2$$

$$A_4 = 2\beta^4(5\ell - 3) + 8\varepsilon^2\beta^2(1-\mu^2)[6\ell - 5] + 64\varepsilon^5(1-\mu^2)^2$$

$$A_5 = -2\beta^5 - 16\beta^3\varepsilon^2(1-\mu^2) - 64\varepsilon^5\mu(1-\mu^2)^2$$

and

$$I = \frac{2b}{5(4ac - b^2)a^{5/2}}\left\{1 + \frac{16ac}{3(4ac - b^2)} + \frac{128a^2c^2}{3(4ac - b^2)^2}\right\}$$

$$+ \frac{2(2c - b)}{5(4ac - b^2)(a - b + c)^{5/2}}\left\{1 + \frac{16c(a - b + c)}{3(4ac - b^2)} + \frac{128c^2(a - b + c)^2}{3(4ac - b^2)^2}\right\}.$$

It is reassuring to note that $\sigma_B(\theta = \frac{\pi}{2}, \varepsilon)$ is one half of the total cross section as it should be, i.e.,

$$\sigma_B(\theta = \pi/2, \varepsilon) = 8\pi\sigma_o \frac{3 + 18\varepsilon + 28\varepsilon^2}{3(1 + 4\varepsilon^2)^3} . \tag{A10}$$

The multiple scattering cross section σ_{MS} can be obtained by considering the cumulative small angle scattering events which lead to a total mean square deflection angle $< \xi^2 >$ in a distance z:

$$<\xi^2> = 2\pi nz \int_0^{\pi/2} \frac{\xi^2 \, d\sigma(\xi)}{d\Omega} \sin \xi \, d\xi. \tag{A11}$$

From (A10) the cross section for 90° scattering by multiple collisions, $\sigma_{MS}(E)$, is usually defined as (setting $< \xi^2 > = 1$ [35]

$$\sigma_{MS}(E) = 2\pi \int_0^{\pi/2} \xi^2 \frac{d\sigma}{d\Omega} \sin \xi \, d\xi \tag{A12}$$

which, after substituting (A4) into (A11), becomes

$$\sigma_{MS}(E) = \frac{4\pi^5 m^2 e^4 a_o^4}{n^4} \frac{1}{\varepsilon^2} \left[\frac{(1 + \varepsilon)^3 \ln(1 + \varepsilon) - \varepsilon - \varepsilon^2/2}{(1 + \varepsilon^3)} \right] \tag{A13}$$

REFERENCES

[1] L. Spitzer, Jr., D. J. Grove, W. E. Johnson, L. Tonks, and W. R. Westendrop, "Problems of the stellarator as a useful power source," USAEC, Report N. Y. O.-6047, 1954.

[2] D. J. Rose, Colham Laboratory Technology Division, Memorandum No. 82, 1968.

[3] C. T. Chang, Nuclear Fusion, vol. 15, p. 595, 1975.

[4] S. L. Gralnick, Nuclear Fusion, vol. 13, p. 703, 1973.

[5] S. L. Gralnick, A Fusion Power Plant, R. G. Mills, Ed., Princeton Plasma Physics Laboratory Report No. MATT-1050, 1974, unpublished, Chapter 7.

[6] L. R. Peterson and A. E. S. Green, J. Phys. B., Ser. 2, vol. 1, p. 1131, 1968.

[7] W. T. Miles, R. Thompson, and A. E. S. Green, J. Appl. Phys., vol. 42, p. 678, 1972.

[8] B. Peart and K. T. Dolder, J. Phys. B., vol. 7, p. 236, 1974.

[9] J. W. McGowan, R. Caudano, and J. Keyser, Phys. Rev. Letters, vol. 36, p. 1447, 1976.

[10] G. H. Dunn and B. Van Zyl, Physical Review, vol. 154, p. 40, 1967.

[11] R. E. Christoffersen, "Configuration-interaction study of the ground state of the H_3^+ molecule, J. Chem. Phys., vol. 41, pp. 960-971, 1964.

[12] H. P. Furth, Nuclear Fusion, vol. 15, p. 487, 1975.

[13] V. J. Johnson, Properties of Materials as Low Temperature (Phase 1), Pergamon Press, 1961.

[14] H. Sorensen, Nuclear Instr. and Methods, vol. 132, pp. 377-379, 1976.

[15] S. Goudsmit and J. L. Saunderson, Physical Review, vol. 57, p. 24, 1940 and vol. 58, p. 36, 1940.

[16] H. W. Lewis, Physical Review, vol. 78, p. 526, 1950.

[17] L. V. Spencer, Physical Review, vol. 98, p. 1597, 1955.

[18] N. F. Mott and H. S. W. Massey, The Theory of Atomic Collisions, Oxford University Press, 1965, p. 455.

[19] H. T. Maecker, H. Schenk and W. J. Peters, Z. Phys., vol. 140, p. 119, 1955.

[20] W. T. Miles, R. Thompson and A. E. S. Green, J. Appl. Phys., vol. 42, p. 678, 1972, private communication, 1975.

[21] R. Andersen, Atomic Data, vol. 3, p. 227, 1971.

[22] R. Geller, Report EUR. CEA. FC 647, 1972.

[23] P. B. Parks, Model of an Ablating Solid Hydrogen Pellet in A Plasma Ph.D. Thesis, University of Illinois, Urbana, 1977.

[24] H. M. Roder, G. E. Child, R. D. McCarty and P. E. Angerhofer, NBS Technical Note 641, National Bureau of Standards, Boulder, Colorado, 1973.

[25] H. J. Allen, "On the motion and ablation of meteoric bodies," in Aeronautics and Astronautics, N. J. Hoff and W. G. Vincenti, Eds. New York: Pergamon Press Inc., 1960, p. 378.

[26] E. J. Opik, Physics of Meteor Flight in the Atmosphere, Interscience, New York, 1958, Chapter 4.

[27] J. A. Owczarek, Fundamentals of Gas Dynamics, International Textbook Co., Scranton, Pennsylvania, 1964, p. 115.

[28] F. Reif, Fundamentals of Statistical and Thermal Physics, McGraw-Hill Book Co., New York, 1965, p. 271.

[29] J. R. Maa, Industrial and Engineering Chemistry Fundamentals, vol. 6, p. 504, 1967.

[30] A. H. Shapiro, The Dynamics and Thermodynamics of Compressible Fluid Flow, The Ronald Press Company, New York, 1973.

[31] K. Kim, R. J. Turnbull, R. Colchin, C. A. Foster and S. Milora, to be published.

[32] O. N. Krokhin, Soviet Physics-Technical Physics, vol. 9, p. 1024, 1965.

[33] D. Rapp and P. Englander-Golden, J. Chem. Phys., vol. 43, p. 1464, 1965.

[34] J. W. Davis and G. L. Kubcinski, Nuclear Fusion, vol. 16, p. 355, 1976.

[35] N. A. Krall and A. W. Trivelpiece, Principles of Plasma Physics, McGraw-Hill Inc., New York, 1973, p. 293.

LIST OF FIGURES

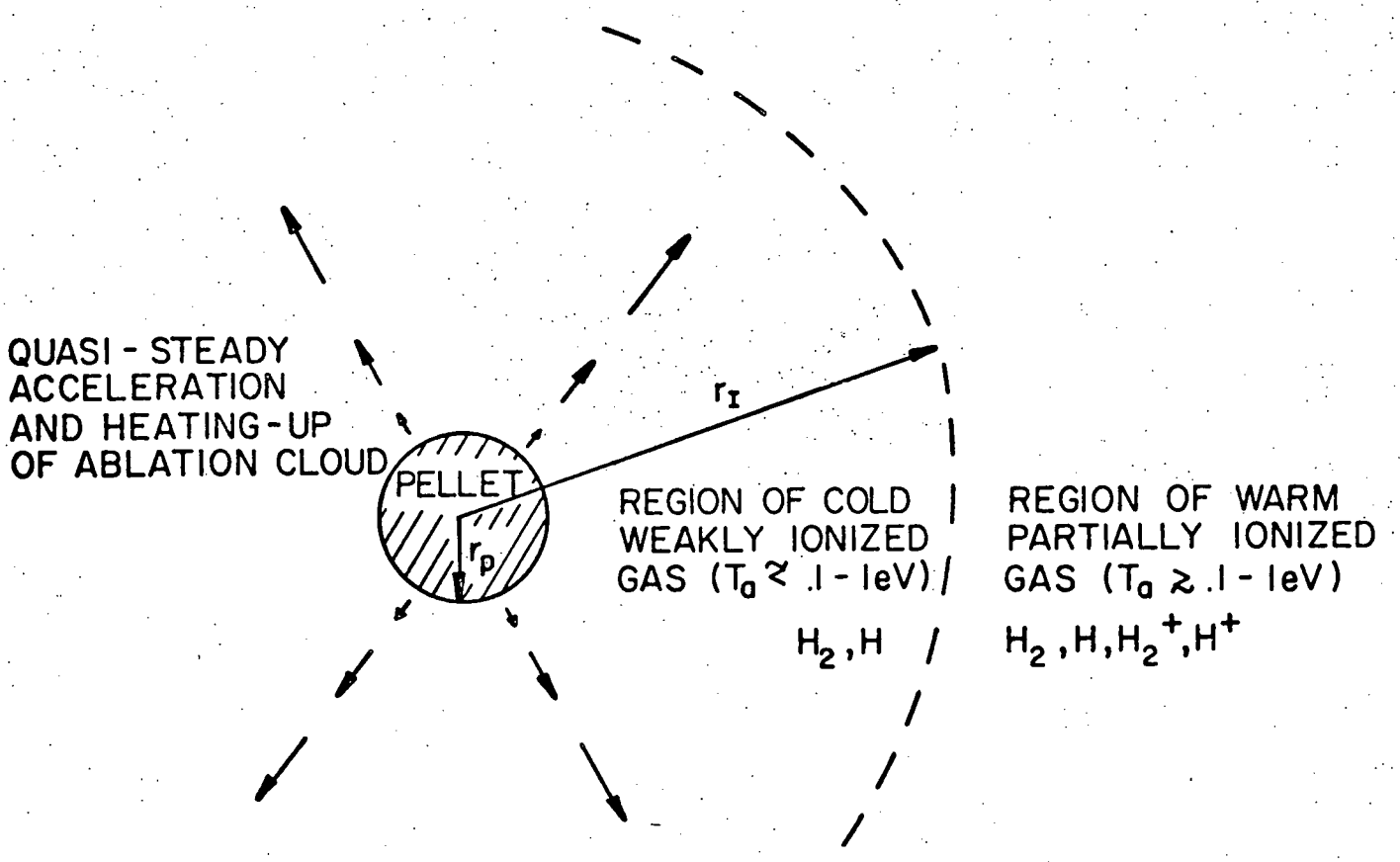
QUASI - STEADY
ACCELERATION
AND HEATING - UP
OF ABLATION CLOUD
PELLET
r_I
r_p
REGION OF COLD
WEAKLY IONIZED
GAS ($T_a \gtrsim .1 - 1eV$)
H_2, H
REGION OF WARM
PARTIALLY IONIZED
GAS ($T_a \gtrsim .1 - 1eV$)
H_2, H, H_2^+, H^+

Figure 1a

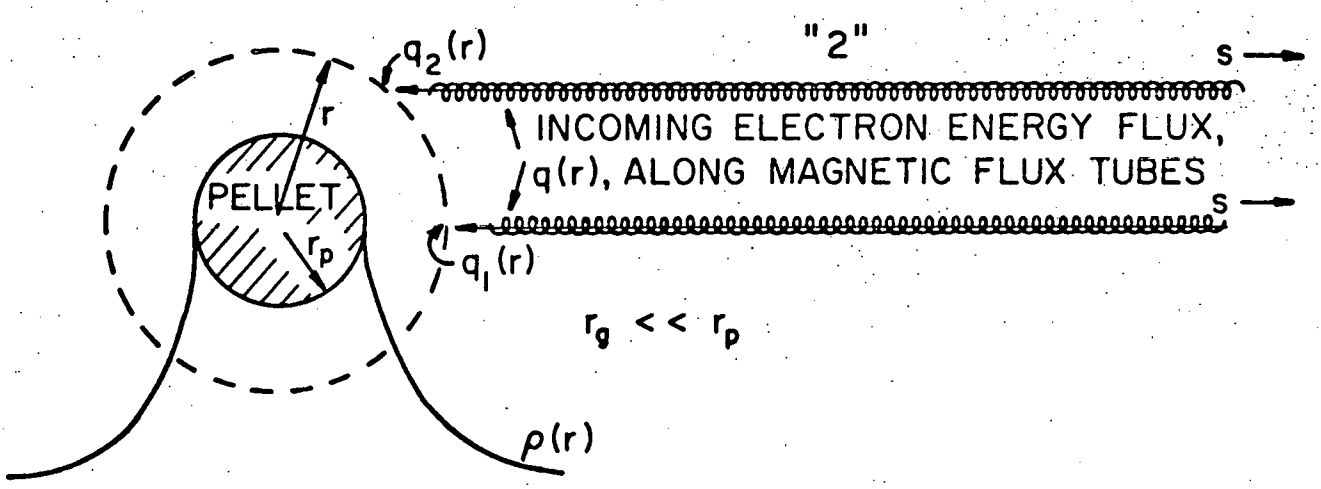
$q_2(r)$
"2"
s
INCOMING ELECTRON ENERGY FLUX,
q(r), ALONG MAGNETIC FLUX TUBES
s
r
PELLET
r_p
$q_1(r)$
$r_g << r_p$
$\rho(r)$

Figure 1b

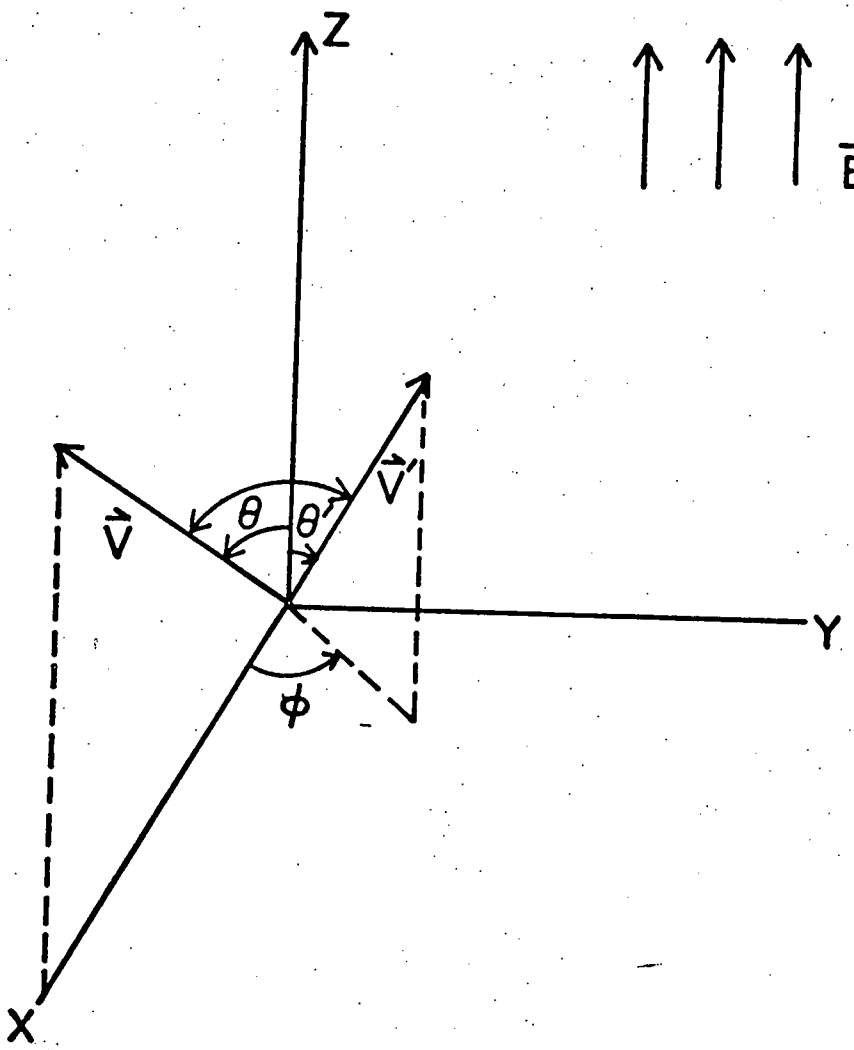

Figure 2

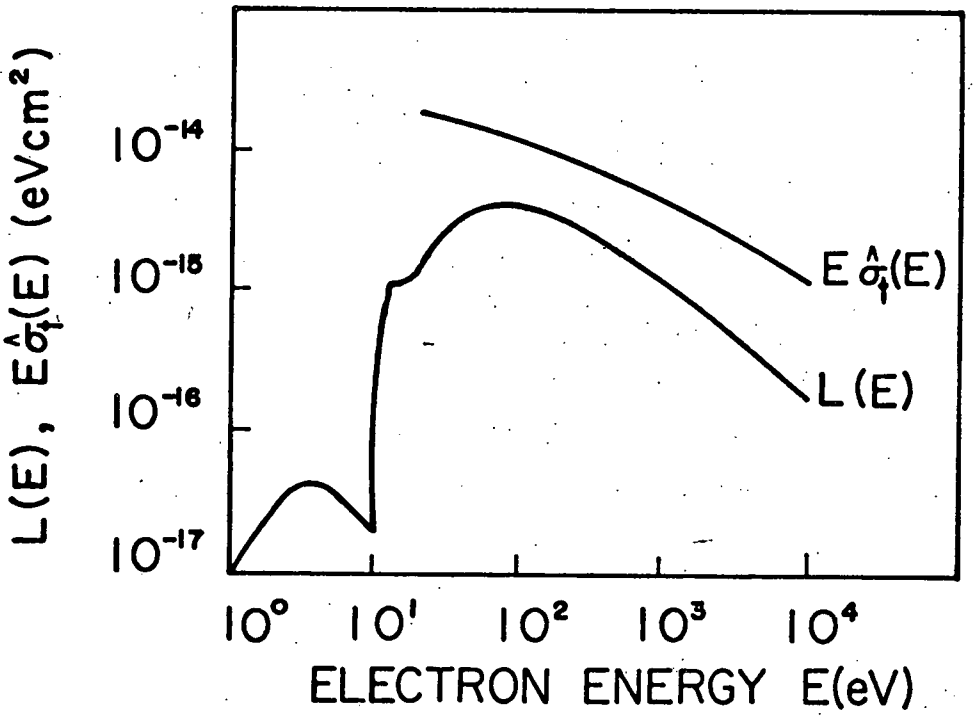
L(E), E$\hat{\sigma}_i$(E) (eVcm^2)
10^{-14}
10^{-15}
10^{-16}
10^{-17}
E $\hat{\sigma}_i$(E)
L(E)
10^0 10^1 10^2 10^3 10^4
ELECTRON ENERGY E(eV)

Figure 3

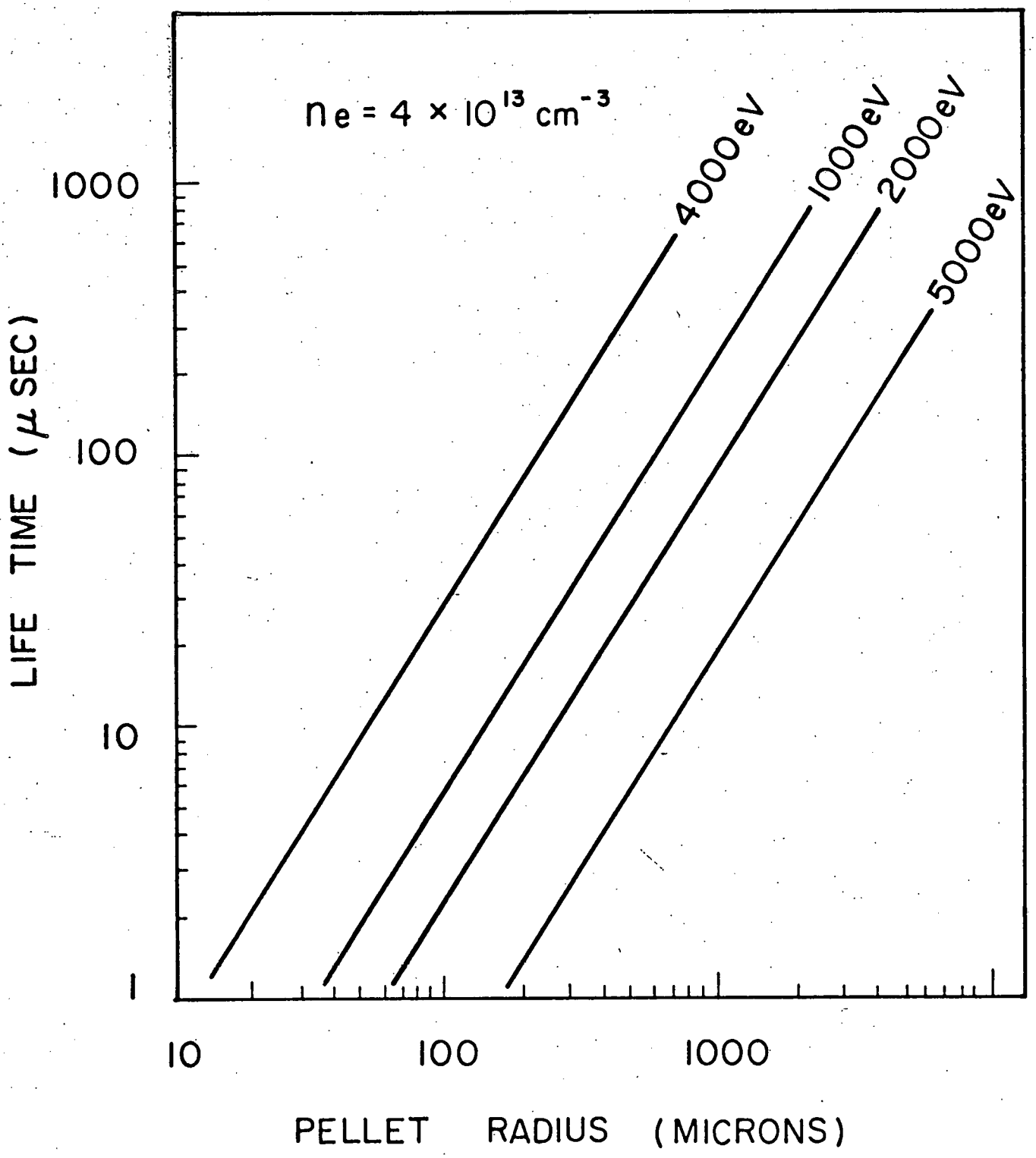
$n_e = 4 \times 10^{13}\ cm^{-3}$
4000eV
1000eV
2000eV
5000eV
1000
100
10
1
LIFE TIME (μ SEC)
10
100
1000
PELLET RADIUS (MICRONS)

Figure 4a

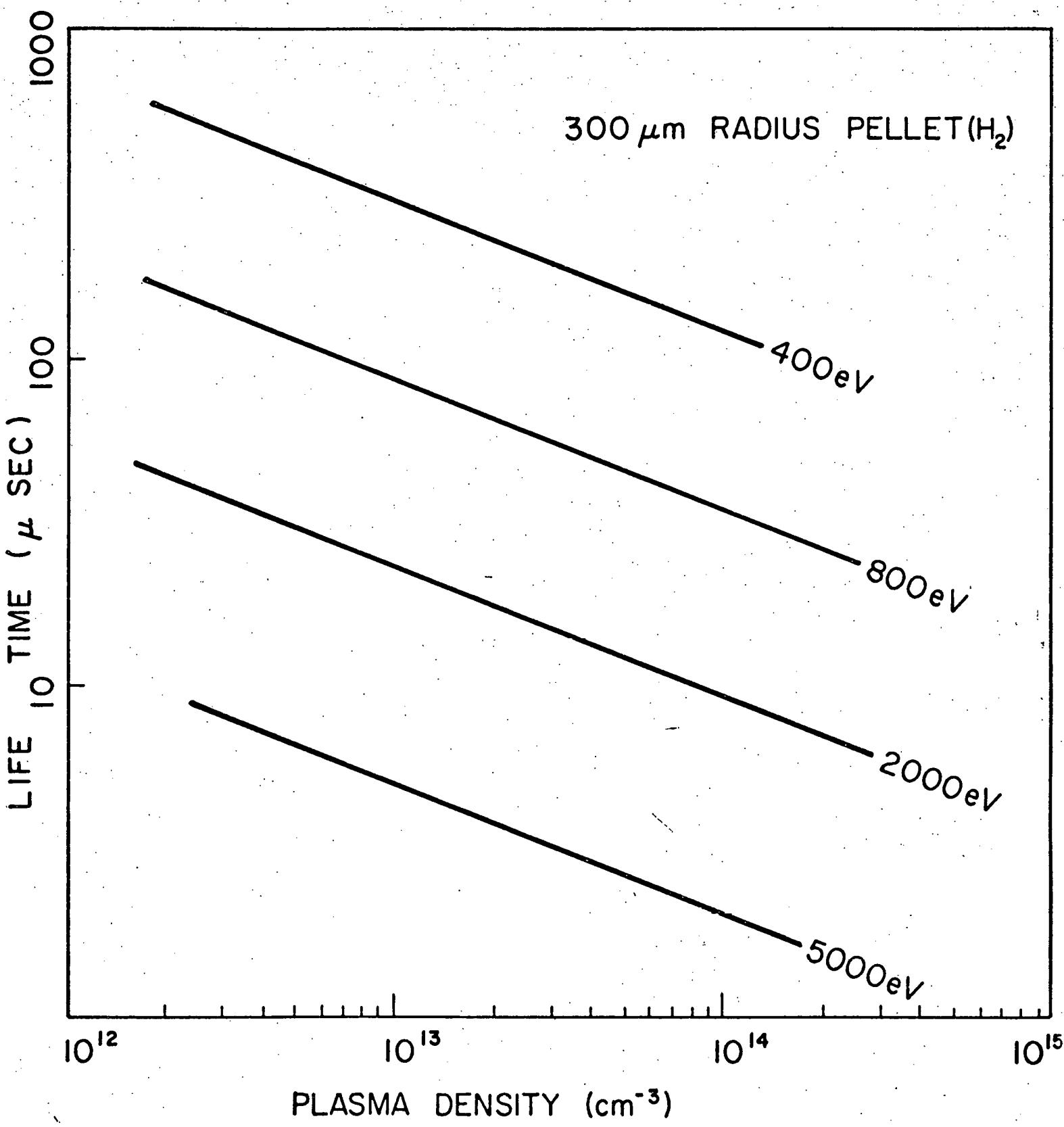
300 μm RADIUS PELLET (H2)
400eV
800eV
2000eV
5000eV
LIFE TIME (μ SEC)
1000
100
10
10^12
10^13
10^14
10^15
PLASMA DENSITY (cm^-3)

Figure 4b

A TECHNIQUE FOR PRODUCING UNIFORM CHARGED DROPS OF CRYOGENIC LIQUIDS

J. P. Woosley and R. J. Turnbull
Department of Electrical Engineering
University of Illinois
Urbana, Illinois 61801

Abstract

We have investigated and developed a reliable method to produce uniformly charged liquid nitrogen drops. An apparatus has been built which is capable of producing and charging drops in the 200 micron diameter range. Rayleigh's method of uniform droplet production which consists of a smooth liquid jet being broken up into uniform drops by an acoustic wave is used. The diameter of the drops is controlled by the inside diameter of the nozzle and the frequency of the acoustic wave. Charges injected into the jet through field emission or field ionization subsequently end up on the drops thereby producing uniformly charged drops. The charge per drop is determined by the amount of charge injected into the jet and by the number of drops produced per second. The maximum charge which could be placed on a single drop such that it maintained its integrity was 1/5 of its Rayleigh limit. The method described here could be applied to other insulating cryogenic liquids such as liquid hydrogen.

1. INTRODUCTION

Charged particles of very small size have a wide range of interesting applications in many fields of applied science.[1] In particular, uniformly charged insulating cryogenic particles have recently become of interest due to two very important applications in controlled thermonuclear fusion (CTF)—first the refueling of Tokamaks, and second targets for laser fusion experiments.

Proposed Tokamak reactors, due to their long pulse time, will have to be refueled. The most promising method seems to be by injection of macroscopic pellets of deuterium-tritium.[2] With charged pellets the refueling could be accurately controlled by deflecting out unnecessary fuel. The first pellet injection experiment on a Tokamak, was carried out by Foster et al in 1975.[3] Uniform uncharged hydrogen pellets of 70 micron diameter were injected into the Oak Ridge Tokamak (ORMAK) at a speed of 95 meters per second.

In laser fusion, intense laser light is focused on a uniform macroscopic pellet of deuterium-tritium positioned in a specially designed reactor. In a preliminary design, the pellets from the pellet generator are allowed only to reach the burn area by a zigzag path.[4] Charged pellets can be easily manipulated through this path and they can be accurately positioned in space, thereby allowing the prefocused laser light to evenly illuminate them. Pellets of extreme uniformity are required and they must be produced at a rate of 100 per second in order to provide a useful amount of power.[4] Rayleigh's method of pellet production which is described in the next paragraph can easily satisfy these requirements.

The method of droplet production which was first investigated by Lord

Rayleigh in 1879,[5] consists of applying a pressure drop across a nozzle (capillary) which results in a smooth liquid jet. The liquid jet is then broken up into uniform liquid drops by the effects of surface tension and an applied acoustic wave. In 1956 Magarvey and Taylor[6] used Rayleigh's method to produce water drops from 0.3 to 20 millimeters (mm) in diameter using three droplet generators. In 1960 Schotland[7] made further improvements by using hypodermic needles tuned to resonance. By changing the hypodermic needle only he produced drops from 0.3 to 1.0 mm in diameter.

Schneider and Hendricks[8] in 1964 and Lindblad and Schneider[9] in 1965 used a PZT bimorph piezoelectric transducer in conjunction with an audio oscillator to produce the acoustic wave energy necessary to break up a water jet into uniform drops. The range over which the droplet diameters could be varied was from 50 to 700 microns. Individual drops could be selected by charging all the drops except one. The charged drops were deflected out, thereby leaving the desired drop. Magarvey and Blackford,[10] and others[11-13] have produced uniformly charged drops. The method used for charging the drops in all cases has been basically the same since conducting fluids were used. The method is known as induction charging and consists of applying a voltage between the conducting jet and a concentric cylindrical electrode. The electric field induces charge to flow in the jet which subsequently breaks up into charged drops.

Generation of uniformly charged drops of insulating cryogenic liquids is naturally much more difficult. First, to produce cryogenic drops the jet assembly (capillary, mechanical transducer, etc.) must be cooled down to cryogenic temperatures. This requires a heat exchanger and some form of thermal insulation. Secondly, in charging insulating liquids, the simple method of charge induction will not work. A more complex and

generally more difficult method has to be used. Two such methods are field emission and field ionization. These two charging methods were used by Halpern and Gomer in 1969[14,15] to measure electron and ion mobilities of a few cryogenic insulating liquids.

In this paper we are reporting on a reliable method of producing uniformly charged cryogenic drops. In the actual investigation, liquid nitrogen was chosen over liquid hydrogen because the physical properties of liquid nitrogen are similar to those of liquid hydrogen yet the boiling temperature of nitrogen is higher so that it is easier to produce a liquid jet. The jet, produced by a pressure drop across a nozzle, will be broken up into uniform drops by surface tension and an applied acoustic wave. The drops will be charged by field emission and field ionization. This method of charging consists of applying a high potential to a very sharp tungsten tip immersed in the jet. Depending upon the polarity of the applied potential, the high field at the tip will field emit electrons into the jet or field ionize the jet. The charged jet will then break up into uniformly charged drops.

2. EXPERIMENTAL APPARATUS

The apparatus used to produce uniform drops of liquid nitrogen consists of three major parts, the heat exchanger, the vacuum chamber used for thermal insulation, and the jet assembly.

The heat exchanger is used to provide a source of liquid nitrogen at a controlled temperature and pressure. This nitrogen is formed by liquefying gaseous nitrogen rather than taking liquid nitrogen directly from a Dewar because of the difficulty in regulating the pressure of the nitrogen from the Dewar to below one atmosphere. The pressure control is necessary to properly form the jet. The heat exchanger which is shown in Figure 1 is a solid copper rod, 2.5 centimeters (cm) in diameter, wrapped with 0.32 and 0.64 cm diameter soft copper tubing, all soft-soldered together for good thermal contact. The nitrogen for the jet flows through the .32 cm tubing and liquid nitrogen which is used to liquefy the gaseous nitrogen flows through the .64 cm tubing.

Referring to Figure 2, the nitrogen for the jet is obtained as follows. A bottle of gaseous nitrogen is connected to a pressure regulator and then to a vacuum regulator. The vacuum regulator is connected to a liquid nitrogen sieve, to a filter and then to the 0.32 cm copper tubing (heat exchanger). From the heat exchanger which liquefies the gaseous nitrogen, nitrogen goes by way of the 0.32 cm tubing to the jet assembly. The liquid nitrogen sieve removes all condensible gases. The vacuum regulator controls the pressure of the liquid nitrogen at the nozzle inlet.

The liquid nitrogen used for cooling comes from a pressurized Dewar through a transfer tube and a filter to a needle valve and then to the 0.64 cm copper tubing in the heat exchanger. From the 0.64 cm copper

tubing the liquid nitrogen is exhausted through a 1.3 cm valve using a mechanical pump. Thus, the liquification of the nitrogen for the jet is accomplished by flashing pressurized (≈ 5 p.s.i.g.) liquid nitrogen into the heat exchanger at a pressure below one atmosphere.

The temperature of the heat exchanger is controlled by the amount of liquid nitrogen allowed to flash in and is measured with a vapor pressure thermometer. The thermometer consists of a 0-760 Torr vacuum gauge connected to a closed chamber filled with gaseous and liquid nitrogen in thermal contact with the heat exchanger. By measuring the vapor pressure, the temperature of the nitrogen liquid can be found from a vapor pressure versus temperature curve.

The droplet chamber and the jet assembly are in direct thermal contact with the heat exchanger. The droplet chamber, as shown in Figure 1, consists of a 0.16 cm wall thickness brass tube 6.4 cm in diameter and 25.4 cm long with two brass plates, 0.32 cm thick and 7.6 cm in diameter bolted to the ends. The heat exchanger is soft-soldered to the top end plate with the jet assembly bolted to the opposite side of the plate.

The droplet chamber has 4 windows which allow the drops to be seen at two different points in space. An image of the drops is focused on a frosted glass plate with a strobe light and a plane convex lens. The lens has a diameter of 8 mm and a focal length of 38 mm. Photographs are taken on high speed film by flashing the strobe light once.

A vacuum in the droplet chamber is controlled by a differential vacuum regulator in conjunction with a mechanical vacuum pump. Thermal insulation is achieved by maintaining the heat exchanger and the droplet chamber in a vacuum on the order of 10^{-5} Torr, and also by using thin wall stainless steel tubing for all physical connections except electrical.

The jet assembly, one of the most important parts of the droplet generator, is shown in Figure 3. It consists of a hollow copper rod silver-soldered to a specially designed filter holder. The length of the copper rod (3.5 cm) is such that it has a natural resonance frequency of 50 kilohertz. A Pyrex glass capillary with a 4 mm outside diameter is shaped into an exponential horn using a glass lathe. The exponential horn amplifies an acoustic wave which is sent down the jet by the piezoelectric transducer. The actual amplification of the acoustic wave takes place in the fluid inside the horn with the maximum amplitude of the wave being at the output end where the liquid jet forms. The acoustic wave along with surface tension causes the jet of liquid nitrogen to break up into uniform drops.

The piezoelectric transducer is powered by a signal generator in conjunction with a wideband amplifier. The output frequency of the signal generator, over a limited range, determines the number of drops produced per second. The signal generator also controls a strobe trigger. Since the number of drops produced per second is much greater than the ability of the strobescope to flash (once for each drop) the strobe trigger is required. The strobe trigger is a frequency divider which divides the input frequency by some multiple number. The strobe flash is synchronized with the drops such that they can be seen standing still.

The piezoelectric transducer is a Vernitron PZT-4 ceramic tube with a resonant frequency of 65 kilohertz. The tube has the following dimensions; 2.5 cm length, 1.3 cm outside diameter, and 0.64 cm inside diameter. A Kovar tube with the same dimensions except for length (0.8 cm) is glued to the transducer, thus producing a new resonant frequency of 50 kilohertz.

The drops are charged by a high potential applied to a very sharp

thoriated tungsten needle. The resulting high fields inject charges into the jet which subsequently breaks up into uniformly charged drops. The amount of charge injected into the jet is determined by the current in the tungsten needle circuit which is controlled with a current limiter.

The tungsten needle is electrically insulated from the jet assembly by a glass filament as shown in Figure 3. The glass filament is secured by soft-solder to a brass screw head, which enables the tungsten tip to be moved in and out of the nozzle outlet. A high voltage electrical connection is made to the tungsten needle by slotting the glass nozzle near the end. A small nickel tube is then placed inside the glass nozzle with a high-voltage line soft-soldered to it. Then, RTV, a silicone rubber sealant, is applied around the slot sealing it off. The tungsten needle inside the nozzle is in physical contact with nickel tube, thereby completing the electrical connection. The needle is etched in a 0.4 mole solution of Sodium Hydroxide (NaOH) by a 5 volt, 60 hertz potential. The tip radius was then estimated to be less than 2500 angstroms through measurements taken with a microscope at a magnification of 315. The method of measuring the droplet charge consists of measuring the current before it is injected into the jet with a micro-micro ammeter as shown in Figure 2. By knowing the number of drops produced per sec., one can then obtain the charge per drop.

In the measurement of the charge on the drops, the current measurements are in the nanoampere range. With the tungsten tip at a very high potential ($\simeq$ 10 kilovolts) inaccuracies could therefore be introduced by current leakage along the surface of the high voltage feedthrough. In order to minimize this effect an insulated wire is fed through the hollow feedthrough and glue is applied around the wire to maintain the vacuum

seal. With this added insulation the leakage current was substantially decreased.

As another check, a droplet collection cup at a very low potential (≃ 5 volts) is used to collect the charged drops and the current produced is measured.

3. EXPERIMENTAL RESULTS

The apparatus described in the preceding section has successfully produced uniformly charged liquid nitrogen drops in the 200 micron diameter range. In operating the droplet generator, the following results were noted.

Using the vapor pressure thermometer, no change in liquid temperature could be detected once a continuous jet was produced. A slight drift in temperature (≈ 1.5 K per hour) was noted. The droplet generator could be cooled from 300 K (room temperature) to 64 K by flashing pressurized liquid nitrogen into the heat exchanger. Also, a very slight variation in the vacuum at the nozzle inlet (12.5 mm of Hg) was detected, but with no resulting adverse effects on the jet.

The vacuum chamber used for thermal insulation was generally operated in the 10^{-5} Torr range. The outer case which contains the droplet generator stayed at room temperature except at the upper end plate which was slightly cooled due to the incomplete insulation of the liquid nitrogen inlet and exhaust feeds.

After the droplet generator was cooled down and a continuous smooth jet was produced, the transducer was energized, causing the jet to break up into uniform drops. The range of frequencies over which the jet would break up into equally spaced uniform drops depends upon the pressure drop across the nozzle and the inside diameter at the outlet of the nozzle (exponential horn). The pressure drop across the nozzle could be varied from 125 to 375 mm of Hg, the nozzle inlet vacuum from 0 to 500 mm of Hg, and the droplet chamber vacuum from 250 to 600 mm of Hg.

Ten kilovolts obtained from the high voltage power supply was applied

to the current limiter. The current limiter then applies the appropriate potential to the tungsten tip such that a constant amount of charge is continuously injected into the jet. The charge injection current initially started around 5×10^{-9} amperes and was controllable up to its maximum value of 2×10^{-7} amperes.

In one typical experiment the following results were observed.

The droplet generator was cooled down to 72 K, and the nozzle inlet and droplet chamber vacuums were regulated, respectively, to 100 and 375 mm of Hg. This resulted in a pressure drop across the nozzle of 275 mm of Hg. A smooth jet was produced and broken up into uniform drops by a 17 kilohertz signal applied to the transducer. With this signal and the nozzle outlet having an inside diameter of 88.5 microns, drops having diameters of 177 microns resulted.

A sequence of photographs was taken of the jet as the current injected into the jet was slowly increased. The first sequence, shown in Figure 4, is taken with positive charges being injected into the jet.

The drops without charge are shown in Figure 4a. In the next figure, 4b, the current is 4.5×10^{-8} amperes. Note the fact that the drops are still uniform and spherical. In Figure 4c the current is 6×10^{-8} amperes and the drops have become elongated and are beginning to break apart. In the last figure, 4d, the current is at its maximum value (1.8×10^{-7} amperes) and the drops are completely disrupted and they are electrostatically spraying charges off their surface in a manner similar to the experiments in Reference 16.

In the second sequence of photographs shown in Figure 5, the jet is being injected with negative charges (electrons). The drops without charge are shown in Figure 5a. In the next figure, 5b, the current is

4×10^{-8} amperes and the drops are still uniform and spherical. In Figure 5c, the current is 5.8×10^{-8} amperes and three droplet streams are produced and electrostatically accelerated apart. The smaller drops have a larger charge to mass ratio, and therefore, they are accelerated away faster. When the current is increased breakdown is initiated, a glow discharge develops around the tip, and the current can no longer be held constant. The glow discharge around the tip is shown in Figure 5d. Once this discharge begins, the tungsten tip is immediately destroyed and will neither field emit electrons into the liquid nitrogen jet, nor induce field ionization in the jet. This effect was only observed for negative charge injection.

The method of measuring the charge per drop, as explained in Section 2, was used here. Two current measurements were made, one before the charges were injected into the jet and the other at the collection cup where the charges were being collected. These two measurements agreed very well at low currents ($\simeq 5 \times 10^{-9}$ amperes). At high currents ($\simeq 6 \times 10^{-8}$ amperes), electrostatic repulsion between the drops forced them apart such that all the drops were not collected by the collection cup. The collection cup measurements therefore became progressively lower than the injection measurements as the amount of charge injected into the jet was increased.

From the above current measurements, it was found that a maximum charge of 2.64×10^{-12} coulombs per drop could be achieved without destroying the original size of the drops. The Rayleigh limit ($q_{max} = 4\pi\sqrt{2\epsilon_o T}\, R^{3/2}$) for a drop of this size (188 microns in diameter) is 1.38×10^{-11} coulombs per drop or 5.7×10^{-7} coulombs per gram.[17] Thus the drops could be charged to about one fifth of the Rayleigh limit.

ACKNOWLEDGMENTS

This work was supported by the U. S. Energy Research Development Administration.

LIST OF REFERENCES

1) A. D. Moore, ed. Electrostatics and its Applications, New York, John Wiley, (1973).

2) R. G. Mills, ed. A Fusion Power Plant, Princeton Plasma Physics Laboratory Report, MATT-1050 (1974).

3) C. A. Foster, R. J. Colchin, C. D. Hendricks, and R. J. Turnbull, Bull. A.P.S., 20, 1300 (1975).

4) J. Emmett, J. Nuckolls, and L. Wood, "Fusion Power by Laser Implosion", Scientific American 230 (6), 24 (1974).

5) Lord Rayleigh, "On the Instability of Jets", Proceedings of the London Mathematical Society 10, 4 (1879).

6) R. M. Magarvey and B. W. Taylor, "Apparatus for the Production of Large Water Drops", Review of Scientific Instruments 27, 944 (1956).

7) R. M. Schotland, "Experimental Results Relating to the Coalescence of Water Drops with Water Surfaces", Discussions of the Faraday Society 30, 72 (1960).

8) J. M. Schneider and C. D. Hendricks, "Source of Uniform-Sized Liquid Droplets", Review of Scientific Instruments 35 (10), 1349 (1964).

9) N. R. Lindblad and J. M. Schneider, "Production of Uniform-Sized Liquid Droplets", Journal of Geophysical Research 67 (4), 1421 (1962).

10) R. H. Magarvey and B. L. Blackford, "Experimental Determination of Charge Induced on Water Drops", Journal of Geophysical Research 67 (4), 1421 (1962).

11) E. W. B. Gill and G. F. Alfrey, "The Electrification of Liquid Drops", Physical Society. Proceedings, London 65B, 546 (1952).

12) B. J. Mason, O. W. Jayaratne, and J. D. Woods, "An Improved Vibrating Capillary Device for Producing Uniform Water Droplets of 15 to 500 Micron Radius", Journal of Scientific Instruments 40 (5), 247 (1963).

13) J. M. Schneider, N. R. Lindblad, D. D. Hendricks, and J. M. Crowley, "Stability of an Electrified Liquid Jet", Journal of Applied Physics 38 (6), 2599 (1967).

14) B. Halpern and R. Gomer, "Field Emission in Liquids", Journal of Chemical Physics 51 (3), 1031 (1969).

15) B. Halpern and R. Gomer, "Field Ionization in Liquids", Journal of Chemical Physics 51 (3), 1048 (1969).

16) K. Kim and R. J. Turnbull, "Generation of Charged Drops of Insulating Liquids by Electrostatic Spraying", Journal of Applied Physics 47, 1964 (1976).

17) Lord Rayleigh, "On the Equilibrium of Liquid Conducting Masses Charged with Electricity", Philosophical Magazine 14, 184 (1882).

LIST OF FIGURES

Figure

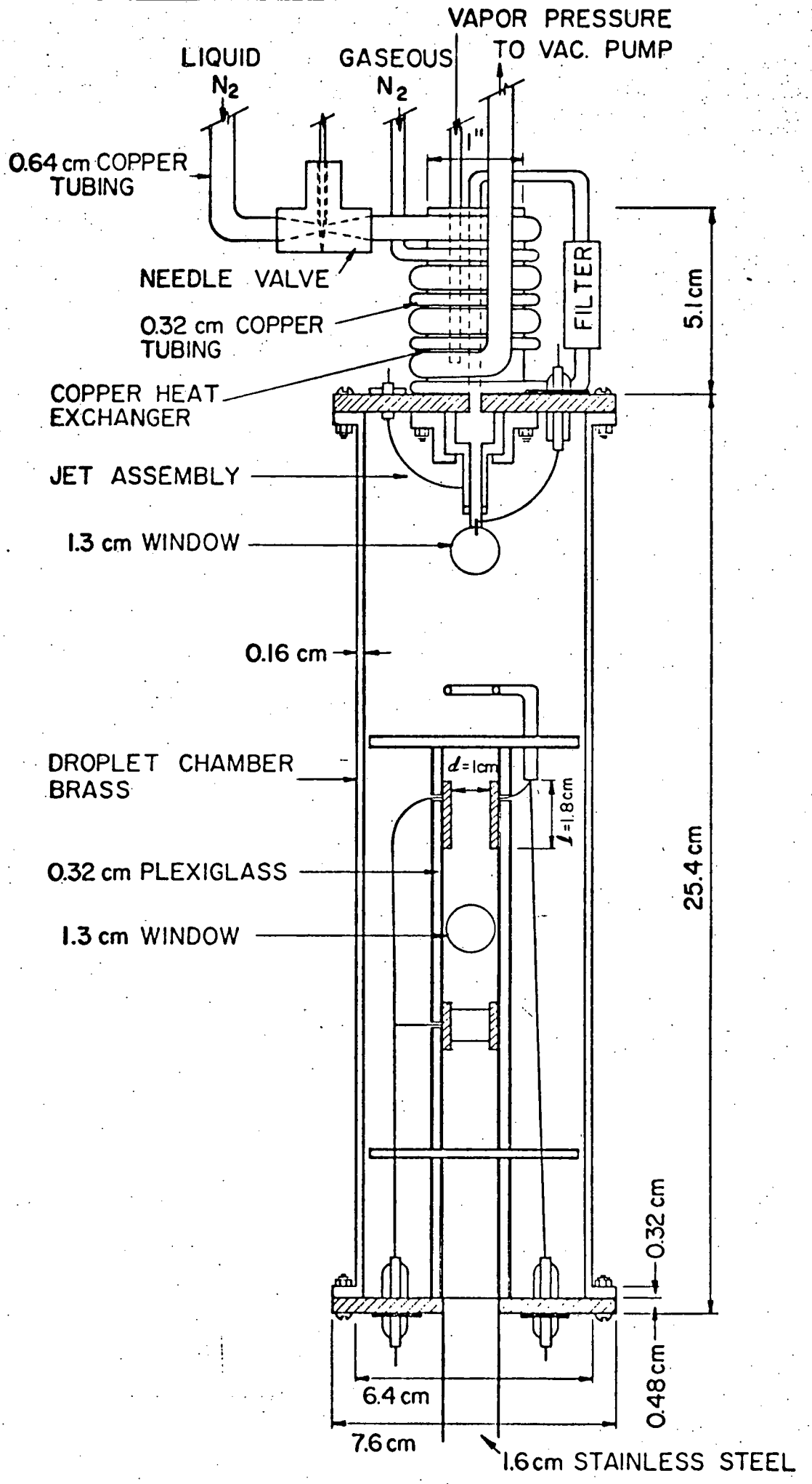
VAPOR PRESSURE
TO VAC. PUMP
LIQUID
N_2
GASEOUS
N_2
0.64 cm COPPER
TUBING
NEEDLE VALVE
0.32 cm COPPER
TUBING
COPPER HEAT
EXCHANGER
FILTER
5.1 cm
JET ASSEMBLY
1.3 cm WINDOW
0.16 cm
DROPLET CHAMBER
BRASS
d = 1cm
l = 1.8cm
0.32 cm PLEXIGLASS
1.3 cm WINDOW
25.4 cm
0.32 cm
0.48 cm
6.4 cm
7.6 cm
1.6 cm STAINLESS STEEL

Figure 1

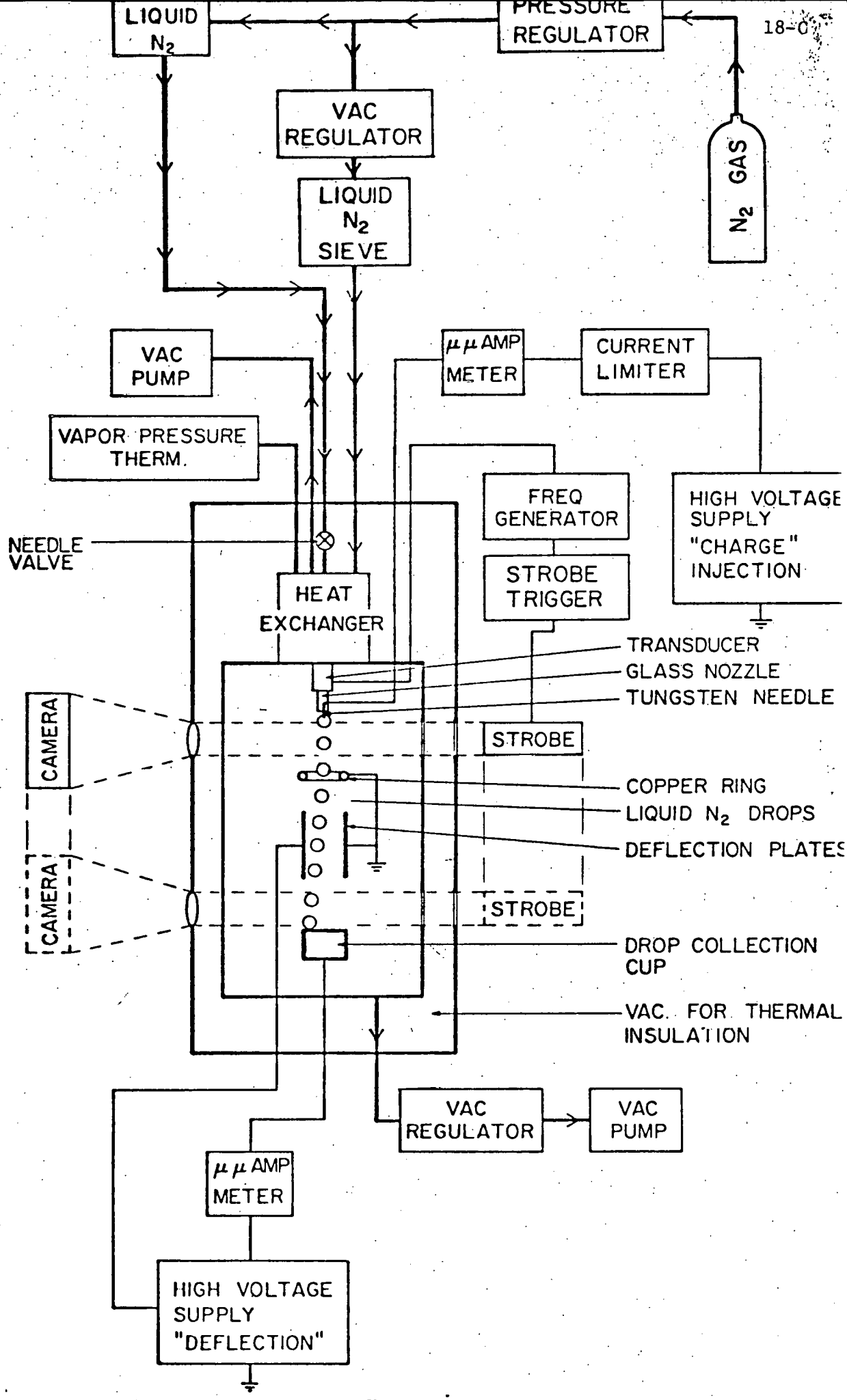
LIQUID N_2
PRESSURE REGULATOR
VAC REGULATOR
LIQUID N_2 SIEVE
N_2 GAS
VAC PUMP
$\mu\mu$AMP METER
CURRENT LIMITER
VAPOR PRESSURE THERM.
FREQ GENERATOR
HIGH VOLTAGE SUPPLY "CHARGE" INJECTION
NEEDLE VALVE
STROBE TRIGGER
HEAT EXCHANGER
TRANSDUCER
GLASS NOZZLE
TUNGSTEN NEEDLE
CAMERA
STROBE
COPPER RING
LIQUID N_2 DROPS
DEFLECTION PLATES
CAMERA
STROBE
DROP COLLECTION CUP
VAC. FOR THERMAL INSULATION
VAC REGULATOR
VAC PUMP
$\mu\mu$AMP METER
HIGH VOLTAGE SUPPLY "DEFLECTION"

Figure 2

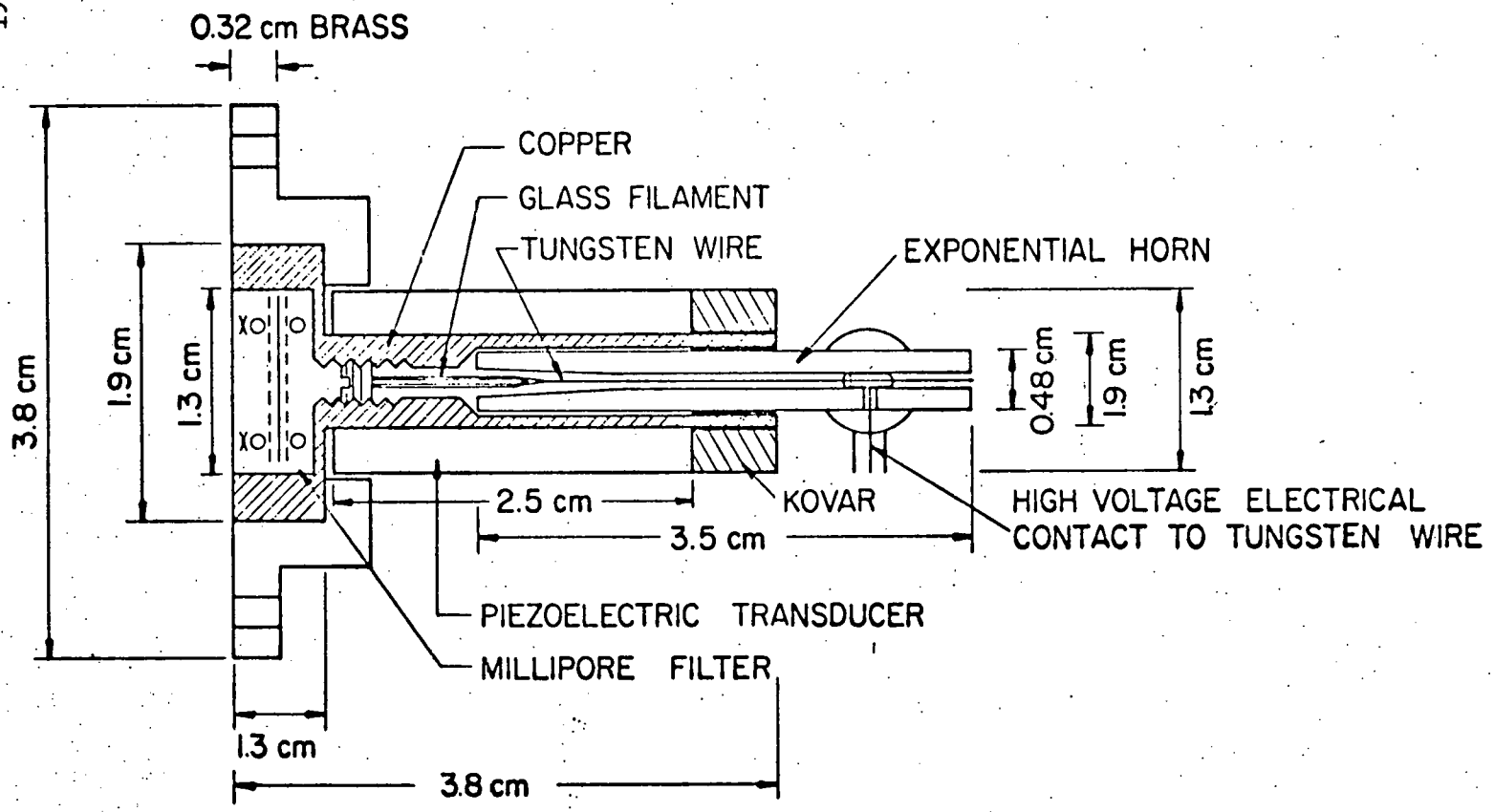
0.32 cm BRASS
COPPER
GLASS FILAMENT
TUNGSTEN WIRE
EXPONENTIAL HORN
3.8 cm
1.9 cm
1.3 cm
0.48 cm
1.9 cm
1.3 cm
2.5 cm
KOVAR
HIGH VOLTAGE ELECTRICAL
CONTACT TO TUNGSTEN WIRE
3.5 cm
PIEZOELECTRIC TRANSDUCER
MILLIPORE FILTER
1.3 cm
3.8 cm

Figure 3

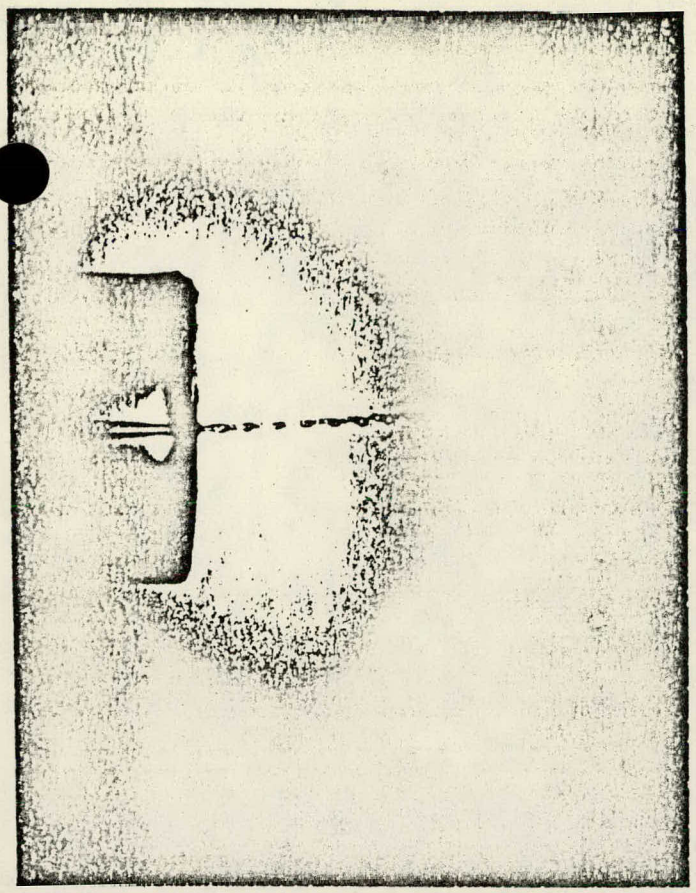

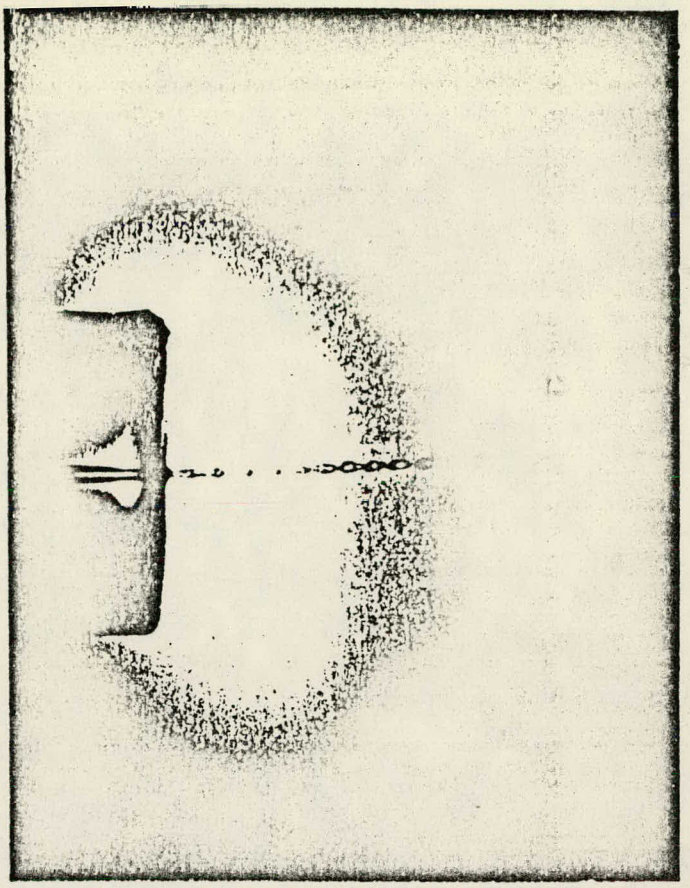

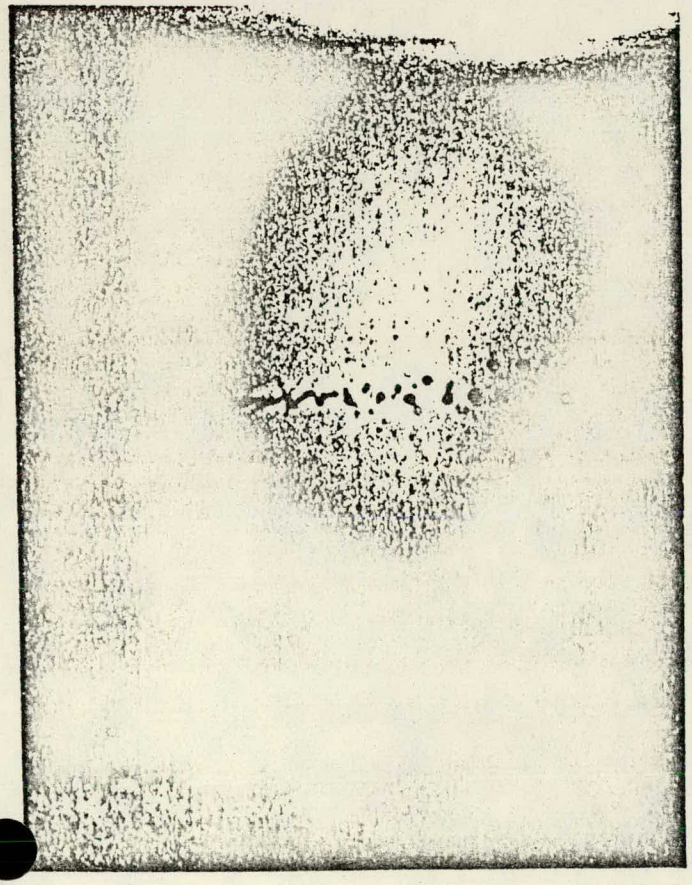

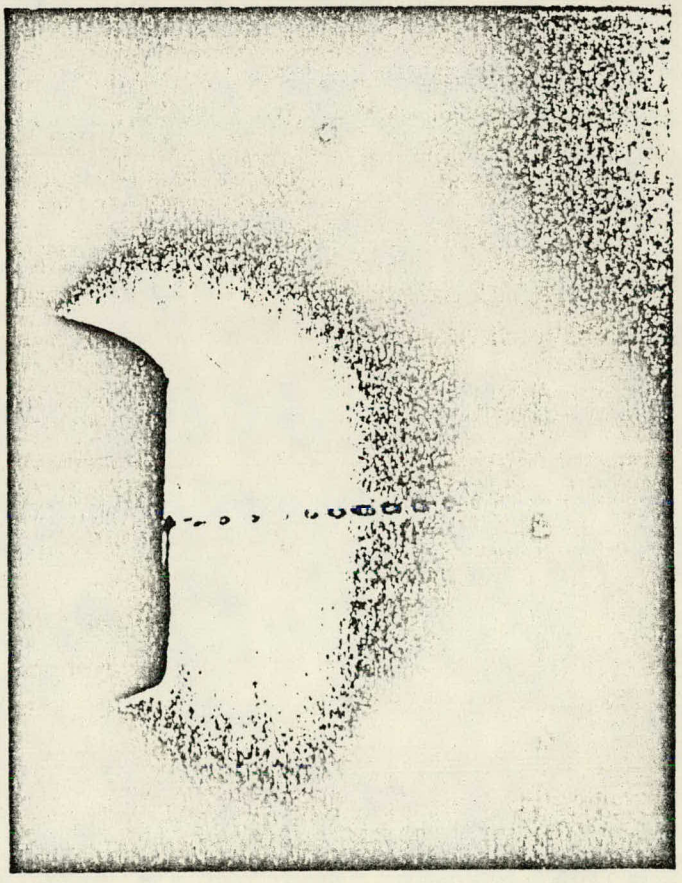

Figure 4

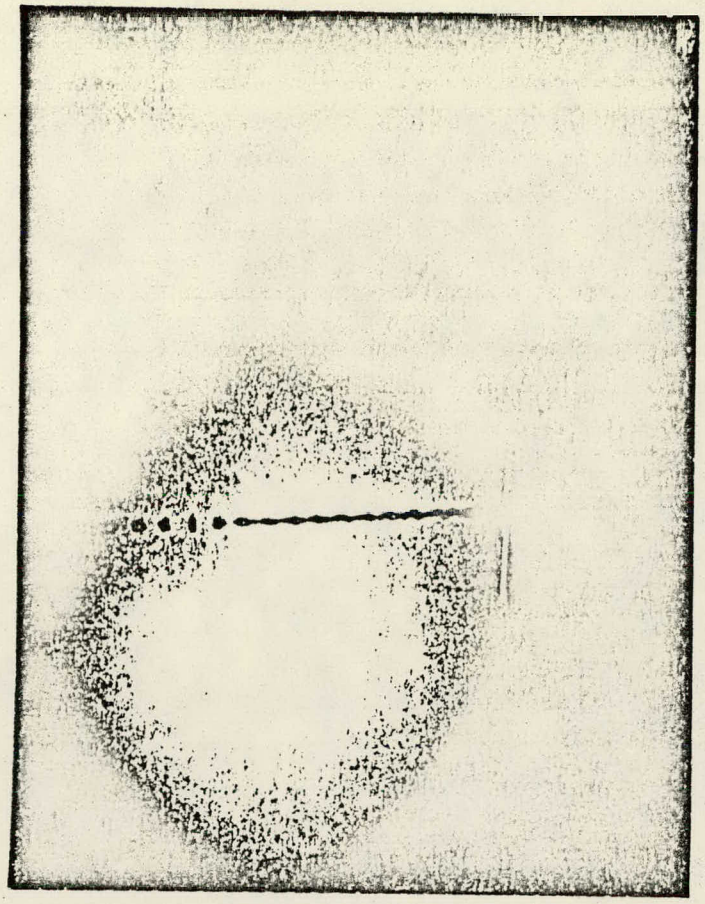

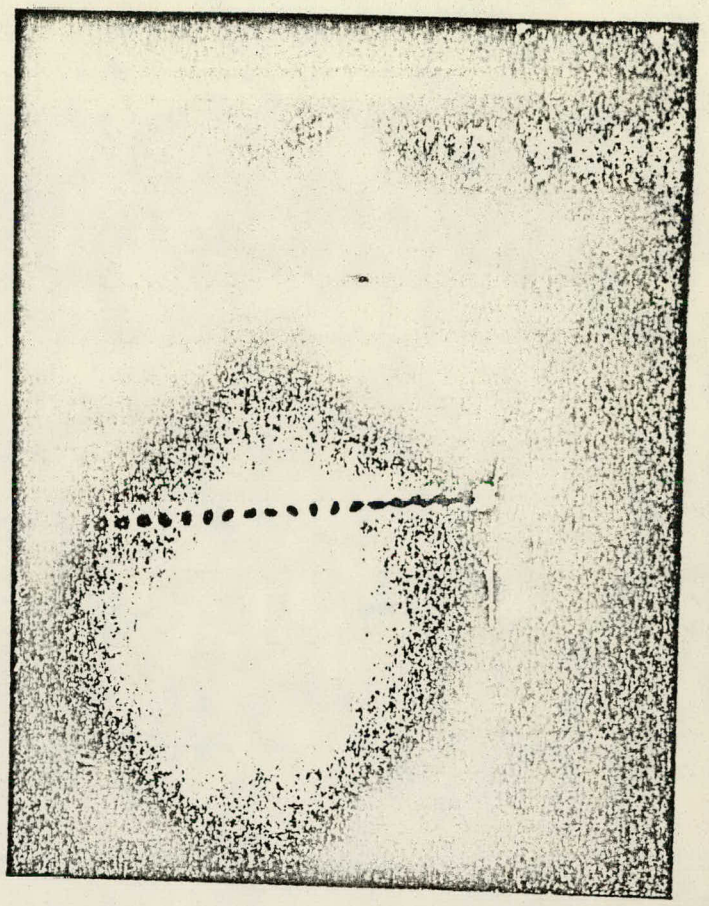

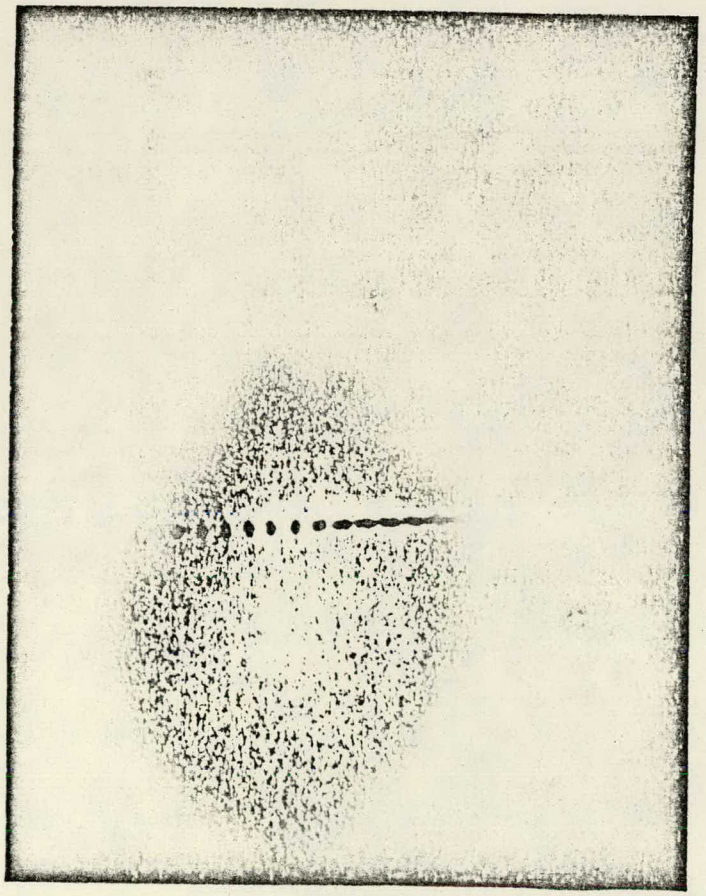

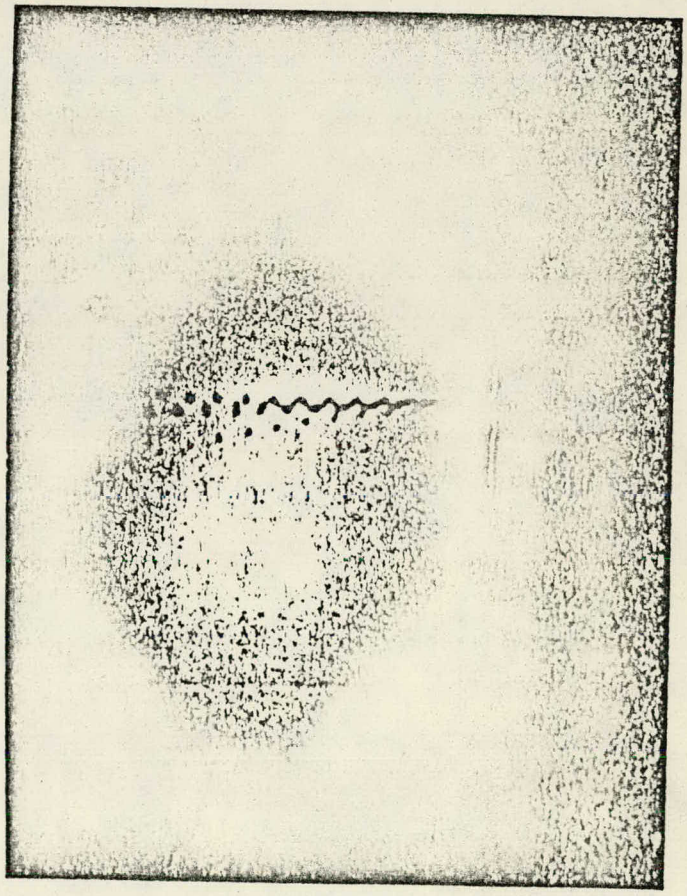

Figure 5

AN APPARATUS FOR PRODUCING UNIFORM SOLID SPHERES OF HYDROGEN

C. A. Foster*, K. Kim,
R. J. Turnbull and C. D. Hendricks**

Department of Electrical Engineering
University of Illinois
Urbana, Illinois 61801

ABSTRACT

An apparatus has been constructed which produces uniform spheres of solid hydrogen for experiments testing the feasibility of using the solid hydrogen pellets for refueling fusion reactors. Two versions of the apparatus were developed, one which produced 70 μm diameter pellets at the rate of 10^5/sec and another which produced 200 μm pellets at the rate of 2.6×10^4/sec.

The first step in the pellet production is to liquefy the hydrogen by flowing it through a liquid helium-cooled heat exchanger. Then, a liquid hydrogen jet is formed by flowing the hydrogen through a nozzle. The jet is broken up into uniform drops by an acoustical excitation. The drops are frozen by evaporation in a pressure less than the triple point pressure of hydrogen. Finally, the drops are injected into vacuum for the experiments.

* Current address, Oak Ridge National Laboratory, Oak Ridge, Tennessee

** Current address, Lawrence Livermore Laboratory, Livermore, California

I. Introduction

Fusion reactors based on the Tokamak principle will be designed to operate with a long cycle time. This requires refueling during the cycle. The injection of small solid pellets of deuterium and tritium appears to be the best method of refueling and as a result, conceptual designs of future reactors include the pellet refueling scheme.[1,2] In order to test the feasibility of pellet refueling we have constructed the pellet generating apparatus described in this report. The generator has been used to study pellet-plasma interactions in conjunction with the ORMAK machine at Oak Ridge National Laboratory. The results of these experiments are reported elsewhere.[3] It also has been used to generate hollow hydrogen spheres which may find use as laser fusion targets.[4]

The pellet generating apparatus, which is shown in Figures 1 and 2, consists of three basic parts:

1. A liquid helium-cooled heat exchanger system which liquefies gaseous hydrogen to produce liquid hydrogen at a controlled temperature and pressure
2. A nozzle and acoustical excitation system which produces a jet of liquid hydrogen and breaks it up into uniform sized drops
3. A vacuum injection system consisting of one or two valves which inject the drops into vacuum and accelerates them by gas dynamic drag

The details of each of these subsystems are described below.

II. Heat Exchanger System

The purpose of the heat exchanger system is to produce sufficient quantities of liquid hydrogen at a controlled temperature and pressure. The hydrogen used was ultra-high purity gas from a cylinder. Using cylinder gas will allow the future use of deuterium or deuterium-tritium mixtures which are not available in bulk liquid form. It also reduces the hazards associated with large quantities of liquid hydrogen. The system normally produced 100 cc/hr of liquid H_2 when 70 μm pellets were being formed and 300 cc/hr when 200 μm pellets were being formed. The temperature was maintained at about 14°K and the pressure was 260 Torr for 70 μm pellets and 125 Torr for 200 μm pellets.

The hydrogen gas was regulated at the tank to about 5 p.s.i.g. This pressure was dropped to the operating pressure with a Conoflow H21AT differential pressure regulator referenced to vacuum. The hydrogen was then pre-cooled to 77°K by passing it through a liquid nitrogen-cooled molecular sieve. It was liquefied by flowing through two series connected liquid helium-cooled copper porous plug exchangers. A schematic diagram of the heat exchanger system is included in Figure 3.

The two copper porous plug heat exchangers were fabricated by sintering 250-400 micron diameter OFHC copper beads into an array of holes drilled into OFHC copper blocks. These were baked for four hours under charcoal in an air furnace held at 1000°C. The heat exchangers were interconnected with thin wall inconel tubing by RF brazing with BT silver solder in a dry hydrogen atmosphere. The brazed assembly was helium leak checked at room temperature and showed no signs of leaking in operating at 14°K.

Each heat exchanger had three separate channels as shown in Figure 3,

one for the helium coolant, a second for the hydrogen reservoir and a third for a vapor pressure thermometer. The liquid helium was continuously transferred from a pressurized storage Dewar through a bayonet coupling transfer tube which fed both heat exchangers. The temperature of each heat exchanger was regulated by throttling the separate helium exhausts with a modified differential pressure regulating valve controlled by the hydrogen vapor pressure thermometers located in the heat exchangers. In operating, if the temperature of a heat exchanger increased above a set point, the pressure in the vapor pressure thermometer would increase, forcing the regulating valve to open. This allowed more helium coolant to flow through the heat exchanger. By adjusting the spring tension on the regulating valve the temperature of the heat exchangers could be set from 12°K to 20°K and was regulated to ± 0.05°K. It was necessary to heat the exhaust helium before it passed through the regulating valves in order to prevent the rubber diaphragms in the valves from freezing.

The apparatus was thermally insulated to allow for operating at 14°K. To accomplish this the heat exchangers were suspended with thin wall inconel tubing in a gold plated vacuum chamber maintained at 10^{-6} Torr by a 2" oil diffusion pump. The heat load to the heat exchangers was 0.05 watts when the hydrogen jet was not operating as compared to 5-15 watts when the jet was operating. The primary heat load was that to cool and liquefy the gaseous hydrogen. The cool-down time of the apparatus from room temperature was approximately 10 minutes.

III. Nozzle and Acoustical Excitation System

The drops of liquid hydrogen are formed by the break-up of a jet. A jet of liquid is unstable and will break up into random sized drops.[5] If uniform sized drops are wanted, they can be obtained by applying an acoustical perturbation to the jet.[6] The method of forming the jet and breaking it into drops is the subject of this section.

The jet was formed by forcing the liquid hydrogen through a glass nozzle connecting the pressurized liquid hydrogen reservoir to a chamber maintained near the triple point pressure of hydrogen. The liquid hydrogen reservoir was maintained at a temperature of about 14°K and a pressure of about 260 Torr for the 70 μm pellets and a pressure of about 125 Torr for the 200 μm pellets. The pressure in the jet chamber is regulated by a Conoflow vacuum regulator to within 1 Torr. The pressure is adjusted in the range 40-54 Torr depending on the desired operating conditions. The pressure in this chamber cannot be too far below the triple-point pressure, or the hydrogen will freeze before the jet breaks into drops. The outlet of the glass nozzle had a diameter of 52 μm for the 70 μm drops and a diameter of 140 μm for the 200 μm drops. To prevent the nozzle from being plugged by particulate the liquid hydrogen was filtered with a Millipore filter having a .47 μm pore size. This filter was placed as close to the nozzle as possible. The parts of the nozzle were ultrasonically cleaned prior to assembly and then tested with liquid Freon 113 to detect any residual particles which could plug the nozzles. The jet velocity was 20 m/sec for the smaller drops and 7 m/sec for the larger drops. This resulted in Reynolds numbers for the jet of about 3000. To prevent turbulence the jet nozzle was made of glass which had a very smooth surface.

The ID of the glass nozzle was in the shape of an exponential horn and was fabricated as follows. A small glass lathe was equipped with a microscope having a vernier eye-piece. A piece of 6 mm OD pyrex tubing was reduced to .152 cm OD x .051 cm ID. The reduced section was then heated with a small torch to form the desired shape and size while observing through the microscope. The glass was then removed from the lathe and scribed at the desired position while observing under a microscope. The scribed glass was broken by pulling the two ends rather than by bending the tube. This procedure produced a perpendicular break since the glass was not under compression on either side. The large end of the nozzle was then scribed and broken by using a pin vice to hold the tip.

In order to break the jet into uniform-sized drops, a piezoelectric transducer was coupled to the jet. Figure 4 is a drawing detailing the acoustical excitation system. For the 70 μm pellets a Vernitron PZT-5H ceramic tube, .64 cm OD x .32 cm ID x 1.27 cm long was used. This transducer was cemented with RTV102 to a kovar washer which has a similar thermal expansion coefficient to the ceramic transducer. The kovar washer was soldered to a copper diaphragm which acted as a free end since the resonant frequency of the diaphragm was much lower than the design frequency. A kovar and lead piece was cemented to the other end of the transducer to lower the resonance of the system. The glass nozzle was cemented with Epoxi Patch 5X resin into a copper jet tube which was designed as follows. The length of copper jet tube was chosen to be a half wave resonator at the 80 KHz design frequency. The ID of the copper tube was drilled so that it formed a ¼ wave resonating chamber for the liquid hydrogen. The resonating chamber was terminated on one end with a ¼ wave plug and the other end fed the entrance of the glass nozzle which was an exponential horn

with an amplification of 17X and a low frequency cut off of 50 KHz.[7] The acoustic perturbation was applied to the jet in the following manner. The transducer drives the base of the copper tube which in turn drives the free end of the copper tube. The glass nozzle, cemented into the free end acts as a piston which pumps the liquid in the resonant cavity. The pressure fluctuations in the liquid cavity are amplified as they travel down the exponential horn. This produced a fluctuation in the exit velocity of the liquid hydrogen, thereby forming the initial waves on the jet. For the 200 μm pellets the system was the same except that because of the lower design frequency (26 KHz) and the longer wavelength of the acoustic wave required for the excitation of the liquid hydrogen jet, the thickness of the copper diaphragm was reduced by a factor of two, whereas the length of the copper jet tube, which was chosen to be a half wave resonator, was increased by a factor of two and a half. This gave rise to an amplification and a cut-off frequency for the exponential horn glass nozzle which were lower than the case of the 70 μm pellets.

IV. Vacuum Injection System

In order to allow for experiments on pellet-plasma interactions, it was necessary to inject the pellets into a vacuum. The mass flux of the 70 μm hydrogen pellets was equivalent to 30 Torr-liter/sec of room temperature hydrogen. (The 200 μm pellets had even larger mass flux.) Therefore, if all the pellets were injected into a vacuum, it would require a 30,000 liter/sec pump to maintain a pressure of 10^{-3} Torr. For that reason it was decided to inject only a small fraction of the pellets into vacuum. The remainder of the pellets evaporated in the chamber near the triple point pressure which has its pressure maintained by a 7 liter/sec mechanical pump acting through a vacuum regulator.

Two different systems were used to selectively inject the pellets into vacuum. For the first system (70 μm pellet system) the selective injection was achieved by use of the small gate valve shown in Figure 5. An aluminum slider with an aperture of 1.5 mm diameter was pulled across a hole by an iron slug solenoid. By discharging a capacitor through the solenoid coil, the slider was cycled closed-open-closed with a minimum open time of 500 μsec. The opening of the gate valve was monitored by a photo pickup on a dummy aperture on the slider. The vacuum seal between the injection tube and the slider was made with a teflon gasket which was held against the slider by a rubber O-ring. The leak rate across this seal was 10^{-3} Torr-liter/sec during operation. The slider gates the opening of a 3 cm long glass injection tube tapered linearly from 1.5 mm ID to 1 mm ID. While traversing the injection tube the 70 μm pellets are accelerated from an entrance velocity of 20 m/sec to an exit velocity of 95 m/sec by the high velocity gas flow in the tube.

In the second selective injection system (200 μm pellet system) two gate valves were used. The first valve was normally closed and the second one normally open. The gate valve had apertures of 3 mm. Between the valves was a stainless steel tube 2.5 mm in diameter and 15 cm long. The tube was used to accelerate the pellets. The exit velocity was about 100 m/sec. The selective injection was achieved by opening the first injection valve and then, after a short time delay, closing the second valve. The time delay could be varied over the range 0.8-42 msec.

In order to aim the jet so that it would pass through the gate valve, micro manipulation of the jet had to be achieved during operation. This was done by coupling micrometer screw adjustments taken from Hoke 1664M4B Micromite Valves to the heat exchanger nozzle assembly in four locations and mechanically floating the heat exchanger assembly inside the vacuum chamber by using a bellows on one end and a bellows and spiraled thin wall tubing on the other end. This allowed the jet to be translated ± .076 cm in the X and Y directions with an angular adjustment of ± 1^{o}. To aim the drops through the gate valve, a pin was placed on the slider which was positioned over the injection tube when the gate valve was closed.

With a low viscosity gas, such as hydrogen at 20^{o}K, any tube or aperture large enough to pass the drops develops a shock wave when any significant pressure drop is applied across it. Since liquid hydrogen has a very low surface tension (2-3 dynes/cm), drops of it are very fragile. These drops are destroyed by a shock wave or by any high velocity gas flow. Therefore, it was necessary to freeze the drops before they reached the gate valve.

A liquid cannot exist in equilibrium at a pressure less than its triple point pressure. If placed in such a low pressure, part of it will evaporate and the remainder will freeze. The rate at which this evaporation-

freezing process takes place is a function of the pressure. As the pressure is lowered from the triple point pressure, the freezing occurs faster and faster. It is this freezing process which we use to freeze the drops before injecting them into vacuum. It is not necessary to freeze the entire drop, but only a thin shell at the surface. The drop will start to freeze at the surface because of thermal conductivity effects.

In our systems, the jet chamber is maintained at a pressure slightly below the triple point pressure. The restrictions on this pressure are that the drops must freeze before reaching the gate valve but the jet must not freeze before it breaks up into drops. In our system this sets a pressure range of 44 to 50 Torr. These pressures are reached by raising the temperature of the liquid hydrogen exiting the nozzle above the freezing temperature of the hydrogen. However, too high a temperature causes bubbles to form as in Reference 4. A small heater loop of .008 cm diameter nichrome wire was placed near the nozzle exit in order to improve the sub-triple point operation of the jet.

V. Auxiliary Equipment

Several windows were placed on the apparatus to observe the jet in operation through an external microscope. An indium sealed double window assembly allowed observation into the cryogenic jet chamber with an objective with a working distance of 14 mm or greater. A Bausch and Lomb 32 mm objective with a 6X eyepiece was used to observe the drops. Photographs were obtained with a 32 mm microscope objective attached to a 35 mm SLR camera.

Another set of windows was placed in a position such that the pellets could be seen just before the injection tube. A third set allowed observation of the exhaust end of the injection tube and a fourth set showed the pellets 30 cm downstream of the injection tube. All of these windows were at room temperature and were cemented in with epoxy resin.

The electronics used in the apparatus were as follows. The output from a wide band oscillator was amplified up to 400 volts peak to peak by a variable gain 50 watt 500 KC amplifier and used to drive the transducer. A strobe lamp which "freezes" the motion of the jet and drops was driven synchronously with the transducer. The synchronous trigger was obtained by detecting the fall of the squared transducer sine wave signal with a logic circuit armed by a unijunction relaxation oscillator running at a frequency of 1-500 Hz which is the operating rate of the strobescope. (The strobescope cannot operate at the transducer frequency.) The shutter gate valve in the first system was driven by a capacitive discharge circuit which could be triggered manually or by a seven volt trigger pulse. A spark gap lamp used in photographing the drops could be activated from the same trigger pulse. The spark lamp was driven by an automotive electronic ignition circuit. In the second system, the gate

valves are run by a SCR trigger circuit with variable time delays. A unijunction transistor time delay circuit was employed to control the delay time between the two valves. A photo detector comprised of an LED-Photo transistor pair was used to detect the opening of the gate valve. A current regulating supply was used to power the nozzle heater.

Several separate low pressure and vacuum systems are used in the apparatus. The vacuum chamber, surrounding the heat exchangers for thermal insulation, was pumped by a 2" diffusion pump backed by a mechanical pump. This system maintained the cryogenic chamber at 10^{-6} Torr. The various vacuum references used in the differential pressure regulators and gauges were pumped to 10^{-2} Torr by a mechanical pump. The jet chamber was pumped by a mechanical pump throttled by a differential pressure regulator. The vacuum chamber below the gate valves was pumped during testing to 2×10^{-3} Torr with a rough pump. During the ORMAK experiments, it was pumped to 5×10^{-4} Torr by the ORMAK pumping system prior to the initiation of the plasma discharge.

VI. Experimental Performance

The hydrogen droplet generator was capable of generating uniform microspheres of hydrogen over a wide frequency range. For the 70 μm system, Figure 6 shows a jet operating at 260 Torr injecting into 55 Torr at three different frequencies. In practice the mid range from 75 to 120 KHz was most useful. During very low frequency operation the jet tends to break up at a harmonic frequency. The highest frequencies produce drops so close together that they tend to recombine while drifting to the injection port. The effects of varying the acoustical amplitude driving the jet are shown in Figures 7 and 8. Figure 7a shows that with the transducer turned off, a clean jet is produced with no turbulence. Figure 7b shows that with very large acoustical amplitudes, the jet can be acoustically disintegrated. The sequence in Figure 8 shows that as the jet is driven with increased acoustical amplitude, the jet breaks up closer to the nozzle.

Figure 9 shows a comparison of the apparatus operating at the triple point pressure and at 47 Torr 4 cm downstream. After the pellets have drifted 4 cm, they are partially but not completely frozen. The dispersion in the drops is due to the partial freezing of the jet interfering with the breakup. The partially frozen spheres shown in Figure 9 have sufficient strength to withstand an injection into vacuum.

Figure 10 shows the pellets entering and exiting the vacuum injection tube. The pressure is 47 Torr at the entrance of the gate valve and 6×10^{-3} Torr at the exhaust of the injection tube. The intact solid pellets measuring 70 ± 5 μm in diameter have a velocity of 95 m/sec with a velocity dispersion of ± 5% and with an angular dispersion of ± 3^{o}. Similar ranges of performance could be achieved by the 200 μm system.

REFERENCES

1) University of Wisconsin Fusion Feasibility Study Group, "UWMAK-I, A Wisconsin Toroidal Fusion Reactor Design," Report UWFOM-68, University of Wisconsin, Madison, 1974.

2) R. G. Mills, ed., "A Fusion Power Plant," Report MATT-1050, Princeton University Plasma Physics Laboratory, 1974.

3) R. J. Colchin, C. A. Foster, K. Kim, S. Milora and R. J. Turnbull (To be published).

4) C. A. Foster, C. D. Hendricks and R. J. Turnbull, Appl. Phys. Lett., 26, 580 (1975).

5) Lord Rayleigh, Proc. London Math. Soc., 10, 4 (1879).

6) J. M. Schneider and C. D. Hendricks, Rev. Scientific Inst., 35, 1349 (1964).

7) R. W. B. Stephens and A. E. Bates, Acoustics and Vibrational Physics, London, Edward Arnold Publishers (1966).

Figure Captions

1) Exploded Drawing of the 70 μm Hydrogen Pellet Generator

2) Picture of the Assembled Hydrogen Pellet Generator

3) Schematic Diagram of the Hydrogen Pellet Generator

4) Acoustical Excitation Apparatus for Causing the Jet to Break-Up into Uniform Drops

5) Small Solenoid Driven Gate Valve Used in 70 μm Pellet System

6) Formation of Drops at Different Frequencies

7) Acoustical Disintegration of the Jet

   a) No Acoustical Excitation Applied to the Jet

   b) Large Acoustical Excitation Applied to the Jet

8) Drop Formation at Different Amplitudes of Acoustical Excitation

   a) Smallest Amplitude

   b) Medium Amplitude

   c) Largest Amplitude

9) Pictures of Liquid and Partially Frozen Pellets Impacting the Alignment Pin on the Gate Valve

   a) Liquid Drops, Drop Chamber Pressure 55 Torr

   b) Partially Frozen Pellets, Drop Chamber Pressure 47 Torr

10) Pictures of Hydrogen Pellets being Injected into Vacuum

   a) Solid Pellets Before Entering Gate Valve, Drop Chamber Pressure 47 Torr

   b) Solid Pellets Exiting from Injection Nozzle, into a Pressure of 6×10^{-3} Torr

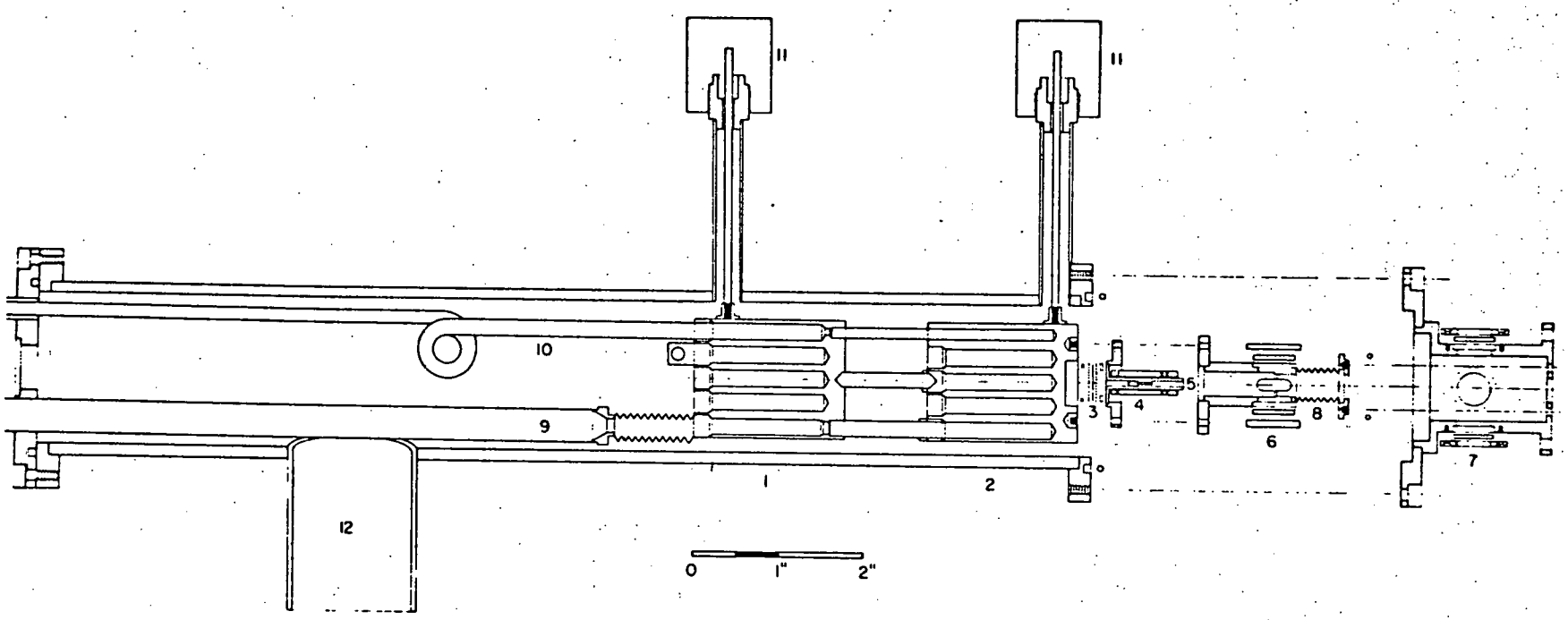

Figure 1

1) Heat exchanger #1
2) Heat exchanger #2
3) Millipore filter
4) Piezoelectric transducer
5) Jet nozzle
6) Indium sealed window
7) Indium sealed window
8) Stainless steel bellows
9) Liquid helium bayonet coupling
10) Gas lines one of 5 shown
    a), b), He exhaust heat exchanger #1, #2
    c), d), Vapor pressure thermometer heat exchanger #1, #2
    e) Hydrogen for jet
11) Jet positioning micrometers 2 of 4 shown
12) High vacuum tube

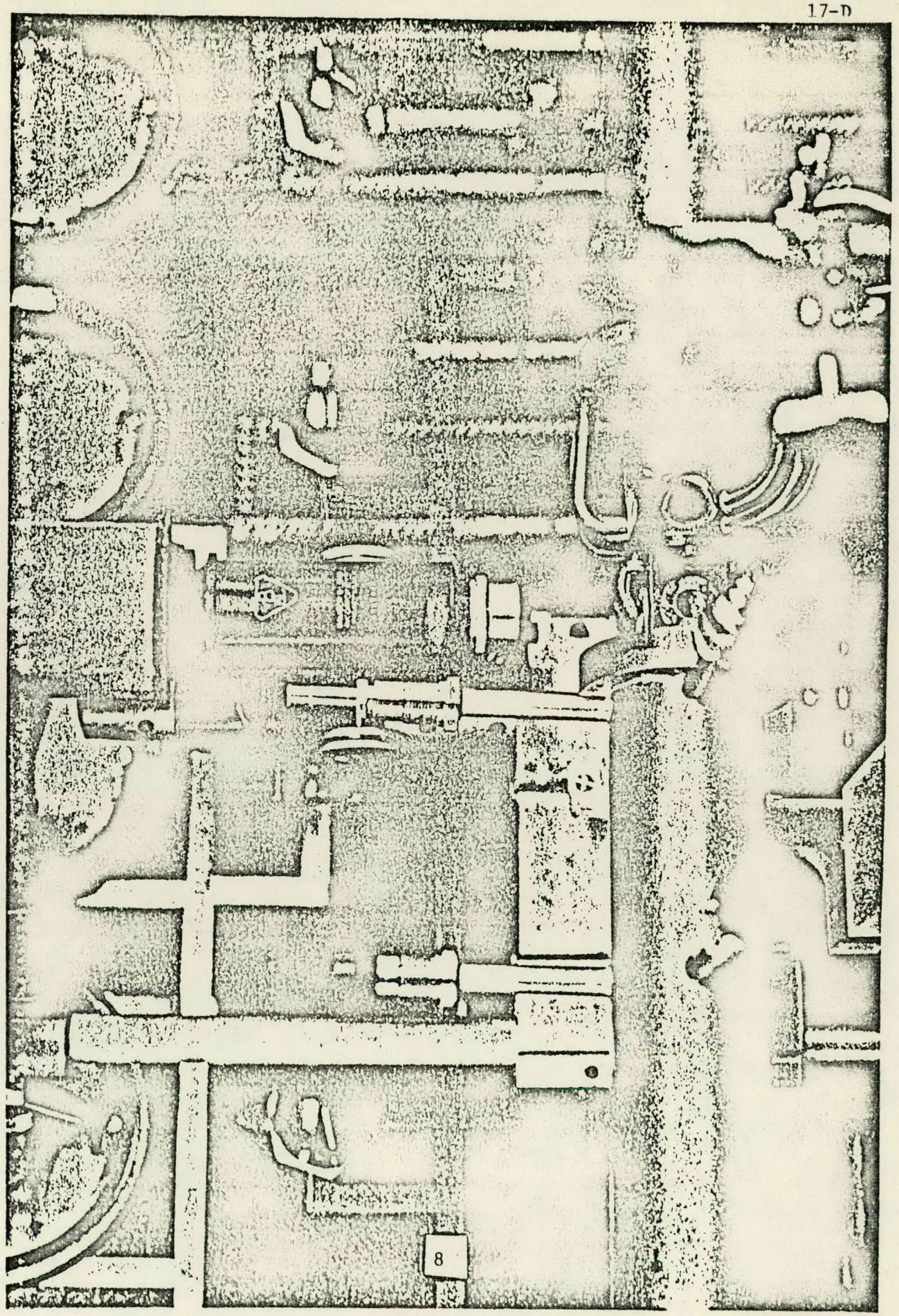

Figure 2

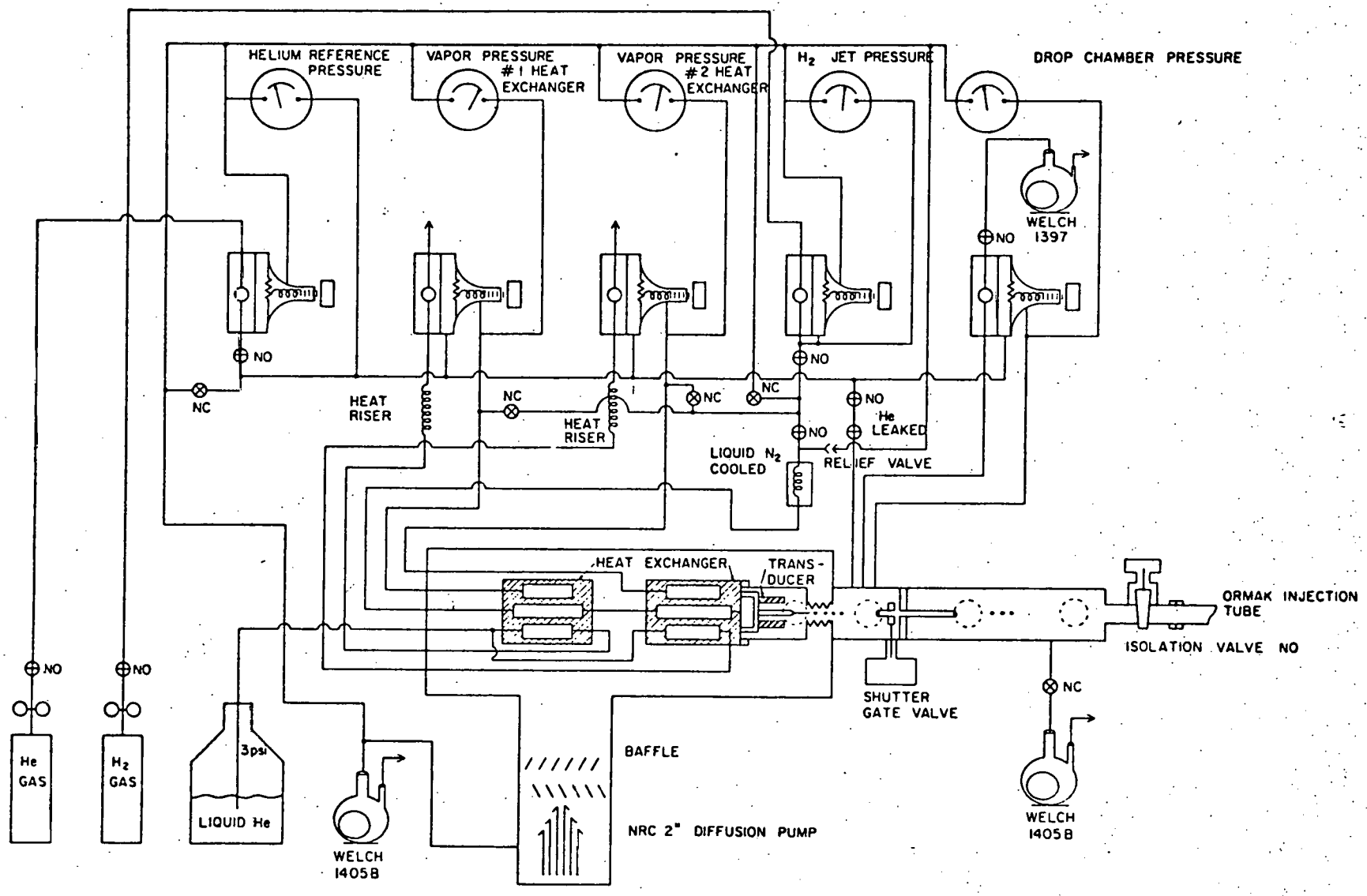
HELIUM REFERENCE PRESSURE
VAPOR PRESSURE #1 HEAT EXCHANGER
VAPOR PRESSURE #2 HEAT EXCHANGER
H_2 JET PRESSURE
DROP CHAMBER PRESSURE
WELCH 1397
NO
NC
HEAT RISER
HEAT RISER
He LEAKED
LIQUID N_2 COOLED
RELIEF VALVE
HEAT EXCHANGER
TRANS-DUCER
ORMAK INJECTION TUBE
ISOLATION VALVE NO
He GAS
H_2 GAS
3psi
LIQUID He
WELCH 1405B
BAFFLE
NRC 2" DIFFUSION PUMP
SHUTTER GATE VALVE
WELCH 1405B

Figure 3

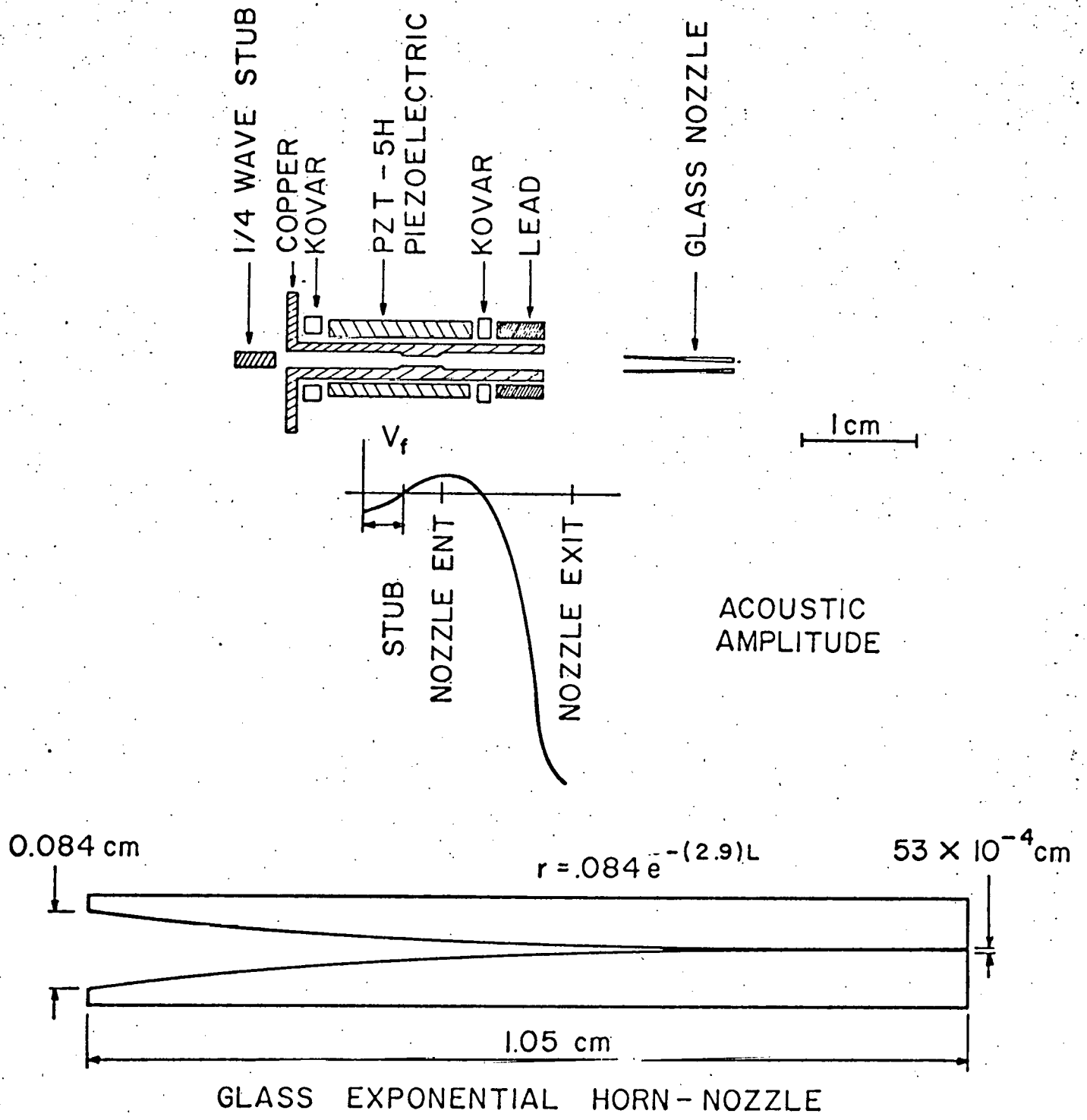
1/4 WAVE STUB
COPPER
KOVAR
PZT-5H
PIEZOELECTRIC
KOVAR
LEAD
GLASS NOZZLE
1 cm
V_f
STUB
NOZZLE ENT
NOZZLE EXIT
ACOUSTIC
AMPLITUDE
0.084 cm
$r = .084\, e^{-(2.9)L}$
53×10^{-4} cm
1.05 cm
GLASS EXPONENTIAL HORN-NOZZLE

Figure 4

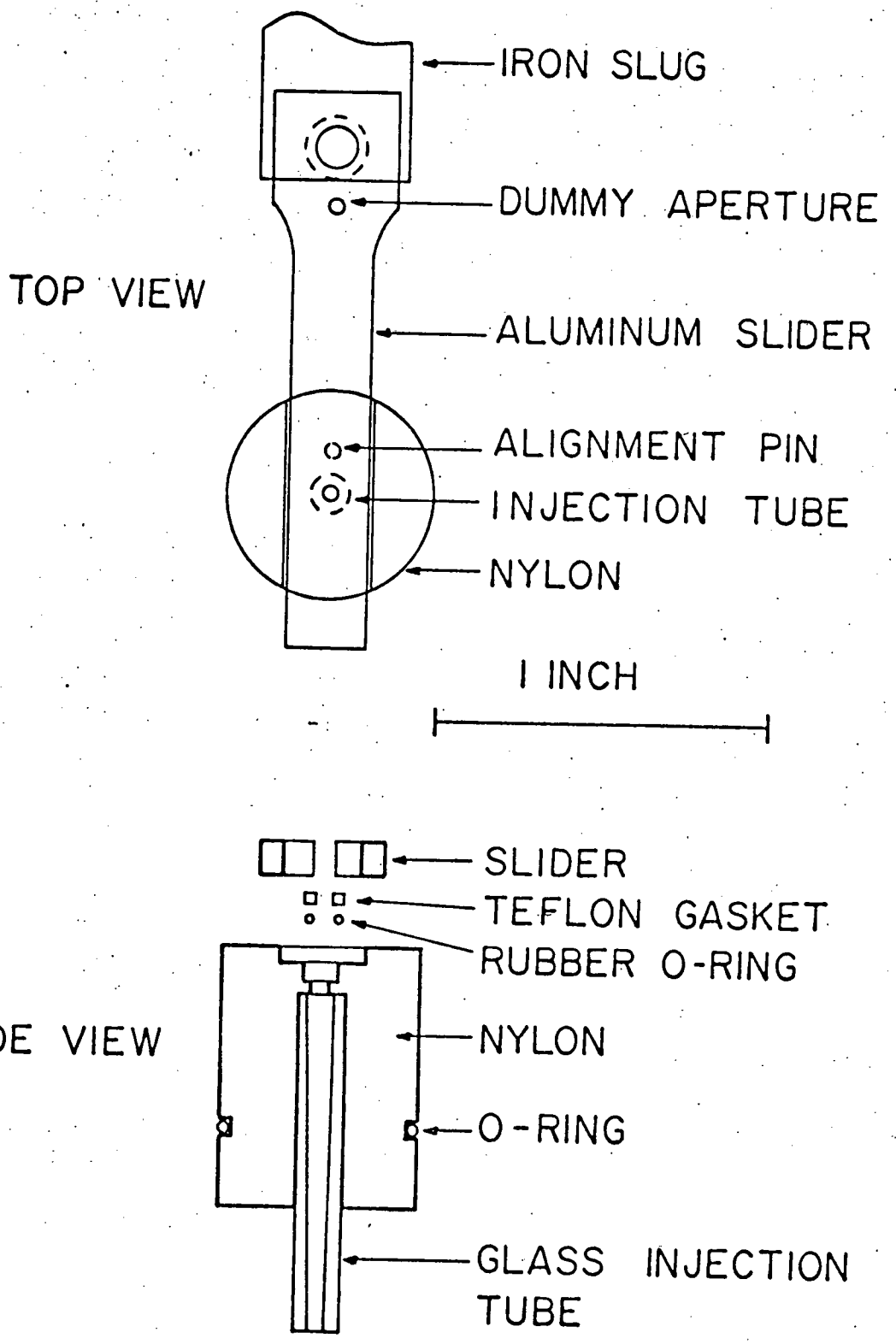
IRON SLUG
DUMMY APERTURE
TOP VIEW
ALUMINUM SLIDER
ALIGNMENT PIN
INJECTION TUBE
NYLON
1 INCH
SLIDER
TEFLON GASKET
RUBBER O-RING
SIDE VIEW
NYLON
O-RING
GLASS INJECTION TUBE

Figure 5

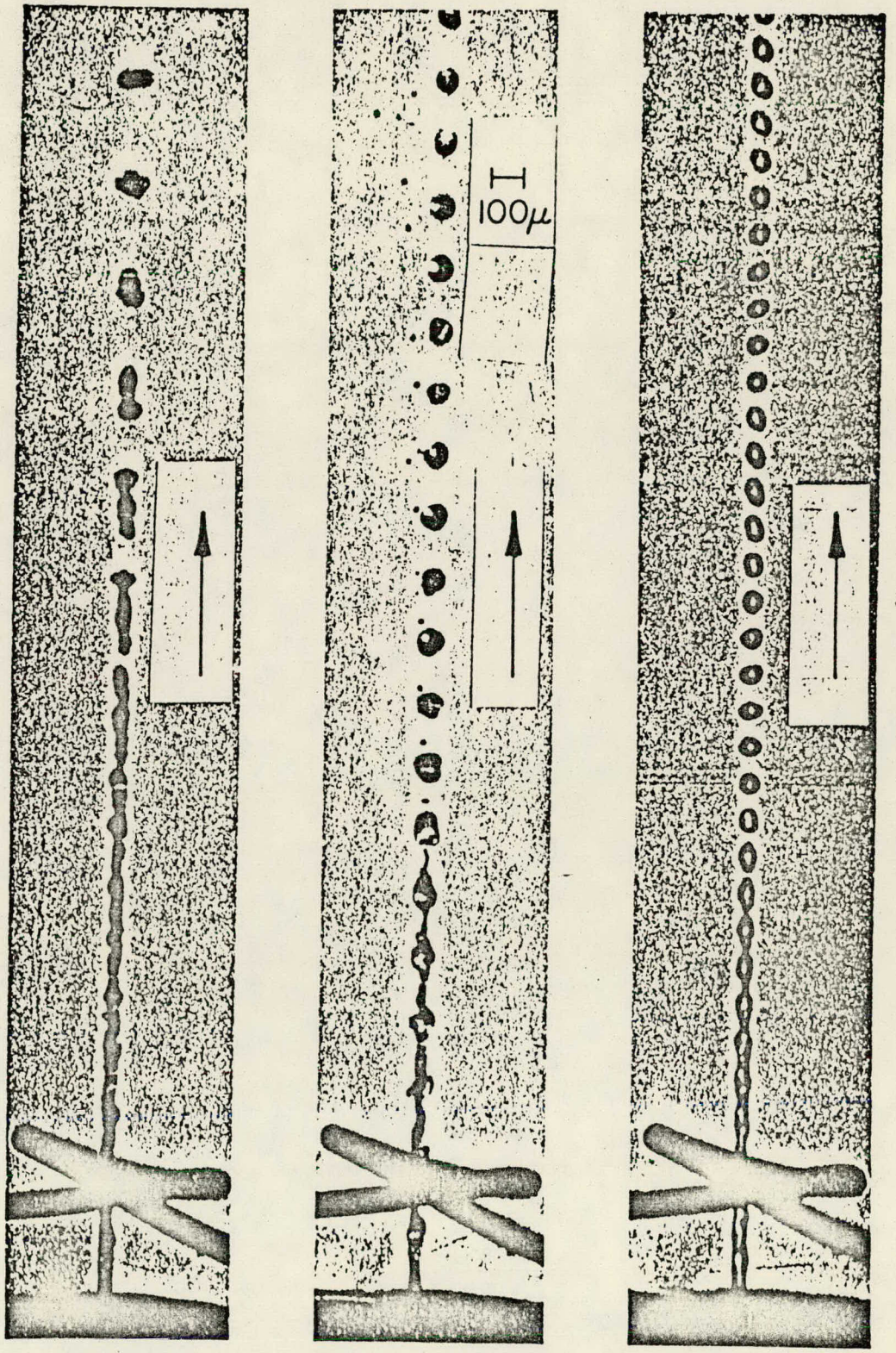

Figure 6

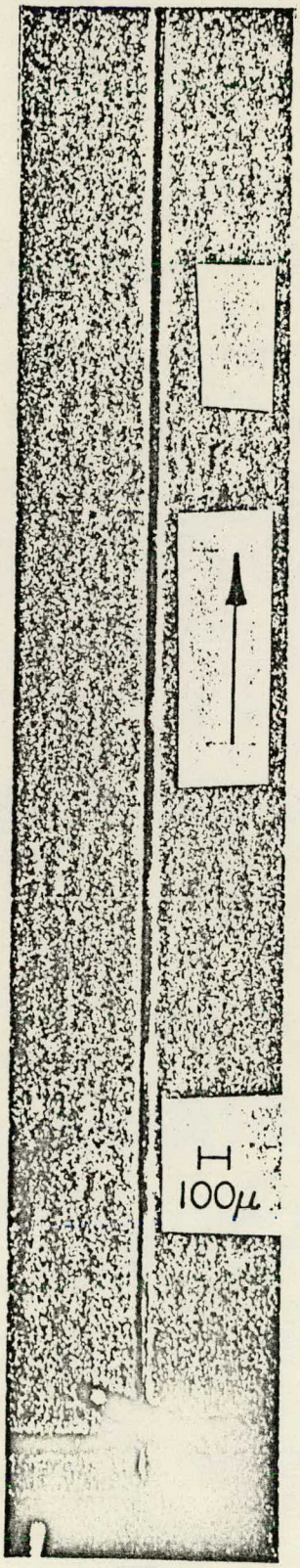

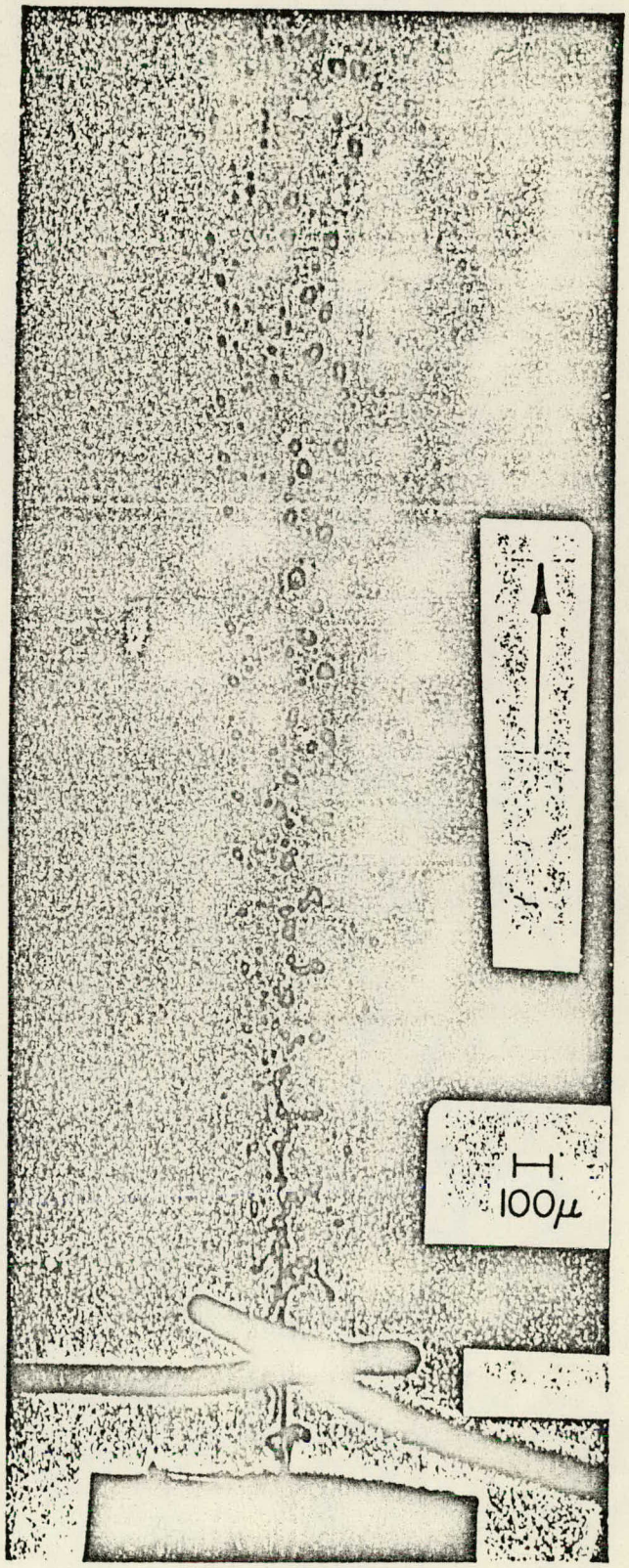

Figure 7

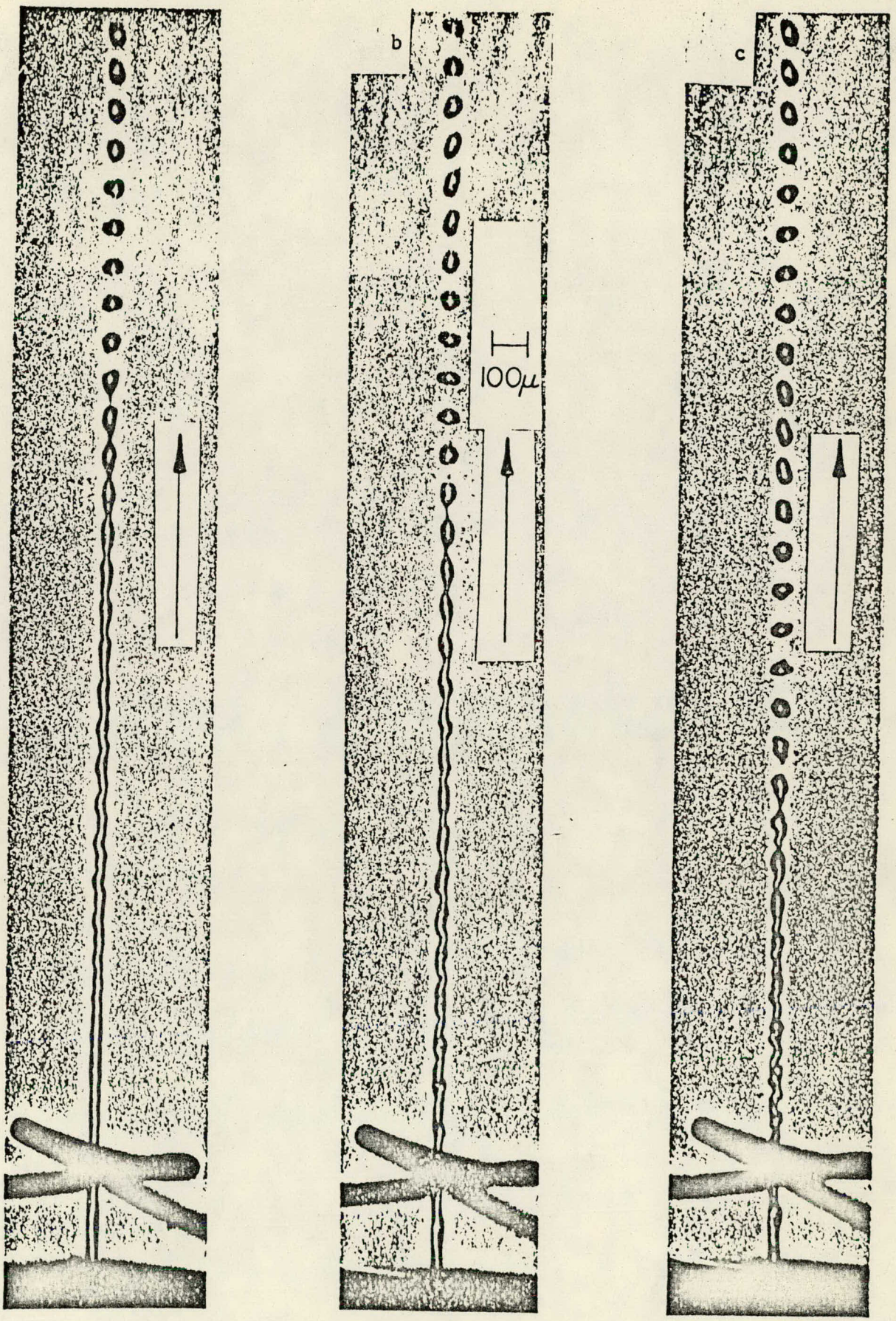

Figure 8

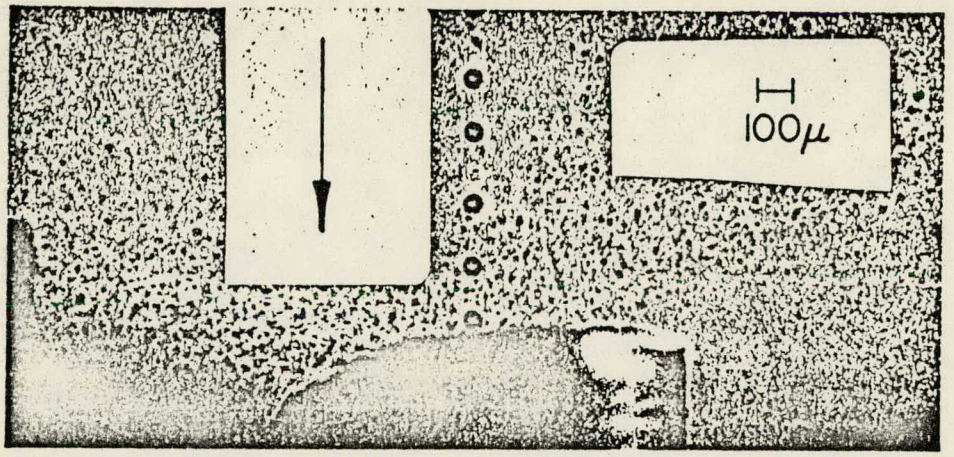

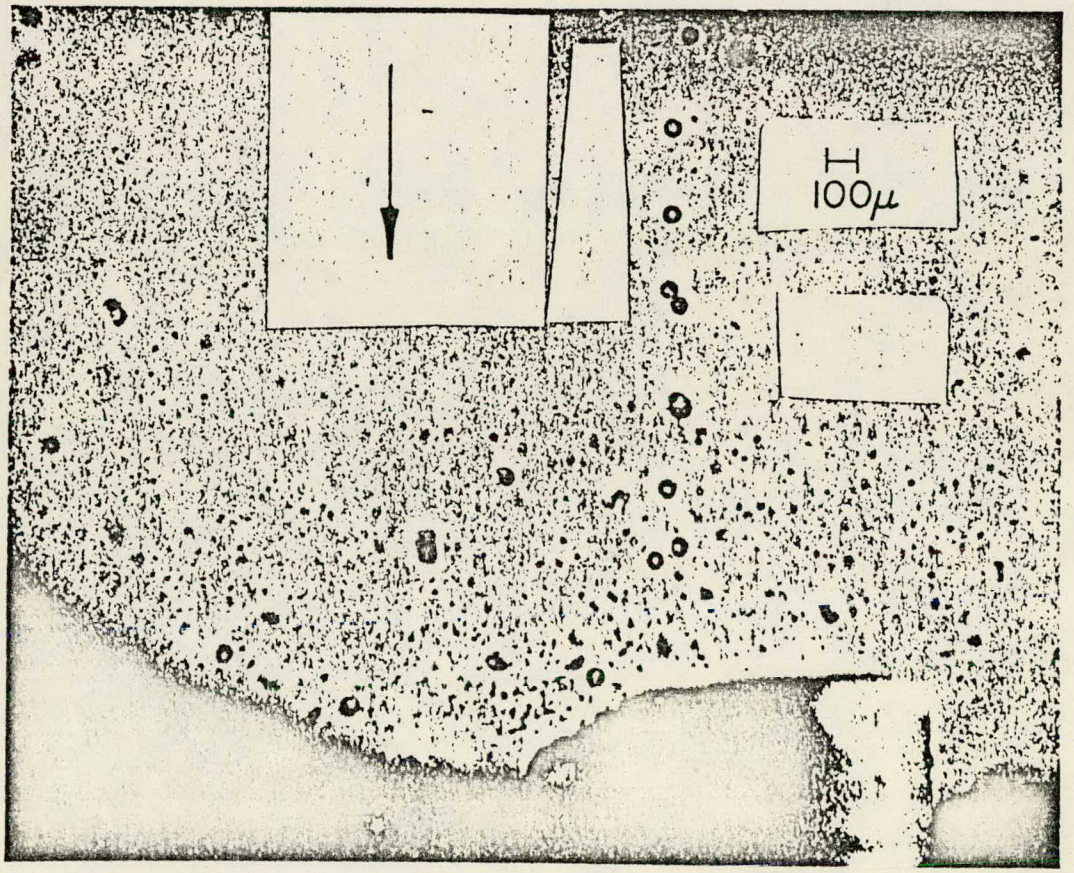

Figure 9

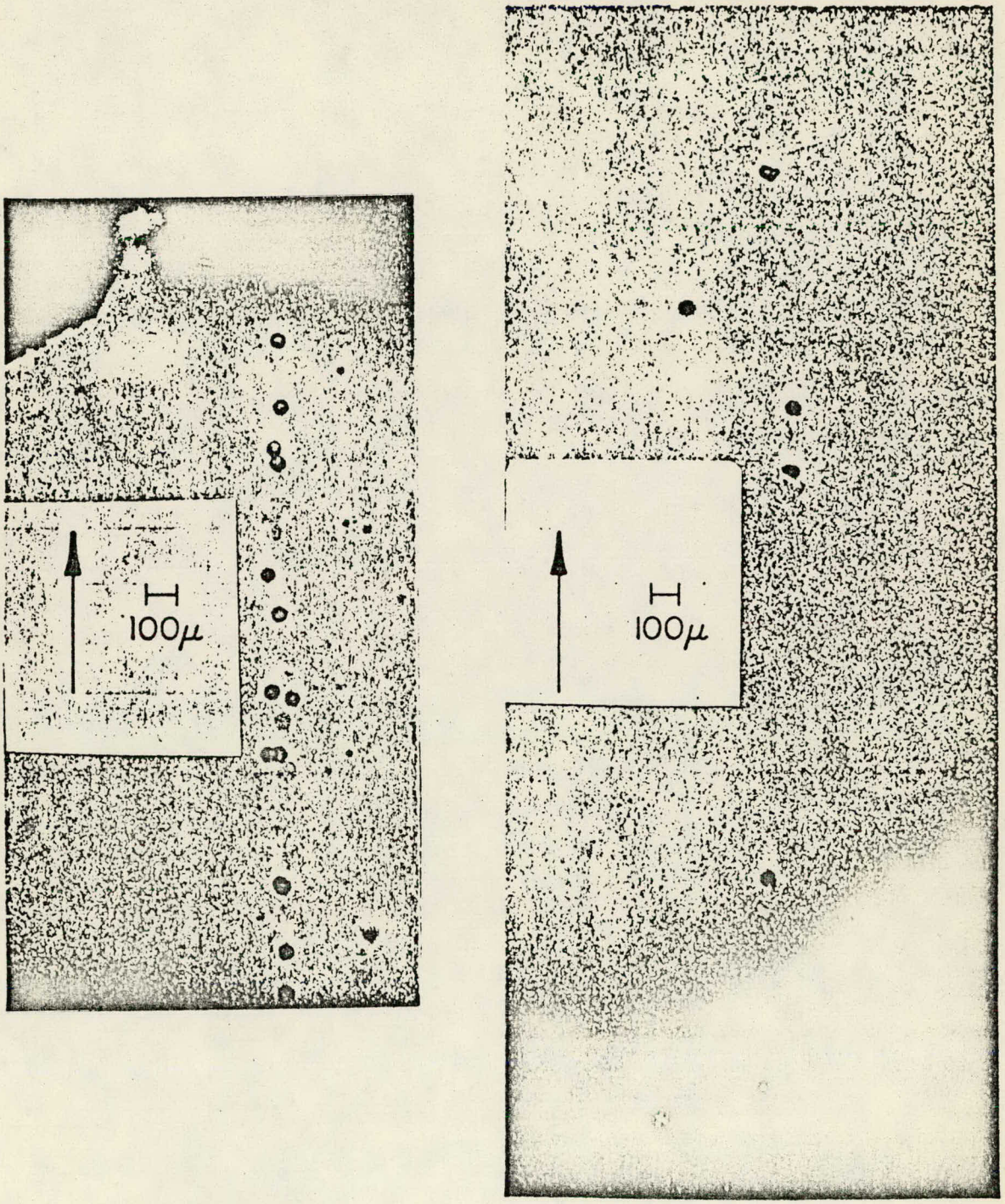

Figure 10